Manu Huttunen

OPTIMIZING THE SPECIFIC ENERGY CONSUMPTION OF VACUUM FILTRATION

ACTA UNIVERSITATIS LAPPEENRANTAENSIS 886

Manu Huttunen

OPTIMIZING THE SPECIFIC ENERGY CONSUMPTION OF VACUUM FILTRATION

Dissertation for the degree of Doctor of Science (Technology) to be presented with due permission for public examination and criticism in the Auditorium of the Student Union House at Lappeenranta-Lahti University of Technology LUT, Lappeenranta, Finland on the 13th of December, 2019, at noon.

Acta Universitatis
Lappeenrantaensis 886

Supervisors Professor Jero Ahola
LUT School of Energy Systems
Lappeenranta–Lahti University of Technology LUT
Finland

Professor Olli Pyrhönen
LUT School of Energy Systems
Lappeenranta–Lahti University of Technology LUT
Finland

Reviewers Professor Risto Ritala
Department of Automation Technology and Mechanical Engineering
Tampere University
Finland

Dr Esko Juuso
Department of Environmental and Chemical Engineering
University of Oulu
Finland

Opponents Professor Risto Ritala
Department of Automation Technology and Mechanical Engineering
Tampere University
Finland

Dr Esko Juuso
Department of Environmental and Chemical Engineering
University of Oulu
Finland

ISBN 978-952-335-458-6
ISBN 978-952-335-459-3 (PDF)
ISSN-L 1456-4491
ISSN 1456-4491

Lappeenranta–Lahti University of Technology LUT
LUT University Press 2019

Abstract

Manu Huttunen
Optimizing the specific energy consumption of vacuum filtration
Lappeenranta 2019
63 pages
Acta Universitatis Lappeenrantaensis 886
Diss. Lappeenranta–Lahti University of Technology LUT
ISBN 978-952-335-458-6 ISBN 978-952-335-459-3 (PDF)
ISSN-L 1456-4491 ISSN 1456-4491

Vacuum filtration is applied in solid-liquid separation in a wide variety of industrial processes for instance in the mining, chemical, and paper industries. The main contributor to the considerable energy consumption of vacuum filtration is the high requirement of pumping air to maintain the pressure difference driving the filtration.

In this doctoral dissertation, the specific energy consumption of vacuum filtration and subsequent thermal drying to achieve a zero moisture content of the filtration product is investigated. The objective of the study is to identify vacuum filtration process variables, which can be manipulated to enhance efficiency and to optimize the energy consumption of the filtration and drying process. The investigation is carried out by analysing the results obtained in experiments with a laboratory-scale Büchner apparatus and a pilot-scale horizontal belt vacuum filter. The analysis of thermal drying is included by calculation. The applicability of a data-driven soft sensor method to estimate the filter cake solid content after vacuum dewatering is studied.

The study shows that it is key to evaluate the specific energy consumption as a function of the solid content of the cake in order to determine the optimal ending criteria for dewatering. It is found that there is an optimal combination of the slurry solid content, the pressure difference, and the slurry loading that results in the minimum specific energy consumption of vacuum filtration and subsequent thermal drying.

Exploiting the thermodynamic nature of vacuum dewatering proved to be highly beneficial to the estimation of the solid content of the filter cake. The developed data-driven soft sensor estimator was able to explain 80 % of the variance in the target variable with a mean absolute error of 0.42 percentage points.

The evaluation of the specific energy consumption of a vacuum filtration process with respect to the solid content of the filter cake and the application of the soft sensor estimator could provide the means to control and optimize the energy consumption of vacuum filtration and subsequent drying.

Keywords: vacuum filtration, dewatering, thermal drying, specific energy consumption, energy efficiency, estimator, soft sensor, filter cake, moisture content, solid content

Acknowledgements

The work presented in this doctoral dissertation was carried out at the Laboratory of Control Engineering and Digital Systems, Department of Electrical Engineering, LUT School of Energy Systems at Lappeenranta University of Technology, now Lappeenranta–Lahti University of Technology LUT, between 2015 and 2019. The research was funded by Tekes, the Finnish Funding Agency for Innovation, currently known as Business Finland.

I want to express my sincerest gratitude to Professors Olli Pyrhönen and Jero Ahola for making it possible for me to embark on the journey that has given me so much motivation and has allowed me to head my career in a new direction. Your guidance along the way is highly valued.

I am grateful to Professor Antti Häkkinen for his support and shared knowledge during this work. A warm thank you to Dr Teemu Kinnarinen and Mr Lauri Nygren for their advice, cooperation, and cakes of many flavours.

I thank my preliminary examiners Professor Risto Ritala from Tampere University and Dr Esko Juuso from University of Oulu for their engagement in the preliminary examination process and their valuable feedback.

Thank you Dr Vesa Karvonen for all your work along the way, your drive and positive attitude, you rock! I am thankful for the extensive experience Mr Bjarne Ekberg made available for this work. Warm thanks to Dr Tuomo Lindh and Mr Mikko Rikkonen for your help and advice in upgrading the pilot-scale filter.

Thank you to my colleagues at the Department of Electrical Engineering for your help in getting this work started and shifting my mindset to the research mode after so many years of working in the industry.

Special thanks to Dr Hanna Niemelä and Mr Peter Jones for your guidance and support in scientific writing.

The financial support of Kymin Osakeyhtiön 100-vuotissäätiö is gratefully acknowledged.

I express my deepest and sincerest gratitude to my loving family. Emma, Eino, and my beloved soulmate Johanna, you are my inspiration.

Manu Huttunen
December 2019
Espoo, Finland

To my wife Johanna, my pillar of strength,
my constant source of encouragement and wisdom.
To my children Emma and Eino,
who impassion me to strive for a better world.
I love you all to the stars and back.

Contents

List of publications

This doctoral dissertation is based on the following papers. The rights have been granted by the publishers to include the papers in the dissertation.

I. Huttunen, M., Nygren, L., Kinnarinen, T., Häkkinen, A., Lindh, T., Ahola, J., and Karvonen, V. (2017). Specific energy consumption of cake dewatering with vacuum filters. *Minerals Engineering*, 100, pp. 144–154. Published.

II. Karvonen, V., Huttunen, M., Kinnarinen, T., and Häkkinen, A. (2018). Research focus and research trends in vacuum filtration – bibliographical analysis, *Filtration*, 18, pp. 40–44. Published.

III. Huttunen, M., Nygren, L., Kinnarinen, T., Ekberg, B., Lindh, T., Ahola, J., Karvonen, V., and Häkkinen, A. (2019). Specific energy consumption of vacuum filtration: Experimental evaluation using a pilot-scale horizontal belt filter. *Drying Technology*, pp. 1–16. Published.

IV. Huttunen, M., Nygren, L., Kinnarinen, T., Ekberg, B., Lindh, T., Karvonen, V., Ahola, J., and Häkkinen, A. (2019). Real-time monitoring of the moisture content of filter cakes in vacuum filters by a novel soft sensor. *Separation and Purification Technology*, 223, pp. 282–291. Published.

Author's contribution

Author Huttunen is the principal author and investigator in Publications I and III–IV, co-authors Nygren and Kinnarinen participated in conducting the experiments, analysing the data, and writing the publications. In Publication II, Dr Karvonen was the corresponding author and Author Huttunen participated in the writing and bibliographical analysis. The co-authors not mentioned above have participated in the project cooperation. In addition, they have contributed to the preparation of the publications by revision comments and suggestions.

Nomenclature

In the present work, variables are denoted using *slanted style*, and constants and abbreviations are denoted using regular style.

Latin alphabet

A	area	m^2
a	experimentally determined slope t/V^2	s/m^6
c	filtration concentration	$kg/m^3_{filtrate}$
E	energy consumption	J
E_S	specific energy consumption	kJ/kg
ΔH	latent heat	kJ/kg
h	width	m
k	permeability, exponential growth rate	m^2, -
L	thickness of the filter cake	m
M	moisture content	% kg/kg
M_s	solids mass flow rate	g/s
$\dot{m}$	mass flow	kg/s
m_s	mass of solids	kg
P	power	W
p	pressure	bar
Δp	applied pressure difference	bar
Q	standard volumetric flow rate, heat transfer	Nm^3/h, J
q_m	mass flow rate	kg/s
q_{sl}	slurry mass flow rate	kg/min
q_V	volumetric flow rate	m^3/s
R	specific gas constant	J/kg K
R_m	resistance of the filter medium	1/m
r	pore radius	m
S	saturation of the filter cake	m^3/ m^3
S_∞	irreducible saturation	m^3/ m^3
s	solid content	kg/kg
T	temperature	°C
ΔT	temperature difference	°C
t	time	s
u	superficial velocity of liquid	m/s
V_f	volume of filtrate	m^3
v	velocity	mm/s
w	mass of cake deposited per unit area	kg/m^2
w_a	specific humidity of air	kg_v/kg_a
x	particle mean diameter	m
z	length on filter belt, thickness of porous medium	m

Greek alphabet

α	specific cake resistance	m/kg
γ	surface tension at the liquid-gas interface	N/m
ε	cake porosity	m^3/m^3
θ	contact angle between the liquid and the solid,	rad
	dimensionless deliquoring time	-
η	efficiency	%
μ	dynamic viscosity of the filtrate	N s/m^2
ρ	density, Pearson correlation coefficient	kg/m^3, -

Dimensionless numbers

k	isentropic exponent
R^2	coefficient of determination

Superscripts

f	filtration
th	thermal
tot	total, i.e., filtration + thermal drying

Subscripts

a	air
av	average
B	filter belt
b	threshold
belt	filter belt
c	filter cake
calc	calculated
d	dewatering, filter cake
dw	dewatering
e	evaporation, actual filter installation
f	filtrate, filtration
g	gas
i	entry surface of the cake
in	input value
l	liquid
m	medium
meas	measured
o	exit surface of the cake
out	output value
R	reduced
r	relative

S	isentropic, specific
s	solids
sep	separation
shaft	vacuum pump shaft
sl	slurry
std	standard
T	isothermal
th	thermal
V	volumetric
v	vapour, evaporation
vp	vacuum pump
w	water

Abbreviations

EDS	energy-dispersive X-ray spectroscopy
LRVP	liquid ring vacuum pump
pp	percentage point
SEM	scanning electron microscope
VSD	variable-speed drive
wt%	weight percent
w/w	weight per weight

1 Introduction

In this doctoral dissertation, the specific energy consumption of vacuum filtration is discussed. In this context, the specific energy consumption is the energy consumed relative to the solids throughput. The focus is on the specific energy consumption with respect to solids and moisture content of the filtration product, i.e., the filter cake. The thermodynamic aspects of vacuum filtration are explored and a data-driven soft sensor for filter cake moisture content estimation is developed.

The specific energy consumption of vacuum filtration is evaluated by analysing the measurements from laboratory-scale Büchner-filter experiments and pilot-scale horizontal belt vacuum filter experiments. The presented methods should be applicable to other types of vacuum and pressure filters as well. In this chapter, the background and motivation of the study are presented together with the objectives and research methods. Finally, the outline of the dissertation is given.

1.1 Background of the study

Vacuum filtration is used for continuous solid–liquid separation in a wide variety of industrial processes for example in the chemical, mining, and paper making industries. It is common to perform the filtration and dewatering operations of slurries with vacuum filters, which are considered robust and reliable technology for dewatering on an industrial scale. Continuously operating vacuum filters are usually applied when the solids to be separated do not contain much fines, settle rapidly, and form a permeable cake that can be dewatered at a moderate pressure difference, or when the cake has to be counter-currently washed in the filter unit (Svarovsky, 2000; Tarleton and Wakeman, 2007; Sparks, 2012). Typical vacuum cake filter designs include for instance rotary discs, drum and horizontal belt filters, and table and tilting pan filters (Tarleton and Wakeman, 2007). Depending on the filter design, different types of filter medium are used, such as polymeric filter cloths or ceramic filter elements. Filtration with horizontal belt vacuum filters is an energy intensive process, both owing to the large volume of air flowing through the pores and cracks of the cake (Ripperger et al., 2013), and because of the leak flow of air into the vacuum system, for instance near the edges of the filter medium. Most of the industrial vacuum filters are operated continuously, and the high production capacities of the industry have substantial energy requirements.

In order to initiate and maintain a flow of filtrate, a pressure difference has to be applied across the slurry and the filter medium (Fig. 1). In the case of vacuum filtration, the slurry and the filter cake on the filter medium are at atmospheric pressure, and the negative pressure difference to p_0 in Fig. 1 is usually generated by suction with a vacuum pump. The vacuum filtration process that follows can be divided into two stages, namely the filtration and dewatering stages. In the filtration stage, liquid is removed from the slurry until the solid particles form a rigid structure, i.e., a filter cake. After the cake formation, liquid in the largest pores of the cake is displaced by air, as long as a cake-specific

threshold pressure is exceeded (Wakeman and Tarleton, 1990; Tien, 2012), and air starts to flow through the cake at an increasing flow rate as a larger proportion of the total pore volume becomes unoccupied by liquid (Wakeman, 1982). While the airflow increases, the rate of dewatering decreases steadily until the saturation of the cake reaches an irreducible level (Hoşten and Şan, 2002; Tien, 2012), which is the minimum saturation of the filter cake obtainable by an infinite pressure difference. The final moisture content of the cake depends on the cake properties and the applied pressure difference (Condie et al., 2000; Wakeman, 2007; Fan, Dong, and Li, 2015), the former being also influenced by the latter and the dewatering time.

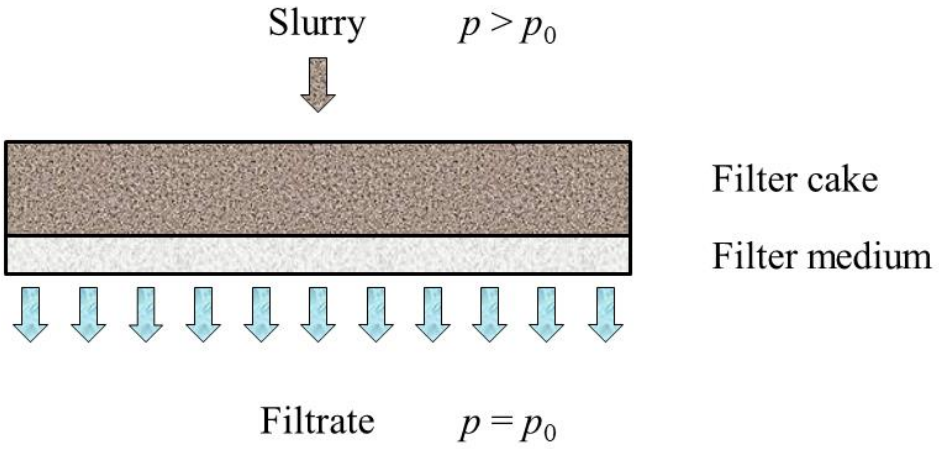

Fig. 1. Cake formation and flow of filtrate through the filter medium. Adapted from (Concha A., 2014).

According to the study reported in Publication II, the research efforts on several filtration categories, including vacuum filtration, have significantly increased over the past decades. In the research context, vacuum filtration plays an important role in various fields, for example in engineering, materials science, and chemistry. Research activity in topics of cake, slurry, and filter medium with regard to vacuum filtration has been steady in recent decades, while activity in filtrate and particle related research has been increasing. The equipment-related search terms of “laboratory” and “continuous” have an increasing trend in the research activity; however, activities on a pilot-scale have remained at a relatively constant level for decades. While Chinese research organizations are the most active producers of publications, the United States is leading in the activity of countries.

1.2 Motivation of the study

In recent years and especially now with the imminent ill effects arising from global warming, the importance of energy conservation and energy efficiency of filtration processes is higher than ever. However, research published on the energy consumption of vacuum filtration has been limited. There is potential for energy conservation and operating cost reduction, because for instance variable-speed control of vacuum pumps to control the pressure difference level or the utilization of modern control technology in filtration processes in general is not yet widely adopted.

The moisture content of a filter cake is probably the most important quality characteristic that should be kept at a constant, desired level in industrial cake filtration applications to maintain consistent product quality and minimize energy consumption. It is often the case that the ultimate desired moisture content of the product cannot be achieved with vacuum filtration only. In this case, a drying stage is added to the process to follow vacuum filtration, and it is usually implemented by thermal drying. The reduction of moisture by vacuum filtration usually requires less energy than thermal drying, and according to Kemp (Kemp, 2005, 2012), a primary method to reduce the energy consumption of thermal drying of materials is efficient dewatering preceding the drying stage. On the other hand, owing to the simultaneous gradually increasing airflow through the cake and the steadily decreasing dewatering rate, the specific energy consumption of the dewatering period can be very high relative to the corresponding moisture reduction.

1.3 Objectives of the study

The main objectives of this study are to investigate the effect of pressure difference, slurry loading, and dewatering time on the specific energy consumption of vacuum filtration and to find means to optimize the energy consumption of vacuum filtration. The research focuses on calcite slurries, but the same methods should also be applicable to other mineral slurries.

A further objective of the study is to develop a model for estimating the moisture content of the filter cake after dewatering. The model uses as inputs basic process variables such as the pressure difference, slurry loading, dewatering time, and other process variables that are measured with standard process instrumentation. The limitations and error sources of these methods are discussed.

Both these objectives aim at reducing the combined specific energy consumption of vacuum filtration and thermal drying. The soft sensor estimate of the moisture content of the filter cake after dewatering can be used as a basis for online energy requirement calculations for the drying stage.

The research topics addressed in this doctoral dissertation are:

- The effects of pressure difference, slurry loading, and dewatering time on the specific energy consumption of vacuum filtration.
- Reaching the minimum energy operating point by varying these process variables.
- Reaching the combined minimum energy operating point of vacuum filtration and successive thermal drying.
- Estimating the filter cake moisture content after vacuum filtration using the above-mentioned basic process variables and other standard process measurements as model inputs.

1.4 Research methods

This study comprises laboratory filtration experiments using a Büchner test apparatus and a pilot-scale horizontal belt vacuum filter as well as filter cake moisture content modelling with machine learning regression algorithms. The laboratory-scale Büchner apparatus test setup presented in Appendix A and the pilot-scale horizontal belt vacuum filter setup described in Appendix B are the sources of experimental data in the study. The slurries for the experiments were prepared from tap water (Lappeenranta City, Finland) and dried tailings obtained from a calcite refining process or Nordkalk Parfill calcite. A variety of slurries were prepared to be filtered with the test equipment in various operating points.

Soft sensor regression for the filter cake moisture content was experimented with five standard machine-learning algorithms, namely regularized linear regression algorithms Lasso, Ridge, and Elastic-Net as well as ensemble decision tree algorithms Random Forest and Gradient Boosting capable of modelling non-linear relationships between variables. Basic signal processing methods such as averaging and mean extraction were used in the pre-processing of the experiment data.

1.5 Scientific contributions

The scientific contributions of this doctoral dissertation are:

- Study results of the effects of pressure difference, slurry loading, and dewatering time on the specific energy consumption of vacuum filtration with the focus on calcite slurries.
- Study results of the total specific energy consumption of vacuum filtration and thermal drying with the focus on calcite slurries.
- A method for determining the leak flow of a vacuum filter.
- A method for estimating the residual moisture content of a filter cake.

The author is also designated as a co-inventor in the following patents and patent applications concerning and closely related to the subjects presented in the doctoral dissertation:

Finnish Patent 127217 B "A system for determining a leak flow of a vacuum system of a vacuum filter," issued 31 January 2018.

Finnish Patent application 20175411 "A method for controlling a vacuum pump," filed 8 May 2017.

Finnish Patent 127626 B "A method and a device for removing liquid from material," issued 31 October 2018.

Finnish Patent application 20175656 "A method and a system for estimating residual liquid content after a liquid removal process," filed 6 July 2017.

Finnish Patent application 20175773 "A method and a system for estimating residual liquid content after a liquid removal process," filed 30 August 2017.

Finnish Patent application 20195281 "A method and a system for monitoring condition of a carrier medium of a liquid separation device," filed 5 April 2019.

1.6 Outline of the doctoral dissertation

This doctoral dissertation studies the specific energy consumption of vacuum filtration with the focus on calcite slurries. The background and motivation of the work are first provided in this introductory chapter. Then, the specific energy consumption of vacuum filtration for experimental tests with a Büchner apparatus and a pilot-scale horizontal belt vacuum filter is discussed. The airflow rates through the filter cake in different operating points of the filters and the specific energy consumption with respect to the solid content of the filter cake are presented. The total specific energy consumption of vacuum filtration and consecutive thermal drying is analysed. Then, a novel soft sensor method for estimating the moisture content of filter cakes is proposed. The conclusions, key findings, and suggestions for future work are presented in Chapter 4.

The rest of the dissertation consists of the following chapters:

Chapter 2 discusses the airflow rates and the specific energy consumption of vacuum filtration. Key results and findings from experimental research with a Büchner apparatus and a pilot-scale horizontal belt filter are highlighted.

Chapter 3 introduces the thermodynamic background related to vacuum filtration and describes a soft sensor method for estimating the filter cake moisture content leveraging this phenomenon. Several regression models constructed with machine learning

algorithms are experimented for moisture content estimation, and their applicability is analysed.

Chapter 4 presents the conclusions and discusses possible paths for future work.

2 Specific energy consumption of vacuum filtration

In this chapter, the focus is on the specific energy consumption of vacuum filtration. First, the principles and theory of cake filtration and dewatering are discussed. Then, power demand in the vacuum filtration process and heat demand in the thermal drying process are addressed. Finally, airflow and the specific energy consumption of cake dewatering and vacuum filtration of the conducted experiments are considered, and the subsequent thermal drying to a zero moisture content of the filter cake is analysed by calculation. The chapter concludes by a summary of results.

2.1 Principles of filtration

In the course of the filtration stage, the solid particles of the slurry are retained on the filter medium forming a matrix with void space, i.e., a filter cake. The liquid filling the void space is held in place by capillary retention forces determined by the size range and surface properties of the particles forming the cake. By applying a pressure difference over the filter cake and the filter medium exceeding the threshold pressure, air has the ability to enter the filter cake and start replacing the liquid.

Darcy's basic filtration equation describing the flow rate u of a filtrate with a viscosity μ through a porous medium can be described as

$$u = \frac{-k}{\mu}\frac{dp}{dz}, \tag{2.1}$$

where dp is the dynamic pressure difference across the thickness dz of a porous medium of the permeability k (Tarleton and Wakeman, 2005).

Irreducible saturation is the minimum moisture content at which the flow of the liquid from the void space of a filter cake ceases at any pressure. From Eq. (2.1) it can be concluded that by increasing the pressure difference over the filter cake the flow rate of the filtrate increases, thus decreasing the time required to achieve a certain moisture content or, on the other hand, a lower moisture content is achieved in the same amount of time (Svarovsky, 2000; Tarleton and Wakeman, 2005).

According to the conventional filtration theory, the average specific cake resistance α_{av} is calculated using experimental data and the integrated, reciprocal form of the Darcy equation presented in Eq. (2.2) (Svarovsky, 2000). A more thorough discussion along with calculation examples concerning the presented filtration equations can be found in the literature, for example in (Svarovsky, 2000; Tien, 2012; Ripperger et al., 2013). The integrated, reciprocal form of the Darcy equation, the general filtration equation for constant pressure operation is given by

$$\frac{t}{V_\mathrm{f}} = \frac{\alpha_\mathrm{av}\mu c}{2A^2\Delta p} V_\mathrm{f} + \frac{\mu R_\mathrm{m}}{A\Delta p}, \tag{2.2}$$

where t is time, V_f is the volume of the filtrate, μ is the dynamic viscosity of the filtrate, c is the filtration concentration, A is the filtration area, Δp is the applied pressure difference, and R_m is the resistance of the filter medium. Solving Eq. (2.2) with respect to α_av, denoting the experimentally determined slope t/V^2 by a, and omitting the resistance of the filter medium yields

$$\alpha_\mathrm{av} = \frac{2aA^2\Delta p}{\mu c}. \tag{2.3}$$

The average porosity of the filter cake ε_av is obtained by the cake dimensions and the void volume of the cake:

$$\varepsilon_\mathrm{av} = \frac{V_\mathrm{v}}{V_\mathrm{c}} = 1 - \frac{m_\mathrm{s}}{\rho_\mathrm{s} AL}, \tag{2.4}$$

where V_v is the void volume ($V_\mathrm{v} = V_\mathrm{c} - V_\mathrm{s}$), V_c is the cake volume, V_s used in the calculation of V_v is the volume of suspended solids in the cake, m_s is the mass of solids, ρ_s is the density of solids, and L is the height of the cake.

Equation (2.4) can be written for a horizontal belt filter as

$$\varepsilon_\mathrm{av} = 1 - \frac{s q_\mathrm{m,sl}}{\rho_\mathrm{s} h_\mathrm{B} v_\mathrm{B} L}, \tag{2.5}$$

where s is the mass fraction of solids in the slurry, $q_\mathrm{m,sl}$ is the feed rate of the slurry in kg/s, ρ_s is the density of solids, h_B is the filter belt width, and v_B is the filter belt linear velocity.

In addition to the properties calculated by Eqs. (2.2)–(2.5), the mathematical dewatering models derived from the conventional or classical filtration theory entail the irreducible saturation and threshold pressure of the filter cake (Condie et al., 2000). Moreover, the underlying assumption of the conventional theory is that the specific cake resistance and the porosity are functions of applied pressure only. In reality, the porosity and the specific resistance of compressible cakes depend on time (creep effect) and solids concentration (rate of cake formation) (Rushton, Hosseini, and Hassan, 1978; Svarovsky, 2000).

2.2 Cake dewatering

The pressure difference applied over the slurry and the filter medium produces a two-phase flow of fluid through rigid porous media (Concha A., 2014). Cake dewatering is done by displacing filtrate (water in this study) in the cake by an immiscible fluid (air in this case). The structure of a filter cake can be considered, in general, as a matrix of solid particles in a liquid and gas mixture.

In case the liquid in the void space of the filter cake is water, the saturation S of the cake is defined as

$$S = \frac{V_{\mathrm{w}}}{V_{\mathrm{v}}}, \tag{2.6}$$

where V_{w} is the volume of water in the cake, which is measured experimentally by evaporating all the pore water off the cake.

In order to understand the reduction of cake saturation by vacuum filtration, the capillary forces affecting in the filter cake bed have to be considered. Surface forces affect at the interface of the two flowing fluids in contact with each other and with the solids of the cake. The surface tension force acts at the interface between the liquid and the solid and retains liquid in the finer pores of the filter cake (Tarleton and Wakeman, 2005).

The two immiscible fluids flowing through the media form unique pathways, which take new routes as the fluid saturation of the filter cake decreases in the course of dewatering. While the liquid saturation is reduced, the liquid pathways become discontinuous, the flow of the wetting fluid stops, and the cake reaches the state of irreducible wetting fluid saturation (Tarleton and Wakeman, 2005).

Reduced saturation S_{R} is defined as:

$$S_{\mathrm{R}} = \frac{S - S_{\infty}}{1 - S_{\infty}}, \tag{2.7}$$

where S_{∞} is the irreducible saturation at which state the flow of the liquid ceases.

Cake solid content s' (mass solid/mass liquid) is calculated by

$$s' = \frac{1 - \varepsilon_{\mathrm{av}}}{S\varepsilon_{\mathrm{av}}} \frac{\rho_{\mathrm{s}}}{\rho_{\mathrm{l}}}, \tag{2.8}$$

where ρ_{l} is the density of liquid.

The cake solid content *s* referred to in this dissertation has the units (mass solid/(mass of liquid + mass of solid)) and can be expressed by

$$s = \frac{s'}{1 + s'}. \tag{2.9}$$

2.3 Power demand in vacuum filtration

For vacuum filtration processes, the desired pressure difference across the filter cake and the medium is often generated by a vacuum pump. By operating a vacuum pump, it evacuates a certain volume of gas from its chamber at each rotation. The volume flow rate $q_{V,in}$ of a pump is described in inlet conditions and expressed by the equation

$$q_{V,in} = \frac{dV}{dt}, \tag{2.10}$$

where *V* is the volume of gas. As the densities of gases vary as a function of pressure and temperature, the actual quantity of gas can be described by the mass flow rate or the standard volumetric flow rate. Assuming the Ideal Gas Law, the standard volumetric flow rate *Q* corresponding to flow in standard conditions can be described by the equation

$$Q = \frac{T_{std}}{T_{in}} \frac{p_{in}}{p_{std}} q_{V,in}, \tag{2.11}$$

where T_{in} is the temperature in the vacuum pump inlet, and T_{std} = 21.11 °C and p_{std} = 101.3 kPa are the standard temperature and pressure, respectively.

In isothermal compression, the temperature of the compressed gas remains constant. Isothermal compression is typically a suitable assumption for cooled compression liquid-ring vacuum pumps (Bannwarth and Ahner, 2005). The isothermal power demand P_T can be calculated using the equation

$$P_T = q_{V,in} p_{in} \ln\left(\frac{p_{out}}{p_{in}}\right). \tag{2.12}$$

Isentropic compression can be assumed for vacuum pumps in certain cases (Silla, 2003). The ideal isentropic power demand P_S for a given inlet volumetric flow rate $q_{V,in}$ generated by the vacuum pump can be calculated by the equation

$$P_{\mathrm{S}} = \frac{k}{k-1} q_{\mathrm{V,in}} p_{\mathrm{in}} \left[\left(\frac{p_{\mathrm{out}}}{p_{\mathrm{in}}} \right)^{\frac{k-1}{k}} - 1 \right], \tag{2.13}$$

where p_{in} is the pressure at the inlet of the vacuum pump, p_{out} is the outlet pressure of the vacuum pump, and k is the isentropic exponent.

2.4 Heat demand in thermal drying

If further drying of the dewatering product is required, thermal drying is an option. With this method, the remaining moisture is removed from the cake by evaporation. The ideal heat required for reaching a desired solid content can be described by the equation

$$\begin{aligned} Q_{\mathrm{v}} &= \frac{1}{\eta_{\mathrm{th}}} \left(q_{\mathrm{m,v}} \Delta H_{\mathrm{w}} + q_{\mathrm{m,s}} \Delta H_{\mathrm{s}} \right) \\ &= \frac{1}{\eta_{\mathrm{th}}} \left(q_{\mathrm{m,s}} \left(\left(\frac{1}{s_{\mathrm{in}}} - \frac{1}{s_{\mathrm{out}}} \right) \Delta H_{\mathrm{w}} + \Delta H_{\mathrm{s}} \right) \right), \end{aligned} \tag{2.14}$$

where η_{th} is the efficiency of thermal drying, q_{m} is the mass flow, ΔH_{w} is the heat demand of warming and evaporating the water, ΔH_{s} is the heat demand for warming the solids, and s is the weight-based solid content of the cake (Kemp, 2012). The subscript v denotes vapour and s solids. For ideal energy consumption, it is assumed that all the supplied energy is consumed by the heating of the liquid and solids and by evaporation of liquid removed from the cake. In the case of removing water, this includes the energy required for heating up the water and solids from their initial temperature to 100 °C and for evaporation. The heat demand for water is calculated by

$$\Delta H_{\mathrm{w}} = \Delta T \mathrm{c}_{\mathrm{w}} + \Delta \mathrm{H}_{\mathrm{e}}, \tag{2.15}$$

where ΔT is the temperature increase from the initial temperature after dewatering to 100 °C, $\mathrm{c_w}$ is the specific heat of water, and $\Delta \mathrm{H_e}$ is the latent heat of evaporation for water. The heat demand for the solids is calculated by

$$\Delta H_{\mathrm{s}} = \Delta T \mathrm{c}_{\mathrm{s}}, \tag{2.16}$$

where $\mathrm{c_s}$ is the specific heat of solids.

The rotary dryer is the most commonly encountered dryer in the mineral processing industry. The thermal efficiencies of rotary dryers typically range from 35 % to 70 % (Mujumdar, 2014). Other convection type dryers suitable for drying post-filter cake

dewatering are for instance flash, fluid bed, and tray dryers (Mujumdar, 2014). It is indicated that convective dryers tend to have a low thermal efficiency of often below 50 % (Kemp, 2012).

2.5 Büchner filter experiments

The Büchner filter setup and operating practice is described in Appendix A. Table 1 summarizes the most important characteristics of the filter cakes resulting from the Büchner filter experiments. As can be observed in Table 1, the experiments with the highest slurry loading of 700 g display a decreasing trend in the final thickness of the filter cakes versus the increasing pressure difference. The highest pressure difference level produced the driest cakes. The calculated average cake porosities ε_{av} ranged from 0.415 to 0.469. The increasing average specific cake resistances α_{av} with the increased filtration pressure imply that the filter cakes were slightly compressible.

Table 1. Variables, separation time, and properties of filter cakes. From Publication I.

Test	**Δp** (bar)	**m_{sl}** (g)	**t_{sep}** (s)	**L** (mm)	**s** (% w/w)	**ε_{av}** (-)	**α_{av} ($\cdot 10^{10}$)** (m/kg)
1	0.4	300	27	6.1	76.1	0.469	1.02
2	0.4	500	56	9.7	79.3	0.435	0.94
3	0.4	700	113	14.5	79.9	0.444	0.96
4	0.6	300	19	5.5	77.4	0.418	1.20
5	0.6	500	43	9.8	80.8	0.445	1.01
6	0.6	700	85	13.9	84.0	0.445	0.99
7	0.8	300	15	5.8	79.7	0.437	1.26
8	0.8	500	40	10.9	84.3	0.469	1.16
9	0.8	700	70	13.2	85.5	0.415	0.99

2.5.1 Airflow through the filter cakes

To better compare the airflow through cakes with different masses, the standard volumetric flow rate relative to the solids mass of the cake m_s, i.e., specific airflow rate, is plotted against the corresponding solid content of the cake (Fig. 2).

Despite some variation in the airflow data caused by minor air leakages and irregularities in the filtrate flow, the following observations can be made on the basis of Fig. 2:

- The airflow rate decreases towards the end of the separation period at Δp = 0.4 and 0.6 bar (Fig. 2 a, b), and is almost constant when Δp = 0.8 bar is applied (Fig. 2 c).

- At the beginning of the dewatering period, the airflow rate remains relatively constant up to a certain point, after which the airflow through the cake increases dramatically (Fig. 2 b, c), unless Δp is low enough to prevent increased airflow (Fig. 2 a).
- Within the studied range of cake thicknesses (see Table 1), the thickest cakes are dewatered better than the thinnest ones, the maximum obtained solid content being 85.5 % w/w.

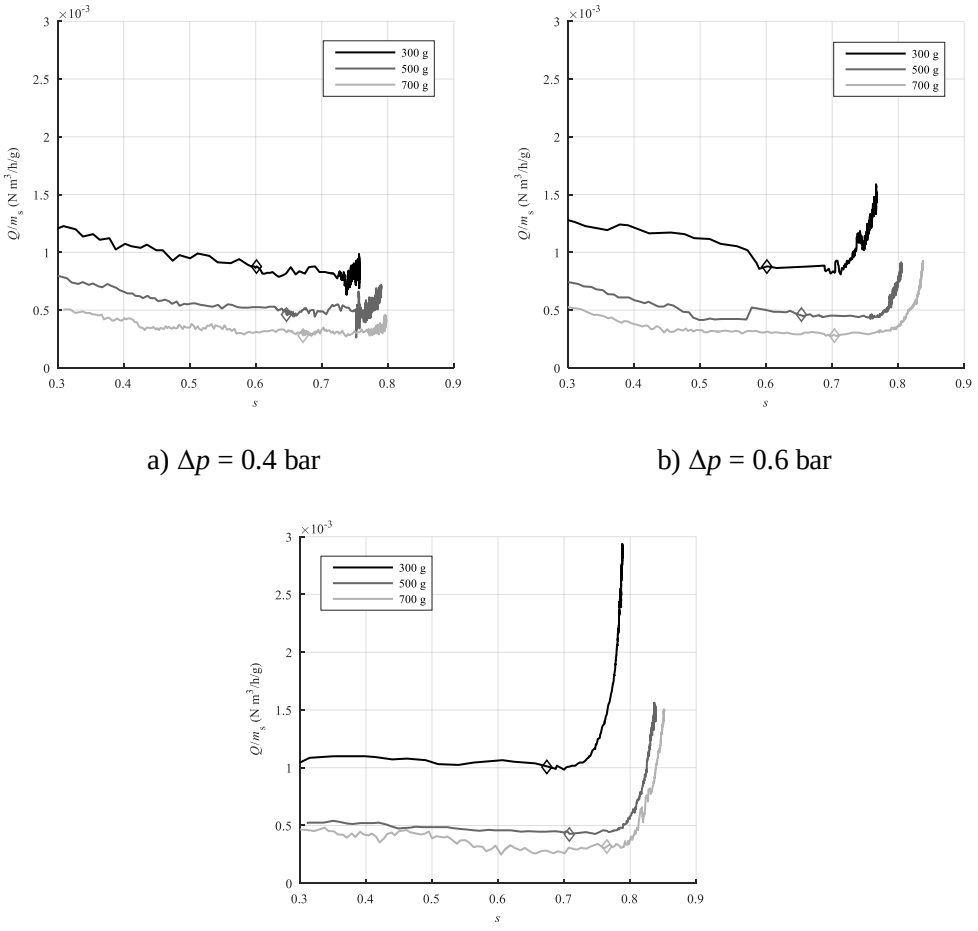

a) Δp = 0.4 bar b) Δp = 0.6 bar

c) Δp = 0.8 bar

Fig. 2. Specific airflow rate as a function of solid content. The diamond symbol indicates the start of the dewatering period. From Publication I.

As can be seen in Fig. 2, the highest solid contents are achieved with the highest slurry loading of 700 g and cake height for every pressure drop level. This is contrary to the expectation of a higher cake having a greater resistance to airflow, thus resulting in a lower airflow rate through the cake (Svarovsky, 2000). However, tiny leakage holes between the inner edge of the Büchner funnel and the filter cake were observed with thinner cakes, even though the pressure difference remained at a constant level. Airflow through the holes rather than through the pores of the cake could result in a higher moisture content at the end of the dewatering period (Tarleton and Wakeman, 2007). A further possible explanation for the more effective dewatering of the thickest cakes is the local variation in the cake thickness, which may cause uneven airflow through the thin cakes. According to (Wakeman, 1998), thicker cakes are washed more effectively than thinner ones and suggested an increased chance of channelling through the thinner cakes as the probable explanation for this.

2.5.2 Specific energy consumption of cake dewatering

Fig. 3 depicts the cumulative specific isentropic energy consumption E_s/m_s of cake filtration and dewatering as a function of solid content. For each experiment there is a certain level for the solid content beyond which the effectiveness of dewatering decreases rapidly and the specific energy consumption increases radically. According to (Rushton, Ward, and Holdich, 1996), the most economical means to filter a cake is to use the lowest possible pressure difference to overcome the capillary retention forces, which may very well be the case with an ideal incompressible cake. However, air leaks and an uneven fluid flow distribution across the filter cake area have to be taken into account. As the air leaks remained nearly constant for each slurry loading level independent of the pressure difference, the leaks account for a major proportion of airflow in low pressure difference tests. Thus, a lower pressure difference does not seem to lead to a lower specific energy consumption compared with higher pressure difference tests. With a lower pressure difference, the cake filtration and dewatering times required to achieve a given solid content are longer compared with the higher pressure difference tests, and therefore, more energy is consumed with the same leak flow rate.

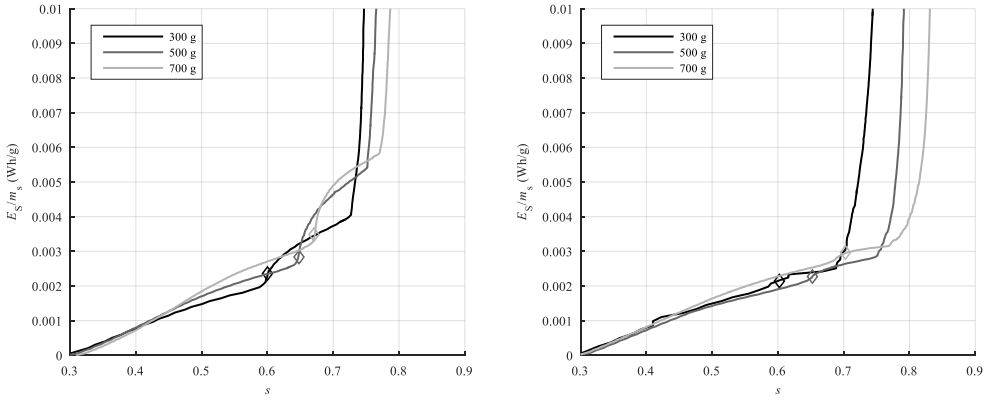

a) Δp = 0.4 bar b) Δp = 0.6 bar

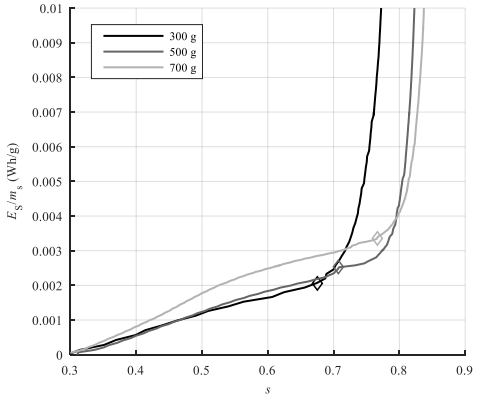

c) Δp = 0.8 bar

Fig. 3. Cumulative specific isentropic energy consumption as a function of solid content. The diamond symbol indicates the start of the dewatering period. From Publication I.

2.6 Pilot-scale horizontal belt filter experiments

The pilot-scale horizontal belt vacuum filter setup and operating practice is described in Appendix B. The objective of the pilot-scale horizontal belt filter experiments was to investigate the effect of the main process variables of the filter on the air and energy consumption as well as on the properties of the filter cake. In preparation for the pilot-scale study, experiments with a Büchner apparatus were conducted to determine the specific cake resistance and porosity, for which the results are presented in Table 2.

The solid content of the slurry s_{sl} was constant 25 wt% in all experiments. Shrinking of the filter cake occurred at the beginning of the dewatering stage in the experiments with a 0.4 and 0.6 bar pressure difference. The initial shrinking of the filter cake decreases the average porosity of the cake during the dewatering stage. Because of this, the average porosity ε'_{av} and cake thickness L' were calculated for the moment of transition from the filtration stage to the dewatering stage by using the volume of solids and liquid in the cake at this instance, with the assumption that the cake was completely saturated. The value of ε'_{av} could be considered an initial value for calculating the average porosity for the duration of the dewatering stage. As can be seen in Table 2, the larger was the filtration pressure difference, the higher was the average specific cake resistance α_{av}, and hence, it can be concluded that the filter cakes were somewhat compressible. Comparing the values of α_{av} with the ones reported in (Holdich, 2003) indicates that they are typical for vacuum filtration of calcium carbonate.

Table 2. Büchner experiment variables, properties of the filter cakes, and filtration time. Slurry temperature T = 22 °C and ssl = 25 wt% in all experiments. From Publication III.

Test	**Δp** (bar)	**m_{sl}** (g)	**w** (kg/m2)	**t_f** (s)	**L** (mm)	**L'** (mm)	**ε_{av}** (-)	**ε'_{av}** (-)	**$\alpha_{av} \cdot 10^{10}$** (m/kg)
1	0.2	300	7.2	186	4.5	5.2	0.41	0.48	4.53
2	0.2	500	12.5	470	6.7	8.5	0.31	0.46	4.51
3	0.2	700	17.7	929	10.6	12.1	0.38	0.46	4.51
4	0.4	300	7.2	108	4.3	5.3	0.38	0.49	4.90
5	0.4	500	12.5	281	7.5	8.7	0.39	0.47	4.93
6	0.4	700	17.9	534	10.8	13.2	0.38	0.50	5.04
7	0.6	300	7.3	78	4.6	7.2	0.41	0.63	4.04
8	0.6	500	12.7	205	7.8	9.3	0.40	0.49	4.99
9	0.6	700	17.8	387	10.8	13.1	0.39	0.50	5.14

Results of the experiments with the pilot-scale horizontal belt filter and the liquid ring vacuum pump are presented in Table 3. The manipulated process variables are the pressure difference Δp and the mass of solids deposited per filtration area w, which was controlled by adjusting the filter belt speed v_{belt} and the slurry infeed rate. The resulting filtration time t_f and distance z_f, dewatering time t_d and distance z_d, cake thickness L, average porosity ε_{av}, throughput of the cake solids M_s, and moisture content M corresponding to the operating point of the experiment are presented. The average porosity was calculated by using the online cake thickness measurement at the end of the dewatering stage.

As can be expected, the results show that a lower moisture content and average porosity of the filter cake is obtained when the pressure difference is increased. It can also be noted that the moisture content and the average porosity vary depending on the mass of solids deposited per filtration area w, the dewatering time, and the distance. The lowest moisture

content along with the lowest average porosity of the filter cake for each pressure difference level is achieved when the dewatering time is the longest. Comparing Tests 6 and 8 within the same pressure difference level, and similarly Test 9 and 12, for which the dewatering time is nearly or exactly the same, it can be observed that a larger slurry loading, i.e., a thicker cake, produces a drier cake. Evaluating the experiments within the same pressure difference levels of 0.3 and 0.4 bar with the slurry loadings of 4.2 to 5.4 and 12.2 kg/m^2, a drier cake is obtained with the thicker filter cake, while the decreasing dewatering time and distance would predict the contrary. This would suggest that an optimum value for the mass of solids deposited per filtration area could be found when seeking for the best dewatering performance. A similar observation was made with another slurry in Publication I. We could suppose that the reason for the worse dewatering performance for the thinnest cakes results from an uneven airflow through the cake, which, in turn, could be due to the lack of the necessary capillary structure in such thin cakes. It is pointed out that the experiments with the solids loading w of 9.5 kg/m^2 that also have the longest dewatering times result in the lowest moisture content.

Table 3. Pilot experiments with a horizontal vacuum belt filter and a liquid ring vacuum pump. Slurry temperature T = 24 °C and s = 26 wt% in all experiments. From Publication III.

Test	Δp (bar)	w (kg/m^2)	v_{belt} (cm/s)	t_f (s)	z_f (cm)	t_d (s)	z_d (cm)	L (mm)	ε_{av} (-)	M_s (g/s)	M (wt%)
1	0.2	4.2	1.1	105	115	77	85	2.5	0.38	4.6	20.3
2	0.2	5.4	1.1	157	173	25	27	3.6	0.44	6.0	20.2
3	0.2	9.5	0.5	293	143	117	57	5.0	0.30	4.6	18.9
4	0.2	12.2	0.5	409	200	0	0	7.2	0.37	6.0	24.6
5	0.3	4.2	1.1	75	83	106	117	2.3	0.32	4.6	19.3
6	0.3	5.4	1.1	114	125	68	75	3.5	0.43	6.0	18.4
7	0.3	9.5	0.5	215	105	194	95	5.0	0.30	4.6	17.6
8	0.3	12.2	0.5	348	170	61	30	6.9	0.35	6.0	18.0
9	0.4	4.2	1.1	59	65	123	135	2.3	0.32	4.6	17.9
10	0.4	5.4	1.1	86	95	95	105	3.4	0.41	6.0	17.0
11	0.4	9.5	0.5	164	80	246	120	4.9	0.28	4.6	17.0
12	0.4	12.2	0.5	286	140	123	60	6.9	0.35	6.0	17.3

Results of the pilot-scale filter experiments with a claw vacuum pump are presented in Table 4. The results are similar to those with the claw vacuum pump; a thicker cake results in a smaller moisture content. For experiments with a pressure difference between 0.2 and 0.4 bar and the longest dewatering times with the slurry loading of 10.3 kg/m^2 result in the smallest moisture content after dewatering. The solid content of the slurry in the claw pump experiments is slightly higher than in the liquid-ring pump experiments. This could be the reason for the higher average porosity values compared with the liquid-ring experiments. An increased solid content generally results in a faster cake formation and a higher porosity.

Table 4. Pilot experiments with a horizontal vacuum belt filter and a claw vacuum pump. Slurry temperature T = 22 °C and s = 28 wt% in all experiments. From Publication III.

Test	Δp (bar)	w (kg/m^2)	v_{belt} (cm/s)	t_f (s)	z_f (cm)	t_d (s)	z_d (cm)	L (mm)	ε_{av} (-)	M_s (g/s)	M (wt%)
1	0.2	4.6	1.1	105	115	77	85	3.3	0.48	5.0	19.4
2	0.2	5.9	1.1	164	180	18	20	4.2	0.48	6.5	19.5
3	0.2	10.3	0.5	276	135	133	65	6.3	0.39	5.0	17.9
4	0.2	13.3	0.5	409	200	0	0	8.1	0.39	6.5	22.7
5	0.3	4.6	1.1	77	85	105	115	3.2	0.47	5.0	18.1
6	0.3	5.9	1.1	118	130	64	70	4.0	0.45	6.5	17.8
7	0.3	10.3	0.5	225	110	184	90	6.1	0.37	5.0	16.9
8	0.3	13.3	0.5	358	175	61	25	7.7	0.36	6.5	17.6
9	0.4	4.6	1.1	59	65	123	135	3.1	0.45	5.0	17.0
10	0.4	5.9	1.1	100	110	77	90	3.9	0.44	6.5	16.7
11	0.4	10.3	0.5	184	90	225	110	5.8	0.34	5.0	16.4
12	0.4	13.3	0.5	286	140	123	60	7.6	0.35	6.5	16.6
13	0.5	4.6	1.1	55	60	127	140	2.9	0.41	5.0	16.4
14	0.5	13.3	0.5	235	115	174	85	7.3	0.33	6.5	16.3
15	0.6	4.6	1.1	50	55	132	145	2.8	0.39	5.0	15.4
16	0.6	13.3	0.5	215	105	194	95	7.2	0.32	6.5	16.0

2.6.1 Airflow rates for the horizontal belt vacuum filter experiments

Standard volumetric airflow rates calculated using the airflow velocity measurements of the horizontal belt vacuum filter experiments are presented in Table 5. In order to estimate the airflow through the filter cake dewatering region, a method to determine the leak flow of the filter was developed. According to the method, a series of test runs were conducted with a 100 % saturated filter cake over the whole area affected by the pressure difference. Assuming that the fluid flow through the fully saturated filter cake is low enough to be ignored, the airflow through the vacuum pump can be considered to arise from the vacuum system leaks. Linear correlation between the pressure difference and the leak flow was observed with a root-mean-squared error of 0.414, R^2 = 0.998, and a p-value of $3.1 \cdot 10^{-5}$. The total airflow for Test 4 with a fully saturated filter cake in both test series serves as a reference point in determining the leak flow for the series.

Table 5. Measured standard volumetric airflow rates for the total flow through the vacuum pump, the estimated volumetric airflow rate, and the air flux through the filter cake in the dewatering area calculated on the basis of leak flow estimates. From Publication III.

Liquid ring vacuum pump experiments						Claw vacuum pump experiments					
Test	Δp (bar)	w (kg/m^2)	$Q_{a,\,total}$ (m^3/h)	$Q_{a,\,cake}$ (m^3/h)	$u_{a,\,cake}$ (m^3/h·m^2)	**Test**	Δp (bar)	w (kg/m^2)	$Q_{a,\,total}$ (m^3/h)	$Q_{a,\,cake}$ (m^3/h)	$u_{a,\,cake}$ (m^3/h·m^2)
1	0.2	4.2	35.0	2.0	23.7	**1**	0.2	4.6	31.5	3.5	41.3
2	0.2	5.4	33.5	0.5	19.0	**2**	0.2	5.9	29.2	1.2	60.6
3	0.2	9.5	36.0	3.0	52.8	**3**	0.2	10.3	33.7	5.7	87.9
4	0.2	12.2	33.0	0.0	-	**4**	0.2	13.3	28.0	0.0	-
5	0.3	4.2	45.0	4.9	42.1	**5**	0.3	4.6	41.0	5.9	51.5
6	0.3	5.4	43.0	2.9	39.0	**6**	0.3	5.9	40.0	4.9	70.3
7	0.3	9.5	49.0	8.9	93.9	**7**	0.3	10.3	45.5	10.4	115.8
8	0.3	12.2	43.5	3.4	114.1	**8**	0.3	13.3	38.8	3.7	124.1
9	0.4	4.2	53.0	5.8	43.2	**9**	0.4	4.6	49.0	6.8	50.6
10	0.4	5.4	55.0	7.8	74.6	**10**	0.4	5.9	48.5	6.3	74.5
11	0.4	9.5	63.0	15.8	132.0	**11**	0.4	10.3	55.5	13.3	121.2
12	0.4	12.2	57.0	9.8	163.9	**12**	0.4	13.3	50.0	7.8	130.6
						13	0.5	4.6	56.0	6.7	48.2
						14	0.5	13.3	58.0	8.7	102.9
						15	0.6	4.6	66.0	9.7	66.6
						16	0.6	13.3	65.0	8.7	91.1

2.6.2 Specific energy consumption of vacuum filtration

The total specific energy consumption $E_s = E/m_s$ to a zero moisture content is illustrated in Figs. 4–6. The proportioned energy consumptions of vacuum filtration and thermal drying are presented. Fig. 4 depicts the total ideal specific energy consumption results of the claw pump experiments calculated using the airflow measurements and the isentropic power demand by Eq. (2.13) and thermal drying to the zero moisture content with a thermal efficiency η_{th} of 100 % by Eq. (2.14) neglecting the heat demand of the solids. Test 3 resulted in the minimum total ideal energy consumption with Tests 6, 7, and 8 close to the minimum. With the pressure difference and the belt speed kept at constant settings while increasing the mass of solids deposited per filtration area (comparing Test pairs 1 and 2, 3 and 4, 5 and 6, 7 and 8, 9 and 10, 11 and 12, see Table 4) decreases the ideal specific energy consumption in the vacuum filtration stage. For the dewatered cakes, the total ideal energy consumption to zero moisture is also decreased. For Test 4, the energy consumption of thermal drying is increased as the filter cake has not been sufficiently dewatered by vacuum filtration. Considering the above-mentioned test pairs, ensuring a reasonable dewatering distance z_d while increasing the mass of solids deposited per filtration area seems to decrease the specific energy consumption of vacuum filtration as well as the total specific energy consumption including the subsequent thermal drying.

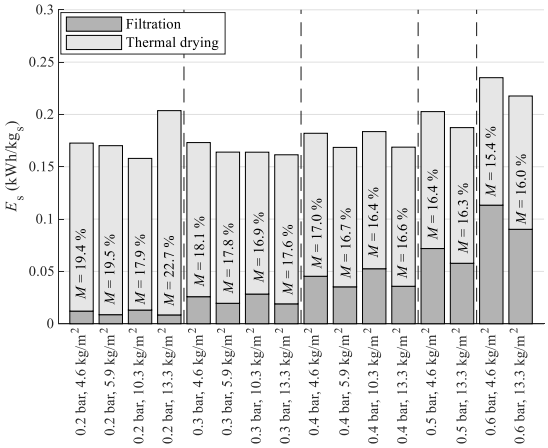

Fig. 4. Ideal specific energy consumption for achieving zero moisture content (M = 0 %) distinguishing between vacuum filtration and thermal drying (thermal efficiency η_{th} = 100 %). The moisture content after vacuum filtration is shown for each experiment. From Publication III.

The total specific energy consumption to zero moisture with a liquid ring vacuum pump and thermal drying is presented in Fig. 5. The results of the claw vacuum pump experiments are illustrated in Fig. 6, respectively. The power consumption data provided by the variable-speed drive served as the basis for calculation of the energy consumption of filtration. A thermal efficiency η_{th} of 50 % was assumed for thermal drying calculations based on the heat efficiency of a spin-flash dryer reported in (Kudra et al., 1989). The minimum specific energy consumption to achieve the zero moisture content with the liquid-ring pump was attained in Test 3 with a 0.2 bar pressure difference and 9.5 kg of solids deposited per filtration area, as can be seen in Fig. 5. Tests 2, 6, and 8 are close to the minimum specific energy consumption. Similarly to the ideal case presented in Fig. 4, when we compare Test pairs 1 and 2, 3 and 4, 5 and 6, 7 and 8, 9 and 10, 11 and 12 (see Table 3), where the pressure difference and the belt speed are fixed for the pairs and the mass of solids deposited per filtration area is increased, we can see that the specific energy consumption decreases in the vacuum filtration stage. With the exception of Test 4, also the total energy consumption to zero moisture is decreased. Similar observations about the effect of solids deposited per filtration area together with the requirement for a reasonable dewatering distance can be made from the liquid ring pump experiments as was made from the ideal specific energy consumption calculations presented in Fig. 4.

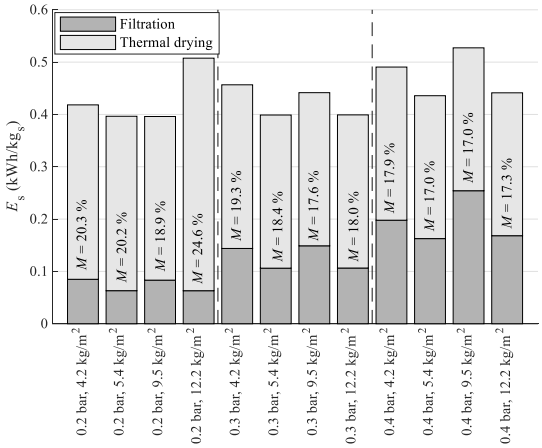

Fig. 5. Specific energy consumption for achieving a zero moisture content (M = 0 %) for liquid-ring vacuum pump experiments, distinguishing between vacuum filtration and thermal drying (thermal efficiency η_{th} = 50 %). The moisture content after vacuum filtration is shown for each experiment. From Publication III.

Similarly to the experiments with the liquid ring pump, the minimum specific energy consumption to achieve the zero moisture content with the claw pump was attained in Test 3 using a 0.2 bar pressure difference and 10.3 kg of solids deposited per filtration area, as depicted in Fig. 6. Results close to the minimum were also reached in Tests 6 and 8. As can be observed in Fig. 6, dewatering the filter cake to the lowest achievable moisture content by using a high pressure difference is not energy efficient. The highest specific energy consumption for the combined dewatering and drying process is due to the unfavourable combination of a low solids loading and a high pressure difference. However, thermal drying of overly wet filter cakes should be avoided when aiming at a low total energy consumption. The claw vacuum pump experiments are analogous to the liquid ring pump experiments considering that keeping the pressure difference and the belt speed fixed and increasing the mass of solids deposited per filtration area (comparing Test pairs 1 and 2, 3 and 4, 5 and 6, 7 and 8, 9 and 10, 11 and 12, see Table 4) reduces the specific energy consumption in the vacuum filtration stage. Correspondingly, with the exception of Test 4, the total specific energy consumption to zero moisture is decreased. Again, similar observations about the favourable effect of increasing the amount of solids deposited per filtration area to the energy consumption can be made from the claw pump results as was made from the ideal specific energy consumption (Fig. 4) and the liquid ring results (Fig. 5). The requirement for a reasonable dewatering distance naturally holds. The specific energy consumption of vacuum filtration using the claw vacuum pump is approximately half of that of the liquid ring pump operated at the same pressure difference, which is mainly due to the higher efficiency of the claw pump.

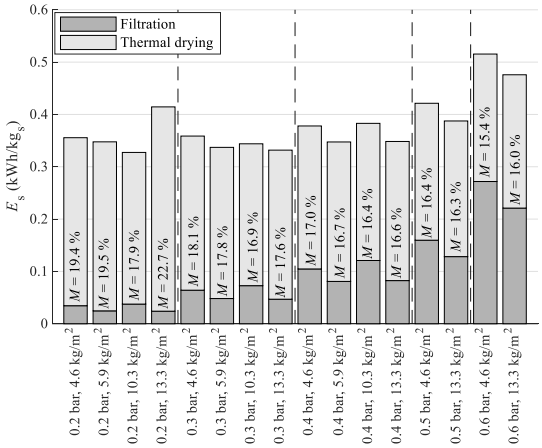

Fig. 6. Specific energy consumption for achieving a zero moisture content (M = 0 %) for claw vacuum pump experiments, distinguishing between vacuum filtration and thermal drying (thermal efficiency η_{th} = 50 %). The moisture content after vacuum filtration is shown for each experiment. From Publication III.

2.7 Summary

Evaluating the specific energy consumption of vacuum filtration as a function of the solid content of the filter cake rather than as a function of time revealed exponential growth after reaching a certain level of cake solid content. The cumulative specific energy consumption with respect to the solid content of the cake clearly illustrates the intensive energy requirement of the cake dewatering stage compared with the filtration stage. To prevent excessive energy consumption during the dewatering stage, the end of dewatering has to be properly timed to avoid the futile effort of pumping air through the cake to obtain a negligible moisture reduction.

According to the pilot-scale experiments, when using a combination of vacuum filtration and thermal drying to reach a moisture level of zero percent, the proportion of energy consumed by vacuum filtration varies between 7 and 53 percent of the total specific energy consumption. The proportion mostly depends on the applied pressure difference, but also on the slurry solid content and loading as well as on the filter belt speed. The smallest total specific energy consumptions for the experiment series are achieved with the pressure difference levels of 0.2 and 0.3 bar. The standard volumetric leak flow of the vacuum system of the filter increases linearly as a function of applied pressure difference. Considering the experiments carried out in this part of the study, the specific energy consumption of vacuum filtration would seem to have a tendency to increase exponentially as the pressure difference increases. Applying the exponential growth formula $E_S(\Delta p) = \mathrm{a} \times \mathrm{e}^{\mathrm{k}\Delta p}$ to the mean specific energy consumption of the claw pump experiments of each pressure difference level ranging from 0.2 to 0.6 bar yields a growth rate of k = 4.9. For these experiments, increasing the pressure difference in order to

achieve a decreased moisture content after vacuum filtration increases the total specific energy consumption including thermal drying to the extent that the process ends up above the optimal range when the applied pressure difference is 0.4 bar or greater.

Although liquid ring vacuum pumps have traditionally been used in filtration because of their availability for large pumping capacities and their ability to handle condensable vapours, their energy efficiency is significantly lower compared with dry pumps. The capacities of liquid ring pumps range to over 37 000 m^3/h, whereas the capacities of dry pumps range only up to 2400 m^3/h (Ryans and Croll, 1981). Although coating options available for dry pumps such as the claw vacuum pump used in this study make the pumps more tolerant to water vapour, the pumping capacity requirements for vacuum filtration are often very high as a result of the combination of leak flow and flow through the cake. As an example, a vacuum pump with a pumping capacity of 7000 m^3/h was used for a 94 m^2 filter area to reach a 0.45 bar pressure difference (Ryans and Bays, 2001). The use of several dry pumps in parallel could be an option to replace the higher capacity liquid ring pumps.

Controlling the pressure difference level with a variable-speed-drive-operated vacuum pump could save energy compared with the traditional bypass valve control. By controlling the slurry infeed, the filter belt speed, and the pressure difference level by means of variable-speed drives would enable the control of the moisture content of the filter cake, and the energy consumption of vacuum filtration could be minimized.

Condition monitoring of the filter vacuum system and estimation of the flow through the filter cake is made possible by the developed leak flow identification method. The ratio of the estimated leak flow and the flow through the filter cake could serve as a metric for the efficiency of the filter.

3 Estimation of filter cake moisture content

In this chapter, the focus is on the estimation of the moisture content of the filter cake after dewatering. First, the thermodynamic aspects of vacuum dewatering are addressed. Then, energy consumption in the dewatering and thermal drying process is discussed, and finally, prediction of the moisture content of filter cakes by applying machine learning regression models is considered. The chapter concludes by a summary of results.

3.1 Thermodynamic background of vacuum dewatering

Regarding the thermodynamic effects of airflow through a filter cake with a partially water-saturated void space, the evaporation of water has to be considered. Fig. 7 describes the heat transfer inside a filter cake caused by evaporation. The difference in vapour pressures at the saturation and interface temperatures acts as the driving force for evaporation of water inside the pores of the filter cake. If the air flowing through the filter cake ($\dot{m}_a$) is unsaturated, there is a difference in vapour pressures and part of the water will evaporate ($\dot{m}_w$). The sensible heat of the water will provide the latent heat (Q_e) for this change of state. At the same time, the water is slightly cooled ($T_w^1 > T_w^2$), the flow of sensible heat from the airflow and the cake solids to the water delivers the latent heat to evaporate a portion of it, and a thermal balance is pursued (Hundy, Trott, and Welch, 2016).

During the dewatering stage, water is both mechanically removed and evaporated from the filter cake by suction and thereby also extracted in the air evacuated by the vacuum pump and as a gas. In this stage, as a filter cake section travels on the vacuum filter belt, its saturation decreases, and consequently, the airflow through the cake increases. The rates of heat transfer between the liquid and gas phases are determined by the properties of the volatile fluid, the dimensions of the interface, and the velocities of flow (Hundy, Trott, and Welch, 2016). Along the whole thickness of the filter cake, heat (Q) is transferred between the liquid water, the cake solids, and the air flowing through. Resulting from this process, the filter cake and the air that has passed through the filter cake to the vacuum box are at a lower temperature than the air entering the filter cake ($T_a^1 > T_a^2$). A more detailed explanation of the governing equations for flow and transport in porous media can be found in (Das, Mukherjee, and Muralidhar, 2018).

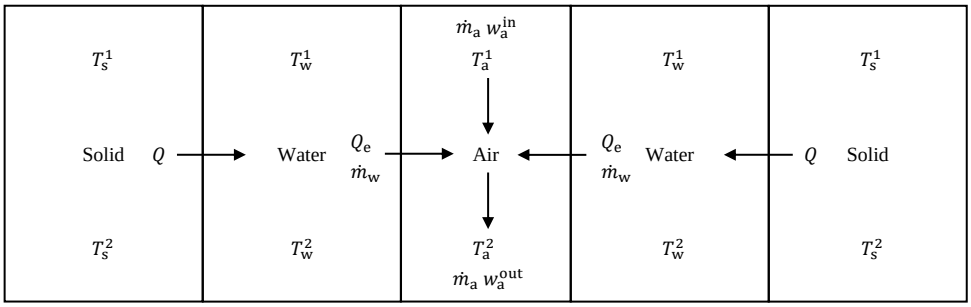

Fig. 7. Diagram of the heat transfer inside the filter cake caused by evaporation. The latent heat Q_e required for evaporation of water will be drawn from the sensible heat of the water. The sensible heat is transferred from the cake solids to the cooled water. In this case $T_x^1 > T_x^2$ and $w_a^{in} < w_a^{out}$. From Publication IV.

The mass of evaporated water is proportional to the mass flow of air through a filter cake and to the change in the specific humidity of the exiting and entering air

$$\dot{m}_w = \dot{m}_a\left(w_a^{out} - w_a^{in}\right), \tag{3.1}$$

where $\dot{m}$ is the mass flow, the subscripts w and a denote water and air, and w_a is the specific humidity of air (Kovačević and Sourbron, 2017). Furthermore, in an air water vapour mixture, the mass transfer rate is proportional to the rate of heat transfer at the interface (Hundy, Trott, and Welch, 2016).

To investigate how the thermodynamics of vacuum filtration is manifested on the surface of the filter cake, temperature measurements on the longitudinal centre line of the filter cake in the dewatering region were conducted, and the minimum, mean, and maximum values for each pressure difference level are depicted in Fig. 8.

For these experiments, the slurry solid content was kept unchanged, only adjusting the slurry infeed and filter belt speed to vary the slurry loading on the belt. As the mean surface temperature profiles depicted in Fig. 8 illustrate, evaporation of water during dewatering decreases the surface temperature of the cake towards the end of the dewatering stage. As can be seen, increasing the pressure difference over the filter cake increases the surface temperature change.

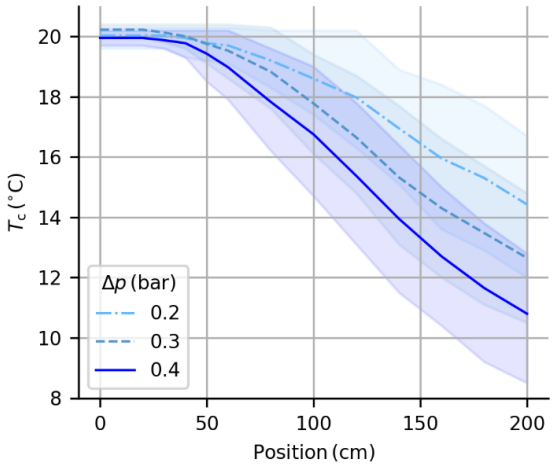

Fig. 8. Mean filter cake surface temperature T_c profiles along the filter belt (lines) and variation between the minimum and maximum temperatures resulting from varying slurry loadings (filled area) at the corresponding pressure difference levels. From Publication IV.

3.2 Energy consumption

In search of a low specific energy consumption for the combined dewatering and thermal drying process, a series of 80 filtration experiments were conducted by operating the pilot-scale horizontal belt filter in varied operating points. The summary statistics of the filtration experiments are presented in Table 6.

Table 6. Summary statistics of the settings for all the experiments. The symbols μ and σ denote mean and standard deviation. From Publication IV.

	Δp (bar)	s_{sl} (-)	ρ_{sl} (kg/m^3)	q_{sl} (kg/min)	M_s (g/s)	v_{belt} (mm/s)	w (kg/m^2)
μ	0.34	0.33	1259	1.1	5.8	6.6	9.7
σ	0.11	0.07	69	0.2	0.9	2.3	3.2
min	0.20	0.26	1192	0.6	4.4	5.0	4.4
25 %	0.30	0.28	1214	1.0	5.0	5.0	6.5
50 %	0.31	0.29	1221	1.1	5.8	5.0	10.1
75 %	0.40	0.39	1323	1.2	6.5	10.0	12.1
max	0.61	0.44	1384	1.5	7.4	10.0	14.7

The power demand estimates for vacuum filtration were calculated using Eqs. (2.12)–(2.13). The specific energy consumption of vacuum filtration, $E_S^f = E^f/m_s$ with respect to the filter cake solid content is depicted on the left in Fig. 9. As can be seen in the illustration, the specific energy requirement of filtration increases radically as the pressure difference is increased from 0.2 bar to 0.6 bar. Similar findings of the radically increasing specific energy consumption were also observed in Publication I. The increased pressure

difference and energy consumed provides a mere one percentage point (pp) increase in the cake solid content, at best, compared with the driest result with a 0.2 bar pressure difference.

The heat demand of thermal drying of the filtration product to zero moisture was calculated by Eqs. (2.14)–(2.16) and assuming thermal efficiency of η = 50 % based on the heat efficiency of a spin-flash dryer reported in (Kudra et al., 1989). For the calculations, it was assumed that the initial temperature of the moist solids is the same as the vacuum pump inlet air temperature. The majority of the energy consumed during thermal drying is due to evaporation of water, and a small proportion of energy consumption is due to heating up the dewatering product from its initial temperature. The total specific energy consumption to zero moisture, i.e., the sum of the specific energy consumption of vacuum filtration and the specific energy consumption of thermal drying, $E_S^{tot} = E_S^f + E_S^t$ with respect to the filter cake solid content after dewatering is presented on the right in Fig. 9. The experiments with the low specific energy consumption to zero moisture seem to accumulate around the solid content of 0.84. Therefore, it is important to track the filter cake solid content during filter operation in order to minimize the energy consumption. Fig. 9 shows that the total specific energy consumption for the majority of the experiments varies from 1000 to 1150 kJ/kg, and thus, the potential for energy conservation by adjusting slurry concentration, pressure difference, and cake deposited per unit area could be as high as 13 % in this case. The process variable settings along with the resulting key characteristics of the filtration experiments with the total specific energy consumption in the lowest 10 % are presented in Table 7.

Table 7. Filtration experiments with the total specific energy consumption in the lowest 10 %. For symbol definitions, see Nomenclature. From Publication IV.

s_{sl} (-)	ρ_{sl} (kg/m^3)	w (kg/m^2)	M_s (g/s)	Δp (bar)	L_c (mm)	z (cm)	t_f (s)	t_{dw} (s)	s (-)	ε_{av}	M (%)	E_S^{tot} (kJ/kg)
0.39	1323	10.4	5.2	0.20	5.1	130	259	160	0.838	0.27	16.2	1010
0.39	1323	11.7	5.9	0.30	5.7	125	249	170	0.845	0.27	15.5	1011
0.44	1384	7.4	7.4	0.20	4.2	100	100	110	0.835	0.36	16.5	1017
0.39	1323	10.4	5.2	0.30	5.0	105	209	209	0.846	0.24	15.4	1018
0.39	1323	9.1	4.6	0.20	4.4	105	209	209	0.839	0.25	16.1	1020
0.44	1384	14.7	7.4	0.30	7.6	115	229	190	0.840	0.31	16.0	1022
0.44	1384	7.4	7.4	0.30	3.9	85	85	125	0.841	0.31	15.9	1025
0.34	1270	12.1	6.1	0.30	5.8	120	239	180	0.842	0.25	15.8	1029

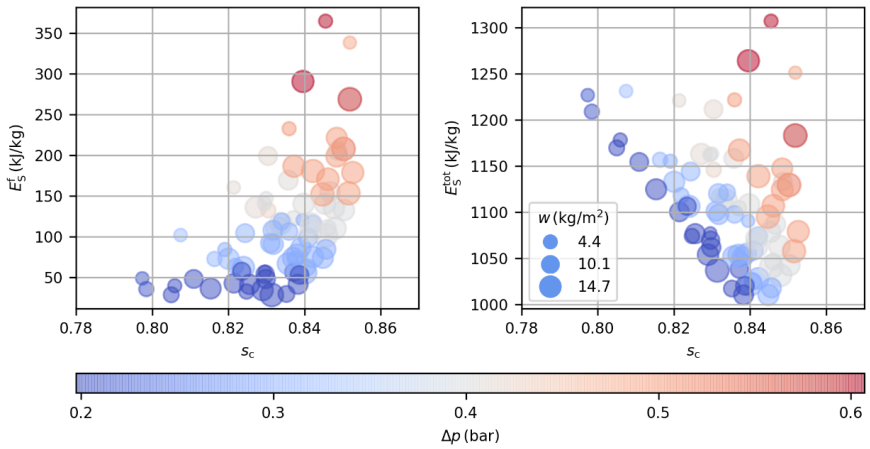

Fig. 9. Specific energy consumption of vacuum filtration E_S^f (left) and the total specific energy consumption to zero moisture E_S^{tot} (right) plotted against the filter cake solid content s_c. The size of the symbol is varied according to the mass of cake deposited per unit area w and the colour according to the pressure difference Δp. From Publication IV.

Within the range of variability in this study, the lowest 10 % of the total specific energy consumption to zero moisture was obtained with pressure differences of 0.2 and 0.3 bar in the vacuum filtration stage. All but one of these experiments resulted from tests having either the highest or the second highest level of the slurry solid content. The majority of the experiments within the lowest 10 % of the total specific energy consumption to zero moisture are from experiments with a slow filter belt speed and a high mass of cake deposited per unit area w. As can be seen in Table 7, the filter cake solid contents after vacuum filtration for all the experiments are between 0.835 and 0.846. The two experiments with the lowest energy consumption were achieved with the slurry solid content of 0.39 and with the highest ratio of filtration time to dewatering time, the second-row experiment having a greater mass of cake deposited per unit area and pressure difference compared with the first-row experiment. Furthermore, compared with the two experiments resulting in the lowest energy consumption, raising the slurry solid content to 0.44 and increasing the filter belt speed produces a thinner, higher porosity cake with only a 6 to 7 kJ/kg (0.6 % to 0.7 %) increase in the total specific energy consumption but a 25 % to 42 % increase in the solids throughput M_s.

3.3 Predicting moisture content of filter cakes using regression models

Mathematical models of processes that are designed to estimate process variables and are based on experimental data are called inferential models, virtual sensors, or soft sensors (Fortuna et al., 2007). Estimating difficult to measure quality variables of processes by soft sensor models that have been developed using data-driven methods has attracted increasing interest in recent years (Lin et al., 2007; Kadlec, Gabrys, and Strandt, 2009; Kadlec, Grbić, and Gabrys, 2011; Souza, Araújo, and Mendes, 2016; Bidar et al., 2017; Ge, 2017; Szymańska, 2018; Yao and Ge, 2018). Basic tools for constructing such models are many machine learning algorithms that have the ability to leverage easy to measure process variables for the purpose of predicting difficult to measure quality or key process variables (Ge et al., 2017). In the case of this study, a reliable soft sensor model for filter cake moisture content estimation could possibly render the use of special equipment that uses for instance x-rays or microwave radiation obsolete.

The aim of the study was to evaluate the applicability of standard machine learning algorithms to the estimation of filter cake moisture content using standard process measurements such as temperature, pressure, and flow as inputs. To this end, five standard algorithms were selected, namely regularized linear regression algorithms Lasso, Ridge, and Elastic-Net and two ensemble decision tree algorithms Random Forest and Gradient Boosting, which are capable of modelling non-linear relationships between variables. In order to avoid overfitting, regularized linear and ensemble decision tree algorithms were selected and trained with fivefold cross validation. The ratio of predictors per observations was kept equal or smaller than 9/80 for the same reason. The Scikit-Learn software package was used for model development.

Due to the limited number of observations, random division of data into 80 % for training and 20 % for testing was performed. Same training and test sets were used for all the algorithms and feature sets. By an exhaustive grid search, the following hyper parameters were explored. The strengths of penalty for the Lasso, Ridge, and Elastic-Net algorithms were 0.001, 0.005, 0.01, 0.05, 0.1, 0.5, 1, 5, and 10. Further, for the Elastic-Net algorithm, the L_1-ratios were 0.1, 0.3, 0.5, 0.7, and 0.9. The number of estimators explored by both decision tree algorithms were 10, 20, 40, 60, 80, 100, and 200. The maximum features settings used in the search for the Random Forest algorithm were auto, sqrt, and 0.33. For the Gradient Boosting algorithm, the explored learning rates were 0.05, 0.1, and 0.2, and the maximum depths 1, 3, and 5. Other settings were left to their default values. Pipelines with a standard scaler were used.

In addition to the direct process variable measurements, two interaction features were formulated to be used as inputs in modelling. The temperature difference ΔT_a between the vacuum pump suction air and the slurry feed as well as the product of the pressure difference and the dewatering time Δpt_{dw} were calculated.

In order to evaluate the linear association between the different process variables, the interaction features, and the filter cake solid content, the Pearson correlation coefficients

ρ between all the variables in the dataset were calculated; the corresponding correlation map is presented in Fig. 10. A strong linear relationship ($|\rho| \geq 0.60$) with the cake solid content is found for the variables of pressure difference Δp, air temperature at the vacuum pump inlet T_{vp}, dewatering time t_{dw}, airflow rate at the vacuum pump outlet Q_a, and interaction features ΔT_a and $\Delta p t_{dw}$. The other variables presented in the correlation map, namely the the mass of cake deposited per unit area w and the temperature of slurry T_{sl}, were also considered to have a relationship (although not a strong linear association) with the filter cake solid content and were therefore included in the analysis.

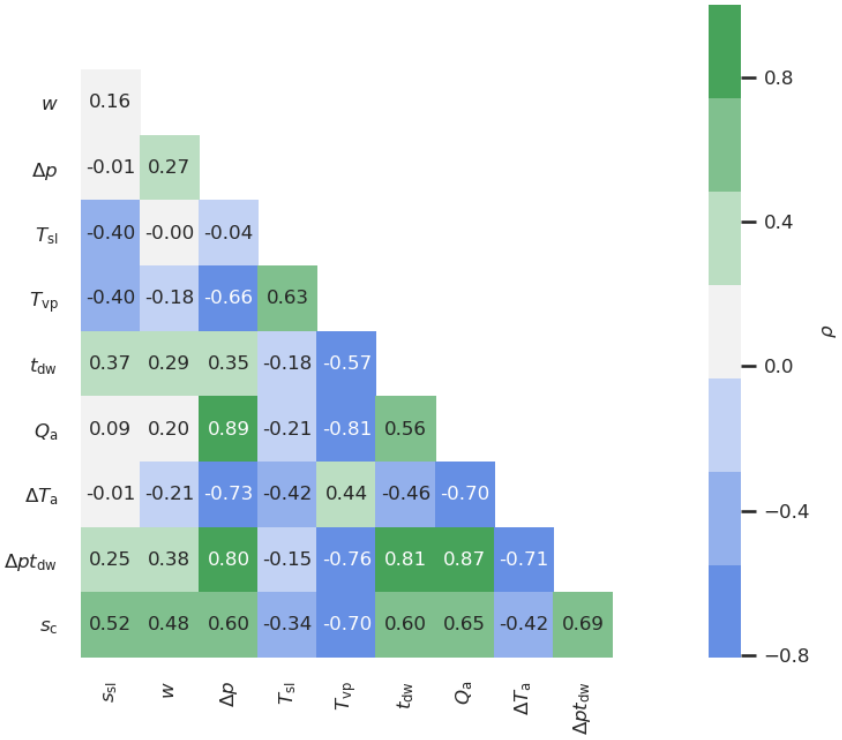

Fig. 10. Correlation map presenting the Pearson correlation coefficients ρ between the experiment settings, process variables, the two interaction features ΔT_a and $\Delta p t_{dw}$, and the filter cake solid content s_c. From Publication IV.

Nine feature sets with varied combinations of process variables were compiled (Table 8) to be used as inputs to the models in order to estimate the cake solid content s_c. For the first feature set, the variables Δp and w were selected. For the other sets, the number of features was increased and varied to see which features would benefit the modelling. As the features Δp and w were the controlled process variables in the experiments, they were

included in each feature set, in two of which Δp was included in the interaction feature Δpt_{dw} alone.

The performance metrics for each algorithm and feature set are presented in Fig. 11. As can be seen for Feature Sets 2 and 3, whether including the dewatering time or the vacuum pump inlet air temperature as an input, the majority of the results seem to favour the latter. This would suggest that the temperature of air inside the vacuum box would have a stronger association with the cake moisture content than the dewatering time also in the multivariable case together with slurry loading and pressure difference. Considering the results for Feature Sets 4 and 5, for the majority of the algorithms including the temperature and flow rate of air as inputs together with w and Δpt_{dw} produces better results compared with the inclusion of the temperature difference ΔT_a in Feature Set 4.

Table 8. Features selected for different feature sets for experimentation as model inputs to predict the cake solid content sc. From Publication IV.

	Feature Set								
Features	**1**	**2**	**3**	**4**	**5**	**6**	**7**	**8**	**9**
s_{sl}						x	x	x	x
w	x	x	x	x	x	x	x	x	x
Δp	x	x	x			x	x	x	x
t_{dw}		x							x
T_{sl}									x
T_{vp}			x		x	x	x	x	x
Q_a					x	x	x	x	x
ΔT_a				x			x	x	x
Δpt_{dw}				x	x			x	x

For Feature Sets 6, 7, 8, and 9, the ensemble decision tree algorithms Random Forest and Gradient Boosting produce considerably better results compared with the linear regression algorithms and raise the coefficients of determination R^2 to the 0.8 region. The fact that these two algorithms have the training and test scores close to each other and are able to explain ~80 % of the variability in the cake solid content indicates the suitability of these algorithms for the non-linear regression problem at hand. The linear regression algorithms Ridge and Elastic Net are able to explain more than 70 % of the variability in the predicted variable, but only once all the features in the dataset are used as inputs. The Gradient Boosting regression algorithm is able to achieve the best accuracy with Feature Set 7 as the input and produces the mean absolute error of 0.41 percentage points (pp) with the R^2 values for training and testing of 0.86 and 0.82, respectively. Furthermore, the relatively high training set R^2 values for the Gradient Boosting algorithm together with the smaller testing set R^2 values could be considered as an indication of overfitting. On the other hand, the corresponding values for the Random Forest algorithm are close to each other giving less indication of overfitting and the mean absolute error values are very close to those obtained using the Gradient Boosting algorithm. Hence, out of the

algorithms evaluated, the Random Forest algorithm would seem to be the best choice for predicting the moisture content of the filter cake for the data set in question.

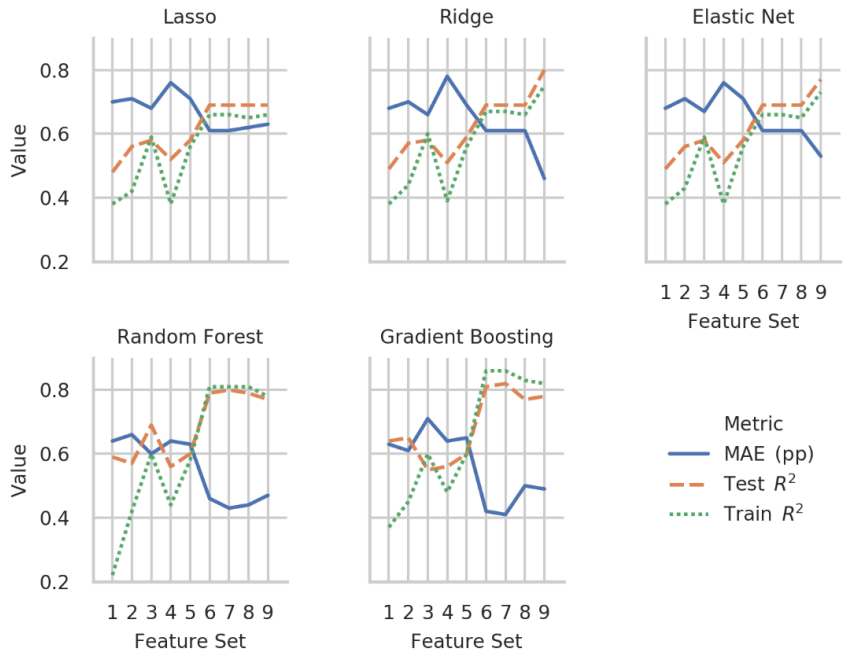

Fig. 11. Performance of the trained models for the filter cake solid content. The mean absolute error MAE is presented as percentage points of the target value. The coefficients of determination R^2 are presented both for the regression model training and testing. From Publication IV.

The predictions and residuals of the best linear regression model obtained with the Ridge algorithm and Feature Set 9 are presented in Fig. 12. The predictions were calculated using the data from both the test and training sets. The randomly dispersed residuals support the applicability of the model with the majority of the absolute values remaining below 0.01, i.e., one percentage point.

Predictions and residuals of the Random Forest model with Feature Set 7 are illustrated in Fig. 13. The majority of the predictions align within ±0.5 percentage points error and only five test set predictions deviate more from the measured values. Two of the experiments with a noticeable prediction deviation from the measured value were conducted with extreme settings for the manipulated process variables. Machine learning algorithms usually produce better results when training on a dataset without irregularities.

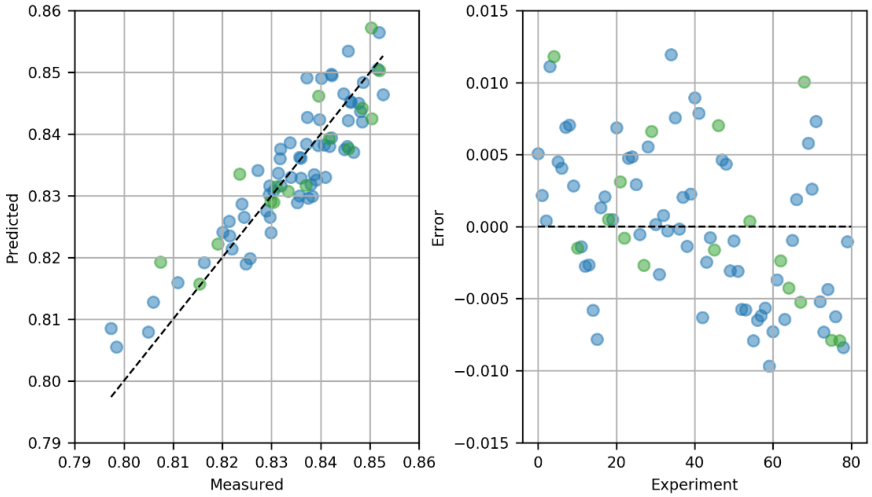

Fig. 12. Soft sensor predictions versus measured values (left) and residuals per experiment (right) for the Ridge regression model with Feature Set 9 as the model input. Blue colour for the training set and green colour for the testing set. Adapted from Publication IV.

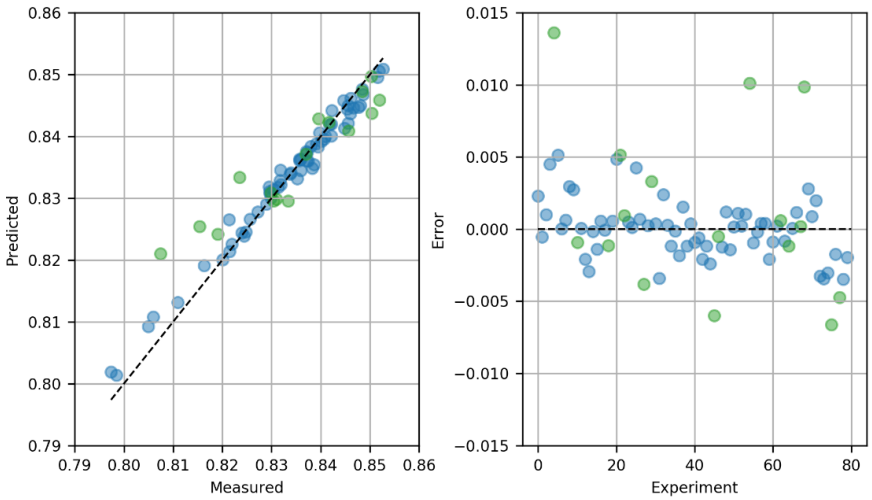

Fig. 13. Soft sensor predictions versus measured values (left) and residuals per experiment (right) for the Random Forest regression model with Feature Set 7 as model input. Blue colour for the training set and green colour for the testing set. Adapted from Publication IV.

3.4 Summary

According to the experiments conducted in this study with the pilot-scale horizontal belt filter, the specific energy consumption of vacuum filtration has a tendency of increasing drastically after a certain level of filter cake solid content is achieved. When combining vacuum filtration with a subsequent thermal drying stage, an optimal operating point for the vacuum filter that is dependent on the combination of the slurry solid content, the applied pressure difference, and the slurry loading was identified. The estimation of filter cake moisture content after dewatering using a data-driven soft sensor approach with standard machine learning regression algorithms and standard process measurements of temperature, pressure, and flow, was successful with the predictions having only minor deviations from the measured values. When considering the prediction of the moisture content of the filter cake after dewatering, it is highly beneficial to leverage on the thermodynamic phenomenon in effect during vacuum dewatering of filter cakes by including the temperature of air passed through the filter cake as a model input.

An important constraint regarding the modelling capability of the data-driven models developed using the methods in this study is that the inputs to the models should remain within the same range as in training of the models in order for the model to output an appropriate prediction for process control purposes. In order to apply the method in industry, a sufficient number of records of the input variables and the corresponding filter cake properties by means of an onsite analysis in an appropriately wide range of operating points of the filter would be essential in order to train a suitable model.

4 Conclusions

The objective of the experimental study reported in this doctoral dissertation was to investigate the airflow rates and the specific energy consumption of vacuum filtration using a laboratory-scale Büchner apparatus and a pilot-scale horizontal belt vacuum filter. The experiments were carried out varying the slurry solid content, pressure difference level, and slurry loadings.

The results obtained with the Büchner apparatus show that dewatering of the filter cake was more efficient when the cake thickness and the pressure difference were greater. This was probably due to a reduction in cake shrinking and cracking with the highest slurry loadings, which most likely prevented the channelling of the liquid flow within the filter cake. It was also found that the specific energy consumption radically increases after reaching a certain level of filter cake solid content. Therefore, it is beneficial to evaluate the specific energy consumption as a function of the solid content of the cake rather than as a function of time in order to determine the optimal ending of dewatering.

Considering the pilot-scale experiments carried out in this study, important factors contributing to the specific energy consumption of vacuum filtration are the means of producing and controlling the pressure difference and the level of applied pressure difference itself. The claw-type vacuum pump used in the experiments proved to be considerably more efficient compared with the liquid-ring pump. A variable-speed-controlled vacuum pump for maintaining a desired pressure difference consumes less energy compared with the traditional bypass valve control. The application of a moderate pressure difference of 0.2 to 0.3 bar produced the most effective results when also taking into account the subsequent thermal drying to a zero moisture content. Furthermore, the pilot-scale experiments indicate that there is an optimal combination of the slurry solid content, the pressure difference level, and the mass of solids deposited per filtration area that results in the minimum total specific energy consumption per solids mass of the filtration and thermal drying stages.

The previously uncharted practice of leveraging on the thermodynamic nature of filter cake vacuum dewatering in order to predict the cake moisture content has proven to be highly beneficial. The heat transfer between the air being forced through the filter cake, the water inside the filter cake, and the solids of the filter cake that results from the evaporation of the void space water can be clearly seen from the results of this study. The regression analysis showed that it was possible to explain 80 % of the variance in the target variable by using the ensemble decision tree regression algorithms and including the vacuum pump inlet air temperature and the airflow rate as model inputs in addition to the traditional vacuum filtration process variables. The mean absolute error for these models was below 0.5 percentage points.

An interesting topic for future research would be the prediction of the moisture content of the filter cake using the cake surface temperature among the model input variables. The surface temperature of the filter cake would be more tolerant to the warming effect

of the leak airflow, which adds additional heat to the air in the vacuum box thus tampering with the cooling effect of evaporation, especially at higher pressure differences.

The proposed method for real-time estimation of the moisture content of the filter cake should be applicable to other types of vacuum filters as well as to horizontal belt vacuum filters, provided that similar process measurements can be made. However, the applicability of the method to air-drying in pressure filters would be another topic for further study. The encouraging results of the pilot-scale investigation suggest that future research on the developed methods should include a trial setup in industry. Yet another interesting topic for future investigation would be the development of a precise mathematical thermodynamic model for the effects of evaporation using the governing equations for mass, momentum, and energy.

References

Bannwarth, H. and Ahner, C. (2005) *Liquid ring vacuum pumps, compressors and systems : conventional and hermetic design*. Wiley-VCH. Available at: https://www.wiley.com/en-us/Liquid+Ring+Vacuum+Pumps%2C+Compressors+and+Systems%3A+Conventional+and+Hermetic+Design-p-9783527312498 (Accessed: 29 April 2019).

Bidar, B. *et al.* (2017) 'Data-driven soft sensor approach for online quality prediction using state dependent parameter models', *Chemometrics and Intelligent Laboratory Systems*. Elsevier, 162, pp. 130–141. doi: 10.1016/J.CHEMOLAB.2017.01.004.

Concha A., F. (2014) *Solid-Liquid Separation in the Mining Industry*. Cham: Springer International Publishing (Fluid Mechanics and Its Applications). doi: 10.1007/978-3-319-02484-4.

Condie, D. J. *et al.* (2000) 'Modeling the Vacuum Filtration of Fine Coal. III. Comparison of Models for Predicting Desaturation Kinetics', *Separation Science and Technology*. Taylor & Francis Group, 35(10), pp. 1467–1484. doi: 10.1081/SS-100100236.

Das, M. K., Mukherjee, P. P. and Muralidhar, K. (2018) 'Equations Governing Flow and Transport in Porous Media', in *Modeling Transport Phenomena in Porous Media with Applications*. Springer International Publishing, pp. 15–63. doi: 10.1007/978-3-319-69866-3_2.

Fan, Y., Dong, X. and Li, H. (2015) 'Dewatering effect of fine coal slurry and filter cake structure based on particle characteristics', *Vacuum*. Pergamon, 114, pp. 54–57. doi: 10.1016/J.VACUUM.2015.01.003.

Fortuna, L. *et al.* (2007) *Soft Sensors for Monitoring and Control of Industrial Processes*. London: Springer London (Advances in Industrial Control). doi: 10.1007/978-1-84628-480-9.

Ge, Z. *et al.* (2017) 'Data Mining and Analytics in the Process Industry: The Role of Machine Learning', *IEEE Access*, 5, pp. 20590–20616. doi: 10.1109/ACCESS.2017.2756872.

Ge, Z. (2017) 'Review on data-driven modeling and monitoring for plant-wide industrial processes', *Chemometrics and Intelligent Laboratory Systems*. Elsevier, 171, pp. 16–25. doi: 10.1016/J.CHEMOLAB.2017.09.021.

Holdich, R. G. (2003) 'Solid–liquid separation equipment selection and modelling', *Minerals Engineering*. Pergamon, 16(2), pp. 75–83. doi: 10.1016/S0892-6875(02)00178-4.

Hoşten, Ç. and Şan, O. (2002) 'Reassessment of correlations for the dewatering characteristics of filter cakes', *Minerals Engineering*. Pergamon, 15(5), pp. 347–353. doi: 10.1016/S0892-6875(02)00038-9.

Hundy, G. H., Trott, A. R. and Welch, T. (2016) *Refrigeration, air conditioning and heat pumps*. Fifth. Oxford: Butterworth-Heinemann.

Kadlec, P., Gabrys, B. and Strandt, S. (2009) 'Data-driven Soft Sensors in the process industry', *Computers & Chemical Engineering*. Pergamon, 33(4), pp. 795–814. doi: 10.1016/J.COMPCHEMENG.2008.12.012.

Kadlec, P., Grbić, R. and Gabrys, B. (2011) 'Review of adaptation mechanisms for data-driven soft sensors', *Computers & Chemical Engineering*. Pergamon, 35(1), pp. 1–24. doi: 10.1016/J.COMPCHEMENG.2010.07.034.

Kemp, I. C. (2005) 'Reducing Dryer Energy Use by Process Integration and Pinch Analysis', *Drying Technology*. Taylor & Francis Group, 23(9–11), pp. 2089–2104. doi: 10.1080/07373930500210572.

Kemp, I. C. (2012) 'Fundamentals of Energy Analysis of Dryers', in *Modern Drying Technology Volume 4: Energy Savings*. Weinheim, Germany: Wiley-VCH Verlag GmbH & Co. KGaA, pp. 1–45. doi: 10.1002/9783527631681.ch1.

Kovačević, I. and Sourbron, M. (2017) 'The numerical model for direct evaporative cooler', *Applied Thermal Engineering*. Pergamon, 113, pp. 8–19. doi: 10.1016/J.APPLTHERMALENG.2016.11.025.

Kudra, T. *et al.* (1989) 'Drying of paste-like materials in screw-type spouted-bed and spin-flash dryers', *Drying Technology*. Taylor & Francis Group, 7(3), pp. 583–597. doi: 10.1080/07373938908916612.

Lin, B. *et al.* (2007) 'A systematic approach for soft sensor development', *Computers & Chemical Engineering*. Pergamon, 31(5–6), pp. 419–425. doi: 10.1016/J.COMPCHEMENG.2006.05.030.

Mujumdar, A. S. (2014) *Handbook of Industrial Drying*. 4rd ed. CRC Press.

Ripperger, S. *et al.* (2013) 'Filtration, 1. Fundamentals', in *Ullmann's Encyclopedia of Industrial Chemistry*. Weinheim, Germany: Wiley-VCH Verlag GmbH & Co. KGaA, pp. 1–38. doi: 10.1002/14356007.b02_10.pub3.

Rushton, A., Hosseini, M. and Hassan, I. (1978) 'The effects of velocity and concentration on filter cake resistance', in *Proc. Symp. on Solid-liquid Separation Practice*. Leeds, pp. 78–91.

Rushton, A., Ward, A. S. and Holdich, R. G. (1996) *Solid-Liquid Filtration and Separation Technology*. Wiley. doi: 10.1002/9783527614974.

Ryans, J. and Bays, J. (2001) 'Run clean with dry vacuum pumps', *CEP Magazine*.

Ryans, J. L. and Croll, S. (1981) 'Selecting vacuum-systems', *Chemical Engineering*, 88(25), p. 72.

Silla, H. (2003) *Chemical Process Engineering: Design And Economics*. Boca Raton: CRC Press (Chemical Industries). doi: 10.1201/9780203912454.

Souza, F. A. A., Araújo, R. and Mendes, J. (2016) 'Review of soft sensor methods for regression applications', *Chemometrics and Intelligent Laboratory Systems*. Elsevier, 152, pp. 69–79. doi: 10.1016/J.CHEMOLAB.2015.12.011.

Sparks, T. (2012) 'Solid-liquid filtration: Understanding filter presses and belt filters', *Filtration + Separation*. Elsevier Advanced Technology, 49(4), pp. 20–24. doi: 10.1016/S0015-1882(12)70193-3.

Svarovsky, L. (2000) *Solid-liquid separation*. 4th edn. Butterworth-Heinemann.

Szymańska, E. (2018) 'Modern data science for analytical chemical data – A comprehensive review', *Analytica Chimica Acta*. Elsevier, 1028, pp. 1–10. doi: 10.1016/J.ACA.2018.05.038.

Tarleton, E. S. and Wakeman, R. J. (2007) *Solid/liquid separation : equipment selection and process design*. Butterworth-Heinemann.

Tarleton, S. and Wakeman, R. (2005) *Solid/Liquid Separation : Principles of Industrial Filtration*. Elsevier Science.

Tien, C. (2012) *Principles of Filtration*. Oxford: Elsevier.

Wakeman, R. (2007) 'The influence of particle properties on filtration', *Separation and Purification Technology*. Elsevier, 58(2), pp. 234–241. doi: 10.1016/J.SEPPUR.2007.03.018.

Wakeman, R. J. (1982) 'An improved analysis for the forced gas deliquoring of filter cakes and porous media', *Journal of Separation Process Technology*, 3(1), pp. 32–38.

Wakeman, R. J. (1998) 'Washing thin and nonuniform filter cakes: Effects of wash liquor maldistribution', *Filtration & Separation*. Elsevier Advanced Technology, 35(2), pp. 185–190. doi: 10.1016/S0015-1882(98)91368-4.

Wakeman, R. J. and Tarleton, E. S. (1990) 'Modelling, simulation and process design of the filter cycle', *Filtration & Separation*. Elsevier Advanced Technology, 27(6), pp. 412–419. doi: 10.1016/0015-1882(90)80534-R.

Yao, L. and Ge, Z. (2018) 'Variable selection for nonlinear soft sensor development with enhanced Binary Differential Evolution algorithm', *Control Engineering Practice*. Pergamon, 72, pp. 68–82. doi: 10.1016/J.CONENGPRAC.2017.11.007.

Appendix A: Büchner apparatus test setup and practice

The Büchner filter used in the laboratory-scale experiments comprised a 100 cm^2 round filter cloth (Tamfelt S1124-22K). TSI 4000 flow meter was used to measure the airflow through the filter and the temperature of the air, a Huba Control pressure sensor was installed for measuring the pressure difference over the filtered material, and a Sartorius CP 4202 S precision balance to measure the mass of the filtrate. Online measurements were recorded at one-second intervals to a computer hard drive. The measurement of filtrate mass as a function of time was made possible by placing the filtrate tank inside a vacuum chamber as illustrated in Fig. 14. The pressure difference was generated by a Vaccon vacuum pump type ejector, which was set to the desired target level using a vacuum regulator. Manual measurements of the mass and the temperature of the slurry to be filtered, the height of the wet cake after filtration, the wet and dry cake mass, and the filtration time were performed. The filtration time for these experiments was considered as the time taken by the cake formation together with the filtration of free water through the filter cake until the point when the descendent water level sank below the surface of the cake. Drying of the wet cakes was performed in an oven at 105 °C. Fig. 14 illustrates the test setup for the Büchner apparatus.

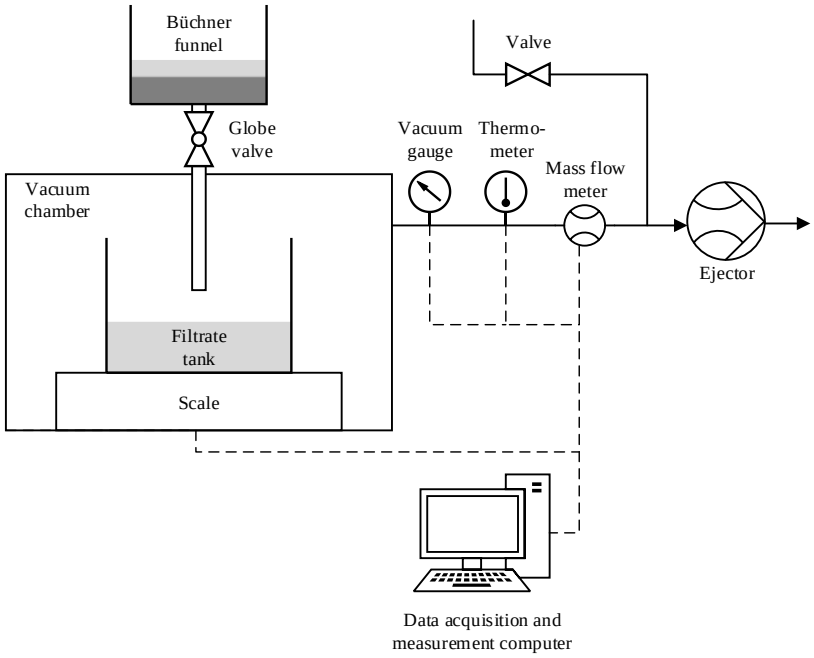

Fig. 14. Büchner test apparatus. From Publication I.

Appendix B: Pilot-scale horizontal belt vacuum filter setup and practice

The device setup and instrumentation of the horizontal belt vacuum filter used in this study are illustrated in Fig. 15. The main operational sections of the device comprised the slurry infeed, filter belt, vacuum generation, and filtrate extraction. Sufficient vertical moving space for the filtrate inside the barometric leg was ensured by dividing the physical layout of the filter into three levels. The applied vacuum of the filter allows the barometric air pressure to push the filtrate level up inside the barometric leg. The frequency-converter-operated pumps and the belt motor enabled the adjustment of the operating point of the filter. The two hose pumps controlled the slurry infeed; the task of the first one was to avoid the settling of the solids along the pumping line by circulating the slurry, and the task of the second hose pump was to control the infeed to the filter belt. A vacuum was generated with one of the vacuum pumps, and the desired pressure difference was controlled by adjusting the rotating speed of the pump with a frequency-converter. The vacuum was applied over the filter medium with the help of a reciprocating tray. The tray had an operating distance of 10 cm, after which the vacuum was cut off and the tray returned to the starting position for reapplication of the vacuum. Because of the operating distance of the tray, the filter had an effective length of 2.1 m, and the width of the filtration area was 0.1 m. The maximum achievable pressure difference was 0.4 and 0.6 bar for the liquid-ring and the claw vacuum pump, respectively.

Recording of the power demand of the vacuum pumps as well as the calculation of the filter belt speed and the slurry infeed rate were enabled by the frequency converters. Measurements of the vacuum pump flow rate, the vacuum pump inlet air temperature, and the generated pressure difference were used to calculate the ideal power demand to produce the pressure drop. Temperature measurements of the slurry fed to the filter belt, the filtrate, and the vacuum pump inlet and outlet flow were recorded. A laser displacement sensor was positioned at the end section of the dewatering stage to measure the filter cake thickness. A digital scale under the filtrate collection tank measured the weight of the produced filtrate.

The filtration process of the device was continuous, i.e., the slurry infeed and distribution on the filter media, the filter cake formation and filtration, and the dewatering until the cake was discharged at the end of the belt all operated continuously during the experiments. The filter cake samples were collected at the cake discharge position after the dewatering section. At the beginning of its return path, the filter belt was sprayed with an amble amount of water to wash the filter media until no solid particles remaining on the media could be detected. Therefore, the effect of the washing of the filter media on the product moisture content and specific energy consumption was outside the scope of the study. The pilot-scale filter instrumentation comprised the devices presented in Table 9.

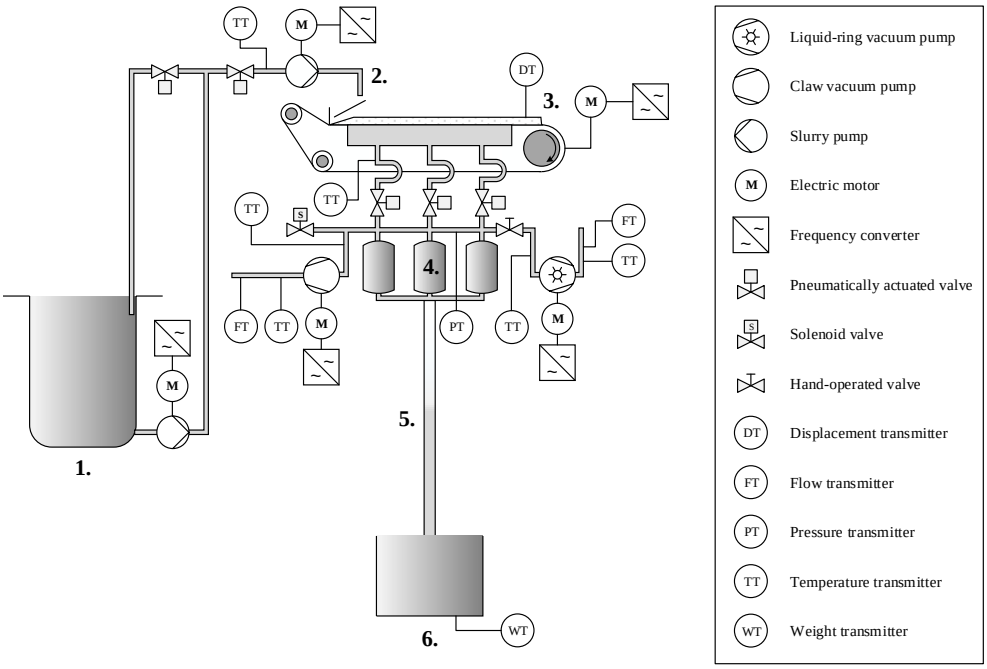

Fig. 15. Horizontal belt vacuum filter device setup and instrumentation: 1) slurry tank, 2) slurry infeed, 3) cake discharge, 4) filtrate intermediate tanks, 5) barometric leg, and 6) filtrate collection tank. From Publication III.

Table 9. Actuator and sensor devices installed in the pilot-scale horizontal belt filter. From Publication III.

Device	**Manufacturer and model**	**Electrical motor**	**Variable-speed drive**
Liquid ring vacuum pump	Robuschi RMV 14	Three-phase motor, 4.0 kW, 1430 rpm	ABB ACS580
Claw vacuum pump	Busch Mink MM1202AVA3	Three-phase motor, 5.1 kW, 3000 rpm	ABB ACS850
Slurry circulation pump	Larox LPP-D 20	Three-phase motor, 0.55 kW, 1400 rpm	Nordac SK300E
Slurry feed pump	Cole-Parmer Masterflex	Three-phase motor, 0.55 kW, 1360 rpm	ABB ACS580
Filter cloth drive	Heynau mini drive	Three-phase motor, 0.18 kW, 1400 rpm	ABB ACS580
Vacuum valves	Gemü		
Slurry control valves	Flowrox PVE25		
Bypass solenoid valve	Schmalz DRV 25 NC		
Cake thickness sensor	Keyence LB-1201 W		
Vacuum pump flow sensors	Schmidt SS 20.260		
Vacuum pressure difference transmitter	Aplisens APR-2000ALW		
Temperature sensors	Aplisens CT-I6		
Filtrate weight scale and transmitter	Dini Argeo PBE300 & DGT20AN		

Publication I

Huttunen, M., Nygren, L., Kinnarinen, T., Häkkinen, A., Lindh, T., Ahola, J., and Karvonen, V.
Specific energy consumption of cake dewatering with vacuum filters

Reprinted with permission from
Minerals Engineering
Vol. 100, pp. 144–154, 2017

Minerals Engineering 100 (2017) 144–154

Contents lists available at ScienceDirect

Minerals Engineering

journal homepage: www.elsevier.com/locate/mineng

Specific energy consumption of cake dewatering with vacuum filters

Manu Huttunen [a,*], Lauri Nygren [a], Teemu Kinnarinen [b], Antti Häkkinen [b], Tuomo Lindh [a], Jero Ahola [a], Vesa Karvonen [c]

[a] LUT School of Energy Systems, Lappeenranta University of Technology, 53850 Lappeenranta, Finland
[b] LUT School of Engineering Science, Lappeenranta University of Technology, 53850 Lappeenranta, Finland
[c] LUT School of Business and Management, Lappeenranta University of Technology, 53850 Lappeenranta, Finland

ARTICLE INFO

Article history:
Received 15 July 2016
Revised 27 October 2016
Accepted 29 October 2016
Available online 5 November 2016

Keywords:
Specific energy consumption
Specific power demand
Cake dewatering
Cake drying
Vacuum filtration

ABSTRACT

The energy consumption of vacuum filtration operations in cake filtration depends on the properties of the cake, the filtration conditions applied, and the progress of the cake dewatering process. Operating a vacuum filter at a high pressure difference requires a high air flow rate and thus has high energy consumption. By taking the filtered solids content into consideration together with the power demand and energy consumed at a certain pressure difference level, it is possible to investigate the specific power demand and energy consumption relative to the filtered cake solids content. When the mother liquor in the void space of the filter cake is replaced by air, the flow rate of air through the cake increases, which has a dramatic influence on the specific energy consumption. In this study, dewatering of calcite mine tailings is investigated with respect to the specific power demand and energy consumption of vacuum generation calculated using the assumption of an ideal isentropic process. The results of this study demonstrate clearly that both the air flow rate and the specific energy consumption in dewatering increase sharply after a certain solid content of the cake is reached. The results suggest that pumping costs in vacuum filtration can be reduced substantially by allowing a slight increase in the residual moisture content of the filter cake.

1. Introduction

Vacuum filtration is a unit operation used in the dewatering of various mineral slurries such as calcium carbonates, phosphates and sulphates. Continuous vacuum belt filters are typically applied when the solids to be separated do not contain much fines, settle rapidly, and form a permeable cake that can be dewatered at a moderate pressure difference, or when the cake has to be (counter-current) washed in the filter unit (Sparks, 2012a; Svarovsky, 2000; Tarleton and Wakeman, 2007). Vacuum filtration with belt filters is an energy intensive operation, partially due to the large volumes of air flowing through the pores and cracks of the cake, as described by Ripperger et al. (2012), and because of the leakage of air into the vacuum box, e.g., near the edges of the filter medium.

A simple way to simulate the operation of horizontal vacuum belt filters in a laboratory is to use a Büchner test apparatus that consists of a cylindrical slurry basin, on the bottom of which the filter medium is installed. The test unit is connected to a vacuum source and experiments are then performed batchwise under various conditions. In cases when the filter cake is not washed, the total filtration time is divided into two periods, namely, separation and drying, the latter of which is often referred to as dewatering. During the separation period, the filter cake is formed and liquid is filtered through the cake until the solid particles form a rigid structure. The height of the cake remains constant, provided that the material is incompressible – a condition that is often assumed in dewatering calculations and modelling (Condie et al., 2000), although not exactly true for real mineral slurries. The separation period can be described mathematically using cake filtration equations derived from Darcy's law (Darcy, 1856). Several properties of the slurry and solids, such as particle size distribution, particle shape, solid concentration and surface charge of the suspended solids, have an effect on the cake formation, and thus also on the flow of liquid through the cake (Besra et al., 2000; Fan et al., 2015; Sorrentino, 2002; Wakeman, 2007). Darcy's law and filtration equations derived from it don't take into account all these properties, thus the results of these equations can only be considered as indicative.

The purpose of the drying period is to remove liquid from the pores of the cake until the target moisture content of the cake is achieved. Removal of pore liquid opens flow channels for air to flow through the cake, which increases the air flow rate (as

* Corresponding author.
E-mail address: manu.huttunen@lut.fi (M. Huttunen).

http://dx.doi.org/10.1016/j.mineng.2016.10.025
0892-6875/

described, e.g., by Wakeman and Tarleton, 1990) and leads to high energy consumption of the vacuum pump. Due to the gradually increasing air flow rate through the cake, the energy consumption of the drying period can become very high relative to the corresponding moisture reduction.

Reduction of moisture content by vacuum filters usually requires less energy than thermal drying. Therefore, mechanical dewatering of the dryer feed is regarded as a primary method for reduction of the energy demand of the drying process (Kemp, 2015, 2012). However, there is a product-specific limit for the best obtainable dewatering result, i.e. irreducible saturation, which is the minimum saturation of the filter cake obtainable by an infinite pressure difference (Campbell, 2006). Heat is sometimes used in the filter unit to further improve the dewatering performance (see e.g. Kinnarinen et al., 2013; Lee, 2006; Peuker and Stahl, 1999, 2000; She and Sleep, 1998).

For a given porous system, the pressure difference required for removal of liquid from pores of different diameters can be approximated using the Laplace-Young equation (Besra et al., 1998a,b), which states that the pressure required to overcome the capillary pressure of a pore is inversely proportional to the pore diameter. This logically means that the largest pores of the cake are dewatered first (Condie et al., 1996). Additionally, decreasing the surface tension and increasing the contact angle have been reported to help obtain low moisture content of the cake (Tao et al., 2000), which is also in accordance with the Laplace-Young equation. However, in practical applications of vacuum dewatering of mineral filter cakes when the aim is to produce readily transportable and storable powders, it is rarely possible to avoid the need for subsequent thermal drying.

Energy consumption has been an important topic of discussion in filtration literature investigating membrane filtration (Blankert et al., 2007), centrifugation and consolidation (Chu et al., 2005), filter presses (Zhu et al., 2016) and mechanical dewatering in general (Lee, 2006). The objective of these previous studies has been to evaluate the operation of solid-liquid separation systems with respect to the mechanical energy requirement of liquid phase operations, which is significantly different from the issue of specific power demand and energy consumption of vacuum systems in which gases are evacuated from a space to create the driving force for separation.

The aim of this paper is to enhance knowledge about energy consumption of vacuum filtration, in particular energy optimization of vacuum filtration dewatering of slightly compressible mineral filter cakes. In addition to the experimental study, the principal theories of cake filtration, dewatering and vacuum pumping are introduced. The study focuses on the power demand and energy consumption of slightly compressible mineral filter cakes during the filtration and dewatering periods. Power demand and energy consumption are discussed from the perspective of the final solids content of the dewatered cake, and it is shown that elimination of the last removable pore liquid using vacuum filtration is a highly energy intensive operation.

2. Theory

2.1. Cake filtration equations

The average specific cake resistance α_{av} is calculated using experimental data and the integrated, reciprocal form of the Darcy equation (Eq. (1)) (Darcy, 1856). More discussion and calculation examples concerning the presented filtration equations can be found in the literature, for instance Ripperger et al. (2012), Svarovsky (2000), and Tien (2012). Integrated form of the so-called general filtration equation for constant pressure operation is given by:

$$\frac{t}{V_f} = \frac{\alpha_{av}\mu c}{2A^2\Delta p} V_f + \frac{\mu R_m}{A\Delta p}, \tag{1}$$

where t is time, V_f is the volume of filtrate, μ is the dynamic viscosity of the filtrate, c is the filtration concentration, A is the filtration area, Δp is the applied pressure difference, and R_m is the resistance of the filter medium. When Eq. (1) is solved with respect to α_{av} using the symbol a for the experimentally determined slope t/V^2 in the calculation and omitting the resistance of the filter medium, Eq. (2) applies for the average specific resistance of the cake:

$$\alpha_{av} = \frac{2aA^2\Delta p}{\mu c}. \tag{2}$$

The average porosity of the filter cake ε_{av} is calculated from the cake dimensions and the void volume of the cake (Eq. (3)):

$$\varepsilon_{av} = \frac{V_v}{V_c} = 1 - \frac{m_s}{\rho_s A L}, \tag{3}$$

where V_v is the void volume ($V_v = V_c - V_s$), V_c is the cake volume, V_s used in the calculation of V_v is the volume of suspended solids in the cake, m_s is the mass of solids, ρ_s is the density of solids, and L is the height of the cake.

2.2. Cake dewatering

Vacuum filtration creates a two-phase flow in porous media. Cake dewatering is done by displacing filtrate, in this case water, in the cake by an immiscible fluid (air in this case). The structure of a cake can be considered as a matrix of solid particles in a liquid and gas mixture.

When the liquid in the void space of the cake is water, the saturation S of the cake is defined as:

$$S = \frac{V_w}{V_v}, \tag{4}$$

where V_w is the volume of water in the cake, measured in experimental work by evaporating all the pore water off the cake in an oven.

To understand reduction of cake saturation by vacuum filtration, the capillary forces in the bed need to be considered. Surface forces affect at the interface of the two flowing fluids in contact inside the cake. The surface tension force acts at the interface between the liquid and the solid and retains liquid in the finer pores of the cake (Wakeman and Tarleton, 2005a).

The Laplace-Young equation (Eq. (5)) determines the pressure difference required to enable gas flow through the capillaries, i.e. the pores of the cake. This pressure difference is often referred to as bubble point pressure or threshold pressure and can be calculated from:

$$\Delta p = \frac{2\gamma\cos\theta}{r}. \tag{5}$$

In the Laplace-Young equation, γ represents the surface tension at the liquid-gas interface, θ is the contact angle between the liquid and the solid, and r is the pore radius.

The two immiscible fluids flowing through the medium form unique pathways, which change as the fluid saturation of the cake changes during dewatering. As the liquid saturation is reduced, the liquid pathways become discontinuous, the flow of the wetting fluid ceases, and the cake reaches the state of irreducible wetting fluid saturation.

Reduced saturation, S_R, is defined as:

$$S_R = \frac{S - S_\infty}{1 - S_\infty}, \tag{6}$$

where S_∞ is the irreducible saturation at which the flow of the liquid ceases.

Cake solid content s' (mass solid/mass liquid) can be calculated using Eq. (7):

$$s' = \frac{1-\varepsilon_{av}}{S\varepsilon_{av}}\frac{\rho_s}{\rho_l}, \tag{7}$$

where ρ_l is the density of liquid.

The cake solid content referred to in this article, s, has the units (mass solid/(mass of liquid + mass of solid)) and can be expressed by Eq. (8):

$$s = \frac{s'}{1+s'}. \tag{8}$$

2.3. Operation of vacuum pumps

The required pressure difference across the cake is generated in vacuum filtration by a vacuum pump. Vacuum pumps are fundamentally compressors, but they are designed to operate at a suction pressure lower than atmospheric pressure (Coker, 2007). The vacuum pump evacuates gas from the vacuum chamber to the atmosphere and, consequently, pressure in the chamber reduces until the gas leaking to the vacuum chamber is equal to the air flow evacuated by the vacuum pump. In the beginning of the filtration, in the cake formation stage, the air flow through the cake can be assumed to be zero, and only liquid passes through the cake. After the cake has formed, the dewatering stage begins, and air displaces the moisture in the cake. Airflow increases with decreasing moisture until it reaches its asymptotic maximum value (Wakeman and Tarleton, 2005b). In the dewatering stage, the vacuum pump consumes significantly more energy than in the cake formation stage, due to increased air flow to the vacuum chamber. Despite the higher energy consumption, vacuum dewatering, with reasonable time limits, is still typically far more cost effective than thermal evaporation (Sparks, 2012b).

In vacuum filters, the air flow through the cake is typically between 0.3 and 2.0 N $m^3/m^2/min$, depending on the application and coarseness of the material. To produce the required air flow, the power demand of the vacuum pump typically ranges from 2 to 15 kW/m^2, while the other devices used, such as the filtrate pump and cloth drive, account only for 0.2–0.4 kW/m^2. (Henriksson, 2000) Therefore, airflow through the cake and vacuum pump efficiency have significant effects on vacuum filter energy consumption and operation costs. The vacuum is typically generated by liquid-ring vacuum pumps (LRVP) (Jorisch, 2015; Silla, 2003), since they are able to handle condensable vapours (Silla, 2003). Mechanical dry vacuum pumps can also be used.

The volumetric flow through a vacuum pump consists of non-condensable and condensable gases. In the case of filtration, the non-condensable gas is typically air and the condensable gas is water vapour. In flow rate estimation of vacuum pumping, it is typically assumed that the non-condensable gases are saturated with condensable vapours (Silla, 2003). Saturated air holds the maximum amount of vapour possible for a particular temperature, i.e. the relative humidity of air is 100%. The air-water vapour mixture can be treated as an ideal gas whose pressure is a sum of the partial pressure of dry air, p_a, and the partial pressure of water vapour, p_v (Çengel and Boles, 2015). The partial pressure of dry air can thus be expressed by the equation:

$$p_a = p_{in} - p_v, \tag{9}$$

where p_{in} is the total pressure of the mixture at the inlet of the vacuum pump. The partial pressure of the water vapour is assumed to be the saturation pressure, which grows as a function of temperature. At a temperature of 20 °C, the vapour pressure of saturated air, p_v = 2.34 kPa. On the basis of the temperature and the partial pressures of the air and water vapour, the density of the air-water vapour mixture, ρ_{in}, can be calculated by the equation:

$$\rho_{in} = \frac{p_a}{R_a T} + \frac{p_v}{R_v T}, \tag{10}$$

where T is temperature, and R_a = 287.0 J/kg K and R_v = 461.5 J/kg K are specific gas constants of dry air and water vapour, respectively (Çengel and Boles, 2015). Higher relative humidity reduces the mass flow and power demand of a vacuum pump, since water vapour has lower density than air, but the effects in industrial filtration applications are negligible.

In operation, a vacuum pump evacuates a certain volume of gas from the chamber on each rotation. The volume flow rate $q_{V,in}$ is described at vacuum pump inlet conditions and is expressed by the equation:

$$q_{V,in} = \frac{dV}{dt}, \tag{11}$$

where V is volume of gas. Since the density of gases varies as a function of pressure and temperature, the volumetric flow rate does not describe the actual quantity of air evacuated, only the volume of gas evacuated at given conditions. The quantity of gas can be described by the mass flow rate or standard volumetric flow rate. The standard volumetric flow rate Q corresponds to air flow in standard conditions, and it can be described by the equation:

$$Q = \frac{T_{std}}{T_{in}}\frac{p_{in}}{p_{std}}q_{V,in}, \tag{12}$$

where T_{in} is the temperature in vacuum pump inlet, T_{std} = 21.11 °C and p_{std} = 101.3 kPa are standard temperature and pressure, respectively (TSI, 2001).

The ideal power demand of a vacuum pump can be calculated on the basis of the volume flow rate, gas density, and inlet and outlet pressure. Isothermal or isentropic compression can be assumed, depending on the vacuum pump type. In isothermal compression, the total heat accruing during the compression is evacuated to the environment and the temperature of the compressed gas remains constant. Isothermal compression is typically used for cooled compression, so it is a suitable assumption for liquid-ring vacuum pumps (Bannwarth, 2005). Isothermal power P_T can be calculated by the equation:

$$P_T = q_{V,in}p_{in}\ln\left(\frac{p_{out}}{p_{in}}\right), \tag{13}$$

where p_{out} is the outlet pressure of the vacuum pump. It is often assumed that the vacuum pump discharges to the atmospheric pressure, thus $p_{out} = p_{std}$.

Isentropic compression can be assumed for vacuum pumps in certain cases (Silla, 2003). In isentropic compression, ideal heat insulation of the system is assumed, so there is no heat transfer through the process boundaries and all the accruing heat remains in the compressed gas. Isentropic power P_S can be used with dry vacuum pumps, and it is calculated by the equation:

$$P_S = \frac{k}{k-1}q_{V,in}p_{in}\left[\left(\frac{p_{out}}{p_{in}}\right)^{\frac{k-1}{k}} - 1\right], \tag{14}$$

where k is the isentropic exponent. Air assumed as an ideal gas has k = 1.4. Since isothermal and isentropic power describe the ideal power demand, the actual power required by the vacuum pump P_{shaft} is calculated by the equation:

$$P_{shaft} = \frac{P_T}{\eta_T} \quad \text{or} \quad P_{shaft} = \frac{P_S}{\eta_S}, \tag{15}$$

where η_T is isothermal efficiency and η_S is isentropic efficiency. The typical isentropic efficiencies of several types of vacuum pumps as a function of pressure ratio are illustrated in a supplementary file (Ryans and Croll, 1981) and (Ryans and Bays, 2001). Since the actual electric power demand of cake filtration depends on the vacuum pump type, as well as the motor and possible electric drive, only ideal energy consumptions of cake dewatering are compared in this paper. The compression is assumed to be isentropic. Isentropic energy consumption E_S for filtration and dewatering can be calculated by the equation:

$$E_S = \int P_S dt. \tag{16}$$

3. Materials and methods

3.1. Preparation of slurry

The slurry for the experiments was prepared from tap water (Lappeenranta City, Finland) and dried tailings obtained from a calcite refining process. This material was selected as the model substance for the experiments due to its coarseness, which is a typical property of solids separated with vacuum belt filters. The solid content of the slurry was constant 30% w/w in all experiments. The particle size distribution of the slurry, measured with a Malvern Mastersizer 3000 laser diffraction particle size analyzer, is shown in Fig. 1.

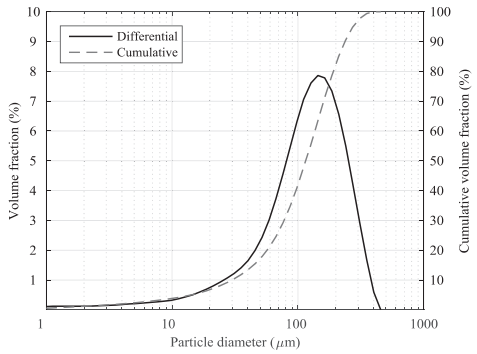

Fig. 1. Particle size distribution of slurry solids.

Table 1
Elemental composition of the solids used for slurry preparation. Values are given in % w/w.

Element	Meas. 1	Meas. 2	Meas. 3	Average
C	10.9	11.1	11.0	11.0
O	44.4	43.7	43.9	44.0
Na	0.6	0.6	0.7	0.6
Mg	1.4	1.5	1.3	1.4
Al	1.4	1.1	1.2	1.2
Si	11.2	11.5	11.8	11.5
K	0.6	0.3	0.2	0.4
Ca	28.9	29.3	29.2	29.1
Fe	0.7	0.9	0.7	0.7

Scanning electron microscope (SEM) images of solids (Fig. 2) were taken and energy-dispersive X-ray spectroscopy (EDS) analysis for elemental composition of the solid phase of slurry (Table 1) was performed using a Hitachi SU 3500 scanning electron microscope. As illustrated in Fig. 2, the shape of the particles is relatively irregular and no clear differences can be observed between the shape of small and large particles.

The main elements present in the solids are O, Ca, Si, and C. On the basis of the elemental composition and the origin of the solids, it can be concluded that the minerals that are present to a large extent comprise forms of calcium carbonate and calcium silicate.

3.2. Equipment and data acquisition

The laboratory experiments were carried out using a Büchner filter with a 100 cm^2 round filter cloth (Tamfelt S1124-22K). Air flow through the filter and temperature of the air were measured with a TSI 4000 flow meter, pressure difference over the filtered material with a Huba Control pressure sensor and mass of the filtrate with a Sartorius CP 4202 S precision balance. Measurements were made online and recorded with a computer at one second intervals. Placing the filtrate tank in a vacuum chamber (Fig. 3) enabled the measurement of filtrate mass as a function of time. The pressure difference generated by the ejector (Vaccon vacuum pump, Medfield, MA) was set to the target level by a vacuum regulator. Mass and temperature of slurry to be filtered, the height of the wet cake after filtration, the wet and dry cake mass, as well as the separation time were measured manually. The separation time is defined as the time required for cake formation and filtration of free liquid through the cake until the descendent water level drops below the surface of the cake. Wet cakes were dried in an oven at 105 °C over night. The measurement setup is illustrated in Fig. 3.

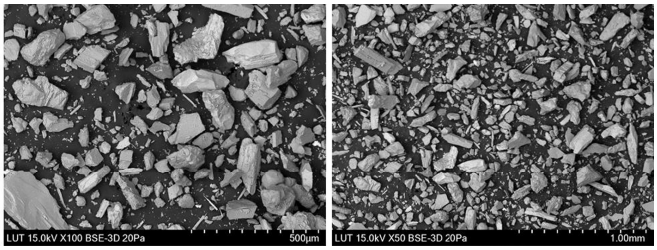

Fig. 2. Scanning electron microscope images of solid particles (100 and 50× magnifications).

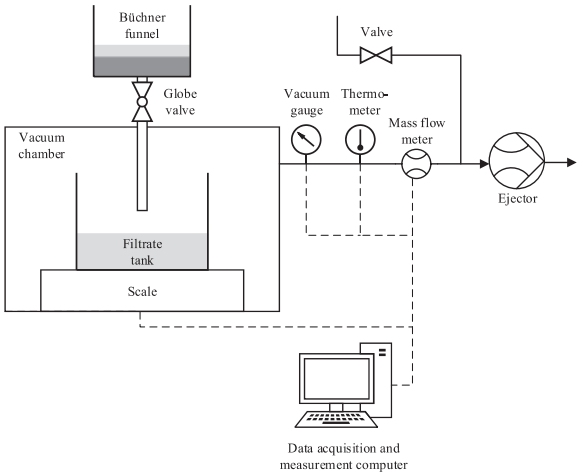

Fig. 3. Büchner test apparatus.

Table 2
Laboratory experiments carried out to study the energy consumption of cake dewatering with a vacuum filter. $T = 20$ °C in all experiments.

Test	Δp (bar)	m_{sl} (g)	m_s/A (kg/m^2)
1	0.4	300	9
2	0.4	500	15
3	0.4	700	21
4	0.6	300	9
5	0.6	500	15
6	0.6	700	21
7	0.8	300	9
8	0.8	500	15
9	0.8	700	21

3.3. Operation of the test filter

To study the energy consumption of cake dewatering with a vacuum filter as regards time and solid contents of the cake, a set of nine laboratory experiments (3^2 full factorial design) were carried out. The experimental plan comprised two variables, namely the pressure difference and the mass of slurry, m_{sl}, fed into the filter. Table 2 shows the range of the applied pressure difference and filtered slurry mass studied in the experiments and the associated mass of suspended solids per filtration area, m_s/A.

During the experiments, the slurry was under continuous mixing in a slurry tank. The required amount of slurry for the test was collected from the slurry tank using a ladle and transferred to a measuring can. Before starting the experiment, the air flow through the filter was blocked with a globe valve (see Fig. 3) and the vacuum chamber pressure was adjusted to achieve the desired pressure difference. Data recording then started. The measured amount of slurry was poured onto the filter medium while simultaneously being manually mixed in the measuring can. Immediately after discharge onto the filter, the manual valve was opened to start the filtration and a stop watch was started.

Determination of the separation time was performed visually. The separation time was recorded using the stop watch for the moment when the descendent water level dropped below the surface of the cake. The total filtration time ranged from 500 to 800 s, depending on the progression rate of the filtration.

4. Results and discussion

4.1. Dewatering characteristics

The mass of filtrate m_f as a function of time is presented in Fig. 4, where the grey lines indicate the dewatering period, which begins after separation time t_{sep} has elapsed from the start of filtration. The overlapping separation curves in Fig. 4 indicate good repetitiveness of the experiments. It is clearly illustrated in Fig. 4 that the duration of the filtration period increases with the increase in slurry mass, which can be explained by the increasing thickness of the cake. An increase in the applied pressure difference has a positive influence on the filtration rate, the improvement being clearest when Δp is changed from 0.4 to 0.6 bar. As an exception to the other experiments presented in Fig. 4, there is a temporary slowdown in the filtrate flow rate in the beginning of the dewatering period when Δp is 0.4 bar (Fig. 4a). This anomaly may be due to a combined effect of the high thickness of the cake and the low pressure difference, which might cause a delay in the beginning of dewatering. Unfortunately, no data is available about the pore size distribution of the cake, so it is therefore impossible to approximate the bubble point pressure of the cake using Eq. (5).

The most important characteristics of the filter cakes are summarized in Table 3. It can be observed in Table 3 that the final thickness of the thickest cakes was reduced when the separation was performed at an elevated pressure difference. The final solid content of the cake was logically highest when the highest pressure difference was used. The calculated values for the average cake porosity ε_{av} ranged from less than 0.42 to approximately 0.47. Comparison of the average specific cake resistances α_{av} implies that the filter cakes were slightly compressible, in other words, α_{av} increased with increased filtration pressure.

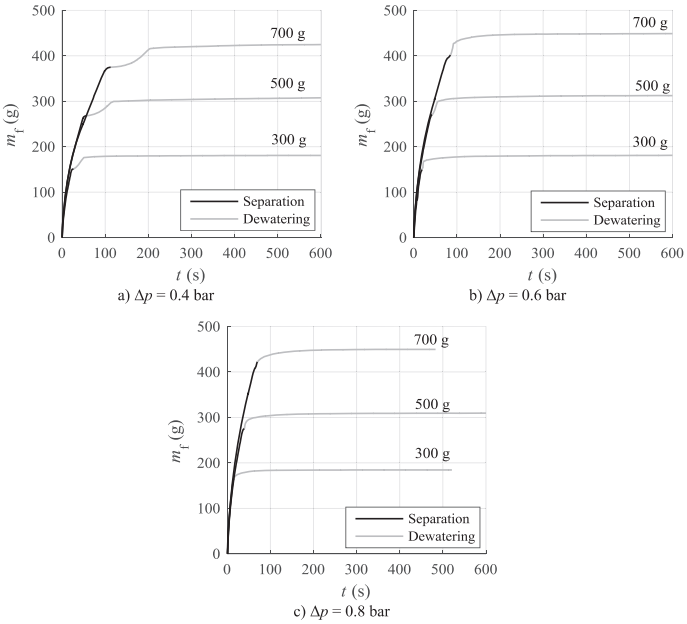

Fig. 4. Filtrate mass as a function of time.

Table 3
Variables, properties of filter cakes, and separation time.

Test	Δp (bar)	m_{sl} (g)	t_{sep} (s)	L (mm)	s (% w/w)	ε_{av} (–)	α_{av} (10^{10}) (m/kg)
1	0.4	300	27	6.1	76.1	0.469	1.02
2	0.4	500	56	9.7	79.3	0.435	0.94
3	0.4	700	113	14.5	79.9	0.444	0.96
4	0.6	300	19	5.5	77.4	0.418	1.20
5	0.6	500	43	9.8	80.8	0.445	1.01
6	0.6	700	85	13.9	84.0	0.445	0.99
7	0.8	300	15	5.8	79.7	0.437	1.26
8	0.8	500	40	10.9	84.3	0.469	1.16
9	0.8	700	70	13.2	85.5	0.415	0.99

4.2. Air flow through the filter cakes

Specific air flow rates, Q/m_s, as a function of time are illustrated in Fig. 5. Specific air flow rate expresses the standard volumetric flow rate calculated by Eq. (12) relative to the solids mass of the cake m_s, which makes the air flow through cakes with different masses more comparable. In the separation stage, the airflow consists of leak airflow and the airflow required to compensate the volume of filtrate flowing into the vacuum box, since airflow through the cake has not yet started. The airflow rate decreases as the filtrate flow rate decreases towards the end of the separation stage and has its minimum value between the separation and dewatering stages. In the dewatering stage, the airflow through the cake increases and approaches its asymptotic maximum value.

The flow curves show that the air flow rate increases at a slow rate during the dewatering period when the filtration pressure is 0.4 bar, while higher pressure differences of 0.6 and 0.8 bar have a more distinct effect on the air flow through the cake. In the beginning of the dewatering period, at the highest Δp (Fig. 5c), the air flow rate rises rapidly until the readily drainable pores have been dewatered, and the increase in the air flow rate then slows down quickly. The thinnest cakes were consistently the most permeable to air flow, but there was not a clear difference between the air flow rates through the thickest cakes, when the mass of slurry fed into the filter was either 500 or 700 g and when pressure differences of 0.6 and 0.8 bar were used (Fig. 5b and c).

When the air flow rates during the separation and dewatering periods are plotted against the corresponding solid content of the cake, the curves give a more realistic impression of how much air has to be pumped out of the vacuum chamber to obtain the desired moisture content of the filter cake. Specific air flow rate as a function of solid content is illustrated in Fig. 6. Even though there is some variation in the air flow data due to minor leakages and irregularities in the flow of filtrate into the vacuum box, the following observations can be made on the basis of Fig. 6:

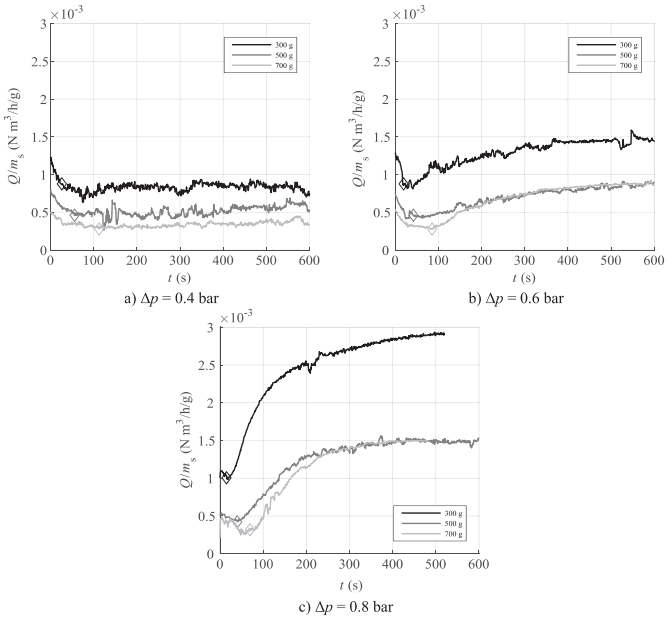

Fig. 5. Specific air flow rate as a function of time. Diamond marker indicates the start of the dewatering period.

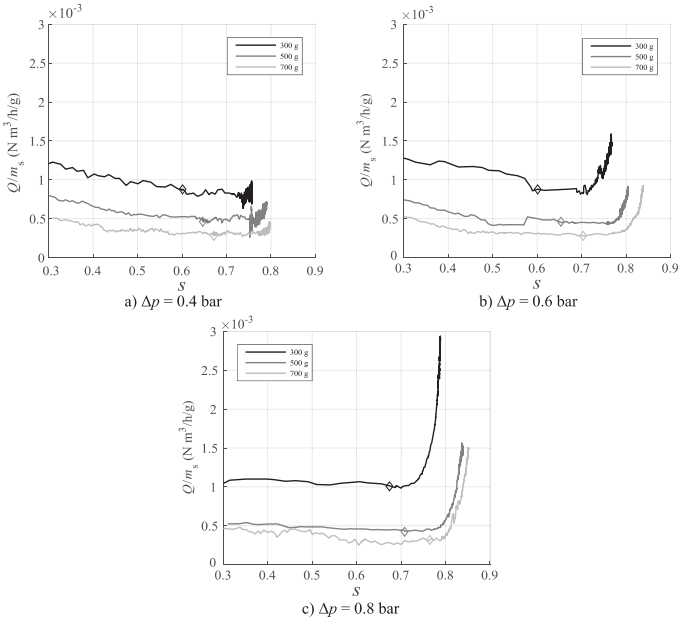

Fig. 6. Specific air flow rate as a function of solid content. Diamond marker indicates the start of the dewatering period.

- The air flow rate decreases towards the end of the separation period at Δp = 0.4 and 0.6 bar (Fig. 6a and b), and is almost constant when the highest Δp of 0.8 bar is used (Fig. 6c).
- In the beginning of the dewatering/drying period, the air flow rate keeps relatively constant up to the point when the largest pores are emptied of water, and the air flow through the cake then increases dramatically (Fig. 6b and c), unless Δp is low enough to prevent excessive air flow (Fig. 6a).
- Within the studied range of cake thicknesses (see Table 3), the thickest cakes were dewatered better than the thinnest ones: the maximum obtained solid content was 85.5% w/w.

As can be seen in Fig. 6, highest solid content is achieved with greatest slurry mass and cake height for every pressure drop level. This is the reverse situation than would be expected, since a higher cake should cause greater resistance to air flow and thus result in lower air flow rate through the cake (Svarovsky, 2000). However, tiny leakage holes at the edges of the Büchner funnel appeared with lower cake heights, which may be the reason for the lower dewatering, even though the pressure difference remained constant. Air flow through the holes rather than through the pores could lead to the higher moisture content at the end of the dewatering (Wakeman and Tarleton, 1999). Additionally, one possible explanation for the better dewatering of the thickest cakes is the local variation of the cake thickness, which may have a negative effect on the evenness of air flow when the cake thickness is only five to six millimetres. Wakeman (1998) has also found that thicker cakes are washed more effectively than thinner ones, and that the probable explanation for this is an increased chance of channelling through the thinner cakes.

4.3. Specific power demand and energy consumption of the cake dewatering

The ideal power demand of a vacuum pump in cake filtration can be determined on the basis of measured air flow rate and pressure drop using the procedure introduced in Section 2.3. Specific isentropic power demand, P_S/m_s, as a function of time is illustrated in Fig. 7. Specific isentropic power demand expresses the ideal isentropic power demand described by Eq. (14) relative to the mass of solids in the cake. Since pressure remains nearly constant during the filtration, the isentropic power curve follows the air flow curve, as can be deduced from Eq. (14). Power demand increases in the dewatering stage, since air flow through the cake is higher. Other factors increasing the power demand are lower cake height and higher pressure difference. Cake resistance is directly proportional to cake height (Svarovsky, 2000), so a lower height cake causes lower resistance, thus increasing the air flow through the cake and the power demand.

Specific isentropic power demand as a function of solid content is illustrated in Fig. 8. These curves, too, follow the shape of the air flow curves presented in Fig. 6. As can be seen, the power demand increases sharply after reaching a certain solid content. This change is most clearly seen in Fig. 8c, where the applied pressure difference is 0.8 bar.

Cumulative specific isentropic energy consumption, E_S/m_s, as a function of time is illustrated in Fig. 9. The specific isentropic energy consumption describes the ratio of isentropic energy consumption calculated by Eq. (16) and the solids mass in the cake. The vast majority of energy is consumed in the dewatering stage. With 0.4 bar pressure drop (Fig. 9a), the energy consumption as a function of time is nearly linear, since the increase in air flow in

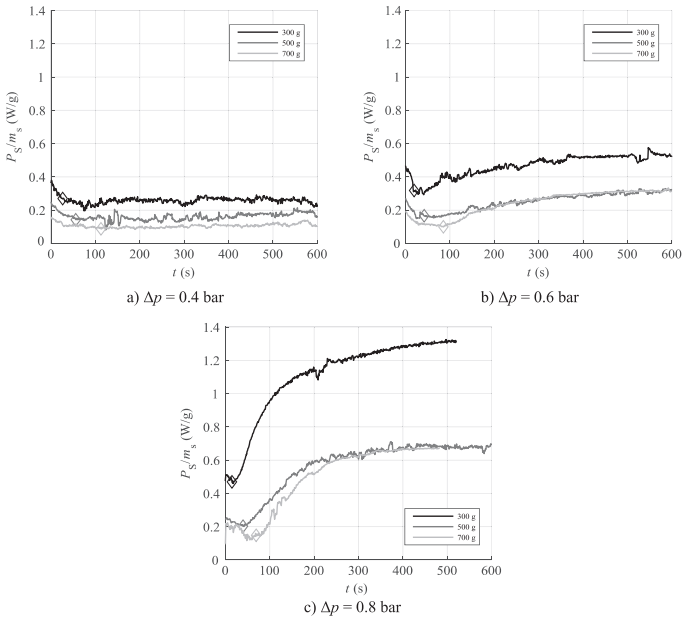

a) Δp = 0.4 bar b) Δp = 0.6 bar

c) Δp = 0.8 bar

Fig. 7. Specific isentropic power demand as a function of time. Isentropic power demand is calculated by Eq. (14). Diamond marker indicates the start of the dewatering period.

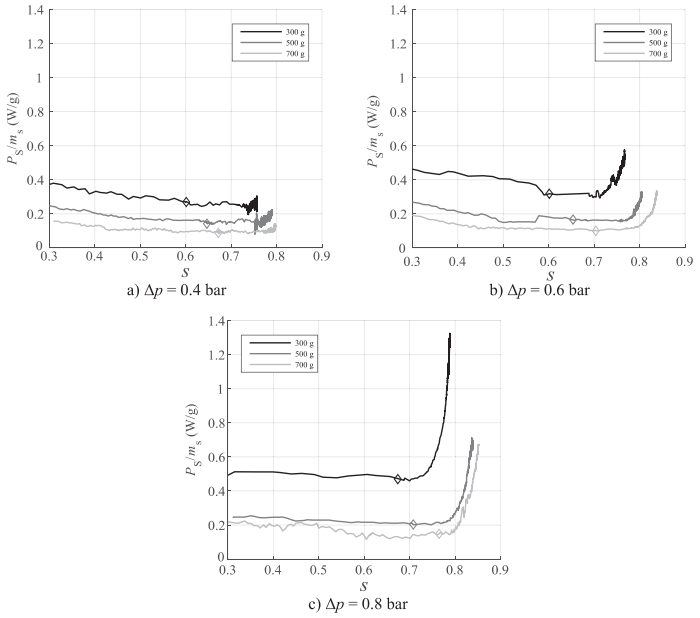

Fig. 8. Specific isentropic power demand as a function of solid content. Diamond marker indicates the start of the dewatering period.

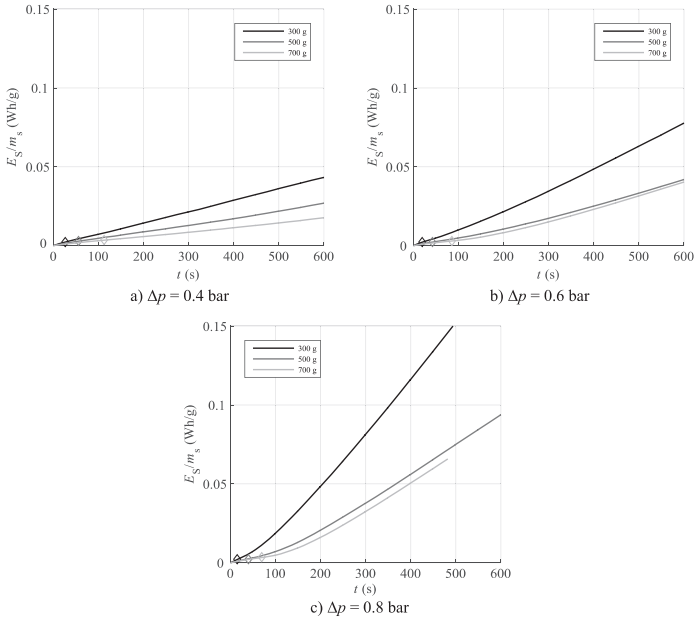

Fig. 9. Cumulative specific isentropic energy consumption as a function of time. Diamond marker indicates the start of the dewatering period.

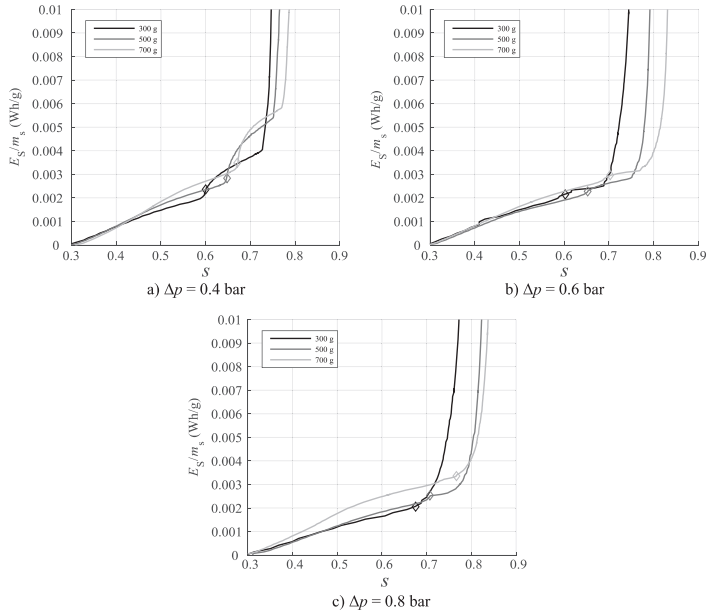

Fig. 10. Cumulative specific isentropic energy consumption as a function of solid content. Diamond marker indicates the start of the dewatering period.

the dewatering stage is relatively low. On the other hand, the effect of higher pressure difference on the cumulative specific energy consumption causes nonlinearity of the curves, as illustrated in Fig. 9b and c.

Cumulative specific isentropic energy consumption as a function of solid content is illustrated in Fig. 10. After a certain amount of moisture has been removed, putting more energy into the process does not seem to lead to a drier cake. According to Rushton et al. (2000), the most economical way to filter the cake is to use the lowest required pressure drop to overcome the fluid drag within the cake, which is the case with an ideal incompressible cake. However, air leaks and uneven flow distribution across the cake area also have to be taken into account. Since air leaks remained nearly constant as a function of pressure drop and account for a major share of air flow in low pressure drop tests, the usage of a lower vacuum level does not seem to lead to less energy consumption than higher vacuum levels. With lower vacuum, the cake filtration and dewatering times are longer, so more energy is consumed with the same amount of leak flow rate.

5. Conclusions

The objective of this experimental study was to investigate the specific power demand and energy consumption of vacuum filtration using a laboratory-scale Büchner filter supplemented with a vacuum box and related instrumentation. Experiments were performed using different slurry loadings and vacuum levels, for which the filtration accumulation and the specific air flow rate through the filter cakes were measured. The results show that the specific power demand and energy consumption of vacuum filtration increases with the progress of the dewatering, and that the shape of the power demand curves consistently follows the shape of the air flow curves. Dewatering of the filter cake was more effective when the cake thickness and pressure difference were greater. This finding, however, does not mean that the dewatering result could be improved by increasing the cake thickness further above the applied range. In this study, the best dewatering result was most likely obtained due to a reduction of cake shrinking and cracking at the highest slurry loadings, which probably prevented channelling of the liquid flow within the cake. When determining the optimal end point of dewatering, it is advisable to evaluate the specific power demand and energy consumption as a function of the solid content of the cake rather than as a function of time, because the specific energy consumption becomes unnecessarily high after reaching a certain level of dewatering. The cumulative energy consumption with respect to time and solid content of the cake illustrate clearly the energy intensive nature of cake dewatering in comparison with filtration in the absence of air flow through the cake. In spite of its high energy consumption, vacuum dewatering is a more energy efficient operation than thermal drying, provided that the end point of dewatering is correctly selected and pumping of air through the cake to obtain a negligible moisture reduction is avoided.

Acknowledgements

The authors would like to thank Peter Jones for providing language help and The Finnish Funding Agency for Technology and Innovation (Tekes) for providing funding for the study.

Appendix A. Supplementary material

Supplementary data associated with this article can be found, in the online version, at http://dx.doi.org/10.1016/j.mineng.2016.10.025.

References

Bannwarth, H., 2005. Liquid Ring Vacuum Pumps, Compressors and Systems. Wiley-VCH, Weinheim.

Besra, L., Sengupta, D.K., Roy, S.K., 1998a. Flocculant and surfactant aided dewatering of fine particle suspensions: a review. Miner. Process. Extr. Metall. Rev. 18 (1), 67–103.

Besra, L., Sengupta, D.K., Roy, S.K., 2000. Particle characteristics and their influence on dewatering of kaolin, calcite and quartz suspensions. Int. J. Miner. Process. 59, 89–112.

Besra, L., Singh, B.P., Reddy, P.S.R., Sengupta, D.K., 1998b. Influence of surfactants on filter cake parameters during vacuum filtration of flocculated iron ore sludge. Powder Technol. 96, 240–247.

Blankert, B., Kattenbelt, C., Betlem, B.H.L., Roffel, B., 2007. Dynamic optimization of a dead-end filtration trajectory: non-ideal cake filtration. J. Membr. Sci. 290, 114–124.

Campbell, Q.P., 2006. Dewatering of Fine Coal with Flowing Air Using Low Pressure Drop Systems Ph.D. Thesis. North-West University, South Africa.

Chu, C.P., Lee, D.J., Chang, C.Y., 2005. Energy demand in sludge dewatering. Water Res. 39, 1858–1868.

Coker, A.K., 2007. Ludwig's Applied Process Design for Chemical and Petrochemical Plants. Gulf Professional Publishing, Burlington.

Çengel, Y.A., Boles, M.A., 2015. Thermodynamics: An Engineering Approach. McGraw-Hill Education, New York.

Condie, D.J., Hinkel, M., Veal, C.J., 1996. Modelling the vacuum filtration of fine coal. Filtr. Sep., 825–834 October 1996.

Condie, D.J., Hinkel, M., Veal, C.J., Boissy, K., Leclerc, D., 2000. Modeling the vacuum filtration of fine coal. III. Comparison of models for predicting desaturation kinetics. Sep. Sci. Technol. 35 (10), 1467–1484.

Darcy, H., 1856. Les Fontaines Publiques de la Ville de Dijon. Victor Dalmont, Paris.

Fan, Y., Dong, X., Li, H., 2015. Dewatering effect of fine coal slurry and filter cake structure based on particle characteristics. Vacuum 114, 54–57.

Henriksson, B., 2000. Focus on separation in the mining industry. Filtr. Sep. 37 (7), 26–29.

Jorisch, W., 2015. Vacuum Technology in the Chemical Industry. Wiley-VCH, Weinheim.

Kemp, I.C., 2015. Reducing dryer energy use by process integration and pinch analysis. Drying Technol. 23 (9–11), 2089–2104.

Kemp, I.C., 2012. Fundamentals of energy analysis of dryers. In: Tsotsas, E., Mujumdar, A.S. (Eds.), Modern Drying Technology Volume 4: Energy Savings. first ed. Wiley-VCH, Weinheim.

Kinnarinen, T., Häkkinen, A., Ekberg, B., 2013. Steam dewatering of filter cakes in a vertical filter press. Drying Technol. 31 (10), 1160–1169.

Lee, J.E., 2006. Thermal dewatering (TDW) to reduce the water content of sludge. Drying Technol. 24, 225–232.

Peuker, U.A., Stahl, W., 1999. Scale-up of steam pressure filter. Chem. Eng. Process. 38, 611–619.

Peuker, U.A., Stahl, W., 2000. Dewatering and washing flue gas gypsum with steam. Filtr. Sep. 37 (8), 28–30.

Ripperger, S., Gösele, W., Alt, C., 2012. Filtration, 1. Fundamentals. In: Ullmann's Encyclopedia of Industrial Chemistry. Wiley-VCH, Weinheim.

Rushton, A., Ward, A.S., Holdich, R.G., 2000. Solid-Liquid Filtration and Separation Technology. Wiley-VCH, Weinheim.

Ryans, J., Croll, S., 1981. Selecting vacuum systems. Chem. Eng. December 14, 72–90.

Ryans, J., Bays, J., 2001. Run Clean With Dry Vacuum Pumps. CEP Magazine.

She, H.Y., Sleep, B.E., 1998. The effect of temperature on capillary pressure-saturation relationships for air-water and perchloroethylene-water systems. Water Resour. Res. 34 (10), 2587–2597.

Silla, H., 2003. Chemical Process Engineering: Design and Economics. Marcel Dekker Inc., New York.

Sorrentino, J.A., 2002. Advances in Correlating Filter Cake Properties with Particle Collective Characteristics. Shaker Verlag, Aachen.

Sparks, T., 2012a. Solid-liquid filtration: understanding filter presses and belt filters. Filtr. Sep. 2012 (July/August), 20–24.

Sparks, T., 2012b. Solid-Liquid Filtration: A User's Guide to Minimizing Costs and Environmental Impact, Maximizing Quality and Productivity. Butterworth-Heinemann, Oxford.

Svarovsky, L., 2000. Solid–Liquid Separation. Butterworth & Co, Witham, Essex.

Tao, D., Groppo, J.G., Parekhm, B.K., 2000. Effects of vacuum filtration parameters on ultrafine coal dewatering. Coal Prep. 21 (3), 315–335.

Tarleton, S., Wakeman, R., 2007. Solid/Liquid Separation: Equipment Selection and Process Design. Butterworth-Heinemann, Oxford.

Tien, C., 2012. Principles of Filtration. Elsevier, Oxford.

TSI, 2001. Standard Flow Rate vs. Volumetric Flow Rate. Application Note.

Wakeman, R., 1998. Washing thin and nonuniform filter cakes: effects of wash liquor maldistribution. Filtr. Sep. 35 (2), 185–190.

Wakeman, R., 2007. The influence of particle properties on filtration. Sep. Purif. Technol. 58, 234–241.

Wakeman, R., Tarleton, S., 1990. Modelling, simulation and process design of the filter cycle. Filtr. Sep. 27 (6), 412–419.

Wakeman, R., Tarleton, S., 1999. Filtration Equipment Selection, Modelling and Process Simulation. Elsevier Science Ltd., Oxford.

Wakeman, R., Tarleton, S., 2005a. Solid/Liquid Separation: Principles of Industrial Filtration. Elsevier Advanced Technology, Oxford.

Wakeman, R., Tarleton, S., 2005b. Solid/Liquid Separation: Scale-up of Industrial Equipment. Elsevier Advanced Technology, Oxford.

Zhu, Y.F., Qian, J.Y., Zhang, Q.K., Kuang, J.Y., Gao, X.F., Jin, Z.J., 2016. Experimental analysis on filter press and energy consumption of diaphragm press drying device in chemical post-processing integrated equipment. Case Stud. Therm. Eng. 7, 92–102.

Publication II

Karvonen, V., Huttunen, M., Kinnarinen, T., and Häkkinen, A.
Research focus and research trends in vacuum filtration – bibliographical analysis

Reprinted with permission from
Filtration
Vol. 18, pp. 40–44, 2018

Research focus and research trends in vacuum filtration – Bibliographical analysis

Vesa Karvonen[a*] Manu Huttunen[b], Teemu Kinnarinen[c], Antti Häkkinen[c]

[a] LUT School of Business and Management, Lappeenranta University of Technology,
P.O. Box 20, FI-53851 Lappeenranta, Finland
[b]LUT School of Energy Systems, Lappeenranta University of Technology,
P.O. Box 20, FI-53851 Lappeenranta, Finland
[c]LUT School of Engineering Science, Lappeenranta University of Technology,
P.O. Box 20, FI-53851 Lappeenranta, Finland
[*]Corresponding author. E-mail address: vesa.karvonen@lut.fi

The term vacuum filtration has many contents, depending on the research context. Thousands of researchers work on their own application areas analyzing results based on vacuum filtration. In this article, bibliographical analysis of commonly used scientific databases is used to define the state-of-the art of vacuum filtration research. The search paths used in this bibliographical study open an interesting view to the extensive world of vacuum filtration research. The results show the usefulness of databases offering a relatively rapid and straightforward way to find answers to questions relevant to individual researchers, research organizations or companies.

INTRODUCTION

The objective of this article is to study the research focus and research trends related to vacuum filtration. The scientific subject areas, the most active research organizations on the affiliation level and home countries of the recognized affiliations are investigated as well. The definition of the word filtration according to Oxford English Dictionary[1] is "The action or process of filtering something; an instance of this" and "The action of passing through a filter; the action of percolating or seeping through a porous medium". The Cambridge Dictionary[2] defines filtration as "The act of passing a liquid or gas through a piece of equipment in order to remove solid pieces or other substances". Filtration as a term is relatively old, the first findings are placed to year 1602 in the medical science context[3]. The word filtration is generic. It is used in many fields of science, e.g. medical, technical, agricultural, and social sciences.

The following research questions (RQ) are posed in this article:

RQ 1: What is the position of vacuum filtration in the field of filtration research?
RQ 2: What are the most important scientific subject areas, research affiliations and their home countries in vacuum filtration research?
RQ 3: What are the most important subtitles or subtopics under the term vacuum filtration and their trends?
RQ 4: What kinds of vacuum filtration equipment are used in vacuum filtration research and how are they related to the main research trends?

RESEARCH APPROACH AND DATA ACQUISITION

There are several databases available for scientists, like the Web of Science[4] (WOS), Google Scholar[5] (GS) and Scopus[6]. They all are excellent tools to find articles, authors and topics. Their search characteristics vary, e.g. when searching for "filtration" WOS uses topic search, GS keyword-based search, and Scopus a combined set covering the title, abstract and keywords of the article.

WOS found 359 763, GS 220 000 and Scopus 274 987 hits for the word filtration. Scopus was utilized in this study by using the search mode "all documents". All documents covers articles, reviews, books and book chapters. The research structure and search paths are shown in Figure 1.

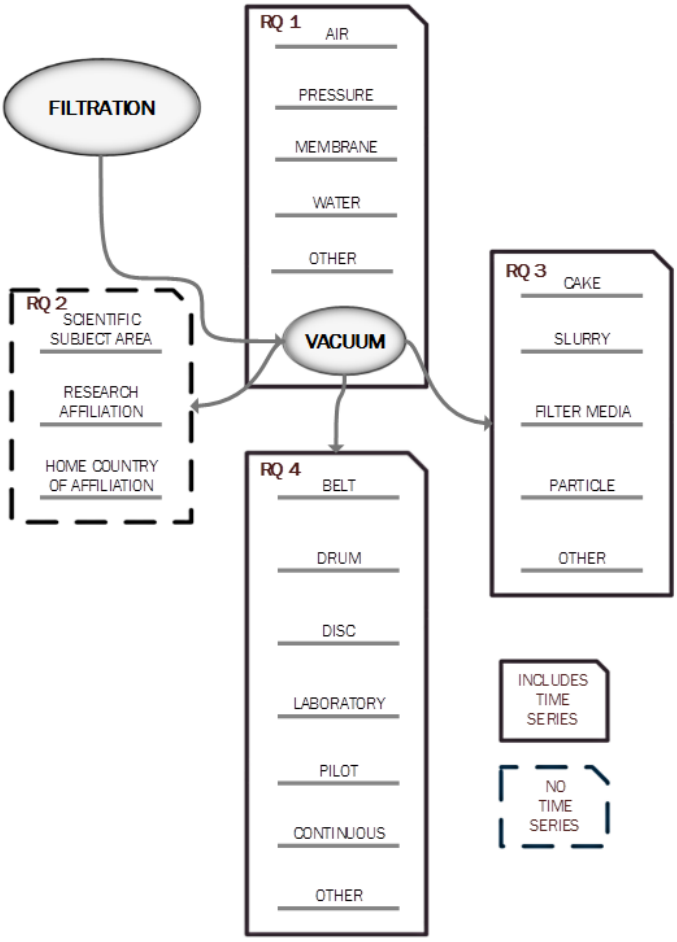

Figure 1. Research structure and search paths.

The data for research question 1 was gathered by combining search words filtration AND the second search words shown in block RQ 1 in Figure 1. The same principle was used for the data

to the other research questions as well (RQ 2 – RQ 4). The data collection for research question 2 was the only RQ where time series were not used. The time series were checked for the following 10-year periods: before 1976, 1976-1986, 1986-1996, 1996-2006 and 2006-2016. The data obtained from the time series enabled a trend analysis showing the relative changes in research activities in the chosen periods. In all data groups, the item "other" is the difference between total hits and the used search words.

RESULTS AND DISCUSSION

This chapter introduces the most important research results and discussion concerning the research questions. Most results are presented in Appendices 1 and 2, the first one showing the data tables, the second one showing the data in the form of figures. Figures 2 and 3 aim at answering RQ 1, Tables 1-3 provide answers to RQ 2, and Figures 4 and 5 represent the data related to RQ 3 and 4, respectively. Besides the data describing the current situation in the field of vacuum filtration, the time series presented in Appendix 2 (Figures 3-5) illustrate the long-term research trends during the past few decades.

The position of vacuum filtration in the field of filtration research

The filtration research carried out globally can be divided into several sub-categories. Figure 2 presents the distribution of some selected filtration-related search words in the field of filtration.

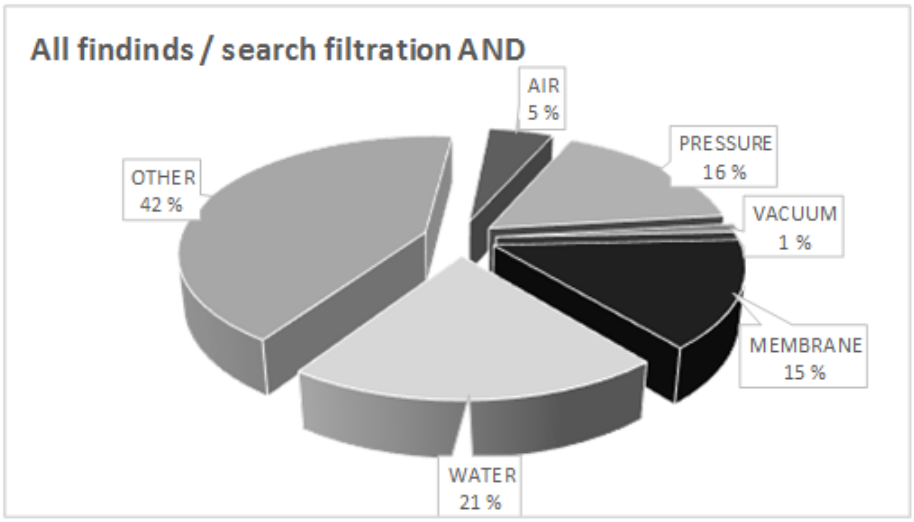

Figure 2. Distribution of selected filtration-related search words in the field of filtration.

Figure 2 shows the research activity in the field of filtration categorized by selected search terms. Water filtration is the biggest of the selected research areas, and pressure filtration is the second. Vacuum filtration research plays a remarkably small role compared to other subtopics in filtration research. Figure 3 shows the search results shown in Figure 2 with time series. The group "other" is not included in this figure. As Figure 3 shows, the research interest in the terms of water, membrane and pressure combined with the term filtration have increased much faster compared

to terms air and vacuum, especially during the last decade, representing over half of the total research activity currently. One reason for that is most probably the importance of pure water, which is one of the focus areas in the United Nations 2030 Agenda[7] policy.

Scientific subject areas, affiliations and their home countries in vacuum filtration research
The TOP-10 list of scientific subject areas in vacuum filtration research (Table 1) shows that engineering, materials science, chemistry, and chemical engineering are the leading categories in this research field. It is interesting to see that vacuum filtration has a role also in many other fields of natural sciences, which indicates generic possibilities for the utilization of the method. This finding might open possibilities to better collaboration between researchers from different fields.

The TOP-10 list of research organizations as scientific article producers (Table 2) show the important role of Asian institutes from China, South Korea and Japan. It seems that some research affiliations are very focused on research in this field.

The TOP-10 list of home countries of the most publishing affiliations (Table 3) shows that the top countries are the United States, China, the United Kingdom, South Korea, and Germany. When comparing the results in Table 3 to the ones in Table 2, it seems that the number of individual research organizations in vacuum filtration research in the United States, the United Kingdom and Germany is big, but they are not as focused on this field of research as their Asian associates.

Subtitles or subtopics under the term vacuum filtration and their trends
Figure 4 shows the overall situation with the selected sub search terms related to vacuum filtration. Particle and cake -related research plays a more important role than slurry, filter media and filtrate issues. When it comes to the time series, Figure 4 shows clearly increased research activity in particle-related issues during the last decades. Note that the group “other” is not included in this figure. One reason to the growth in particle-oriented research may be the great improvements in particle characterization, such as methods used to measure particle size and shape distributions, microscopic characterization techniques, and various on-line measurement methods with advanced software, which offer new possibilities for particle research. At the same time period, cake-related research interest has apparently decreased. The research focus on filtrate and filter has increased evenly during the studied period, but the rate follows the general upward trend in research.

Vacuum filtration equipment in vacuum filtration research and their trends
Figure 5 shows the results of the search linked to vacuum filtration on the equipment level during the last decades. The terms laboratory and continuous received most of the hits with these selected terms. The conventional types of industrial filters, e.g. belt, drum and disc filters, are still important in the research. The biggest growth seems to be in laboratory-related research topics. Interest in drum and belt operated vacuum filter research has dropped to a half during the last three decades. Disc filter research is nowadays on much higher level than the other traditional and commonly used filters. One reason for this might be that there have not been many breakthrough innovations in classic vacuum filter types recently. The very long life span of industrial-size vacuum filtration equipment leads to an incremental development path instead of radical innovations and their market penetration.

CONCLUSIONS

This article contributes to increasing the understanding on different levels related to vacuum filtration. On the general level, the research activity linked to vacuum filtration was compared to the other main categories in the field of filtration research. The study was conducted based on information searched from the Scopus database. Two detailed levels were used in the analysis of research topics on vacuum filtration, the phenomena level and the equipment level. Both levels were also analyzed with respect to certain time periods to find the most important trends covering the long history of research. Not very surprisingly, most of the research where vacuum filtration has an important role is related to various fields of engineering, materials science and chemistry. Chinese research organizations dominate in the list of the most active producers of publications, although the United States is the number one in the corresponding list of countries. The results of the bibliographical analysis suggest also that research activity on cake filtration may be decreasing, while particle-related topics are currently studied more than in the past decades. According to the comparison on the equipment level, the search words "laboratory" and "continuous" have an ascending trend in the time series, but the research activity in pilot scale appears to have been at a relatively constant level for decades. The proper selection of search words and paths is essential in bibliographic analysis. In this study, the data search was executed with maximum three search terms. In order to increase the accuracy of the search, a larger number of words could be incorporated to reduce the possibility of overlapping in the search results. The research approach described in this paper can be developed further to cover other fields of filtration research, which might be useful also for technology providers and process owners in the filtration business. Because of the extremely wide range of filtration research, there is a lot of space to new research openings in this field.

REFERENCES

1. Oxford English Dictionary: http://www.oed.com/view/Entry/70290?redirectedFrom=filtration#eid
2. Cambridge Dictionary: http://dictionary.cambridge.org/dictionary/english/filtration
3. Clowes, W., 1602, *Treat. Cure Struma* 46
4. Web of science: https://apps.webofknowledge.com/
5. Google Scholar: http://scholar.google.fi/
6. Scopus: https://www.scopus.com/
7. UN: http://www.un.org/sustainabledevelopment/development-agenda/

APPENDIX 1

Table 1. Results of the search filtration AND vacuum. TOP-10 list of scientific subject areas according to SCOPUS.

	Scientific subject area	Hits
1	Engineering	1036
2	Materials science	797
3	Chemistry	705
4	Chemical engineering	679
5	Environmental science	377
6	Physics and astronomy	364
7	Medicine	312
8	Biochemistry, genetics and molecular biology	304
9	Energy	213
10	Agricultural and biological sciences	177

Table 2. Results of the search filtration AND vacuum. TOP-10 list of active research organizations according to SCOPUS.

	Research organization	Hits
1	Chinese Academy of Sciences	73
2	Ministry of Education China	63
3	Zhejiang University	27
4	Tsinghua University	25
5	Korea Advanced Institute	22
6	Nanyang Technological University	20
7	Tianjin University	17
8	Sakarya Universitesi	17
9	Shanghai Jiaotong University	17
10	Trinity College Dublin	16

Table 3. Results of the search filtration AND vacuum. TOP-10 list of home countries of vacuum filtration research affiliations.

	Country	Hits
1	United States	679
2	China	516
3	United Kingdom	126
4	South Korea	123
5	Germany	117
6	Japan	96
7	Australia	91
8	Canada	88
9	Russian Federation	66
10	India	65

APPENDIX 2

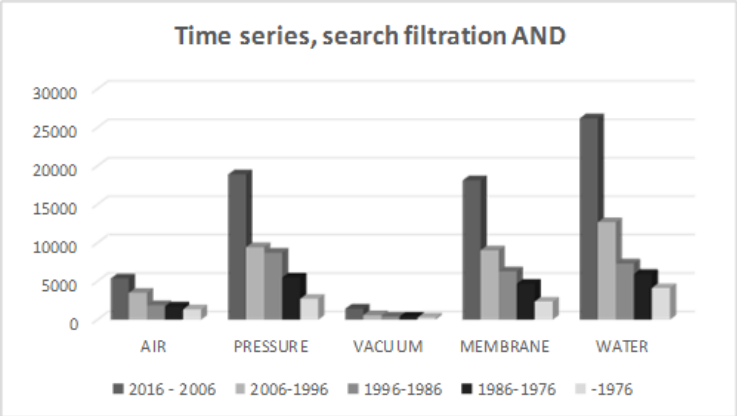

Figure 3. Research trends of selected search words in filtration research.

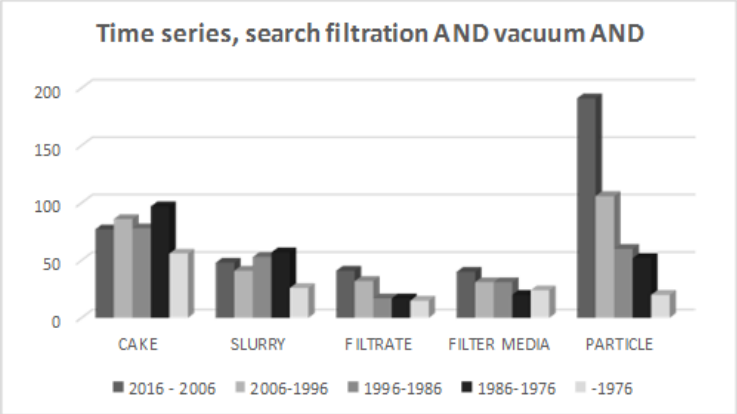

Figure 4. Search results of the combination filtration AND vacuum added by sub search words.

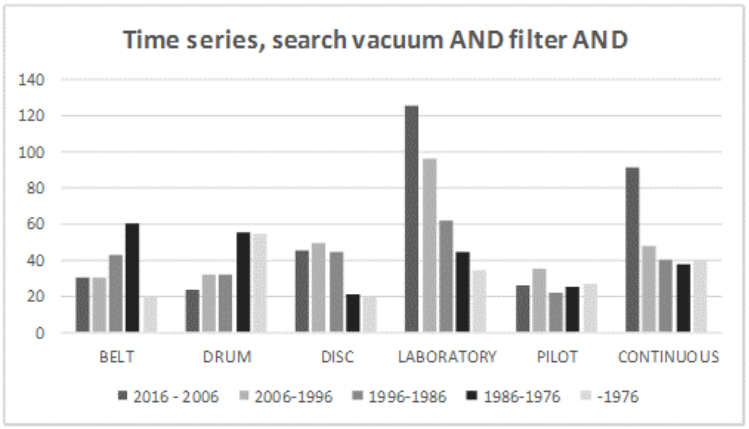

Figure 5. Search results of the combination vacuum AND filter added by sub search words.

Publication III

Huttunen, M., Nygren, L., Kinnarinen, T., Ekberg, B., Lindh, T., Ahola, J., Karvonen, V., and Häkkinen, A.
Specific energy consumption of vacuum filtration: Experimental evaluation using a pilot-scale horizontal belt filter

Reprinted with permission from
Drying Technology
2019

Specific energy consumption of vacuum filtration: Experimental evaluation using a pilot-scale horizontal belt filter

Manu Huttunen[a]*, Lauri Nygren[a], Teemu Kinnarinen[b], Bjarne Ekberg [b], Tuomo Lindh[a], Jero Ahola[a], Vesa Karvonen[b], Antti Häkkinen[b]

[a]LUT School of Energy Systems, Lappeenranta University of Technology, 53850 Lappeenranta, Finland
[b]LUT School of Engineering Science, Lappeenranta University of Technology, 53850 Lappeenranta, Finland
*Corresponding author. E-mail address: manu.huttunen@lut.fi

Abstract

Horizontal belt vacuum filters are used for continuous solid-liquid separation in a wide variety of industrial processes. Despite the low pressure difference (usually $\Delta p < 0.8$ bar), the high air pumping requirement to maintain the pressure difference results in considerable energy consumption. In this paper, the specific energy consumption of vacuum filtration and air flow rates of a pilot-scale horizontal belt filter unit are investigated. The results show that a claw-type vacuum pump consumes only half the energy compared to a conventional liquid ring vacuum pump. A comparison between the specific energy consumption of vacuum filtration and thermal drying of the filter cake to zero moisture revealed that vacuum filtration accounted for less than half of the total energy consumption in the applied experimental conditions at Δp = 0.2–0.5 bar. The majority of the total pumping requirement of the pilot-scale filter resulted from leaks, and only 2–25 % of the air flow found its way through the cake and the filter medium. The results suggest that there is a combination of the pressure difference level and the mass of cake deposited per unit area that together with thermal drying consumes the least amount of energy per solids mass.

Keywords: Energy conservation; Specific energy consumption; Vacuum filtration; Horizontal belt vacuum filter; Cake dewatering; Thermal drying

1. Introduction

In recent years, the importance of energy consumption and energy efficiency of filtration processes has been recognized. Research on a limited number of filtration applications with respect to energy consumption has been reported, including filtration of fine calcium carbonate with an integrated filtration equipment [1], membrane filtration processes for harvesting of microalgae [2–4], and desalination of water [5–12]. However, the energy consumption of vacuum filtration in solid liquid separation processes has not been discussed in the literature, with the exception of the authors' laboratory-scale study [13] on the isentropic energy consumption of vacuum dewatering. Research trends and research focus in vacuum filtration has been studied by Karvonen et al. [14].

Vacuum belt filters are used in minerals processing, mining, and various fields of chemical industry for solid-liquid separation of slurries containing relatively coarse solids. The main benefits of vacuum belt filters include continuous operation, good opportunities for cake washing, and ease of monitoring and control of the separation process [15, 16]. The solids throughput of a vacuum belt filter depends only on the solids content and the feed rate of the slurry, whereas the final moisture content of the cake also depends on other properties of the slurry, such as particle size distribution and particle shape, and operating factors of the filtration process, such as the applied pressure difference, filtration time and dewatering time. In most industrial installations, the moisture content of the product is the quality parameter that sets limits on the production capacity and determines the energy consumption of the filter. The energy issues have become increasingly important in the industry as companies attempt to reduce their operational costs and environmental impacts.

Vacuum pumps typically consume most of the energy required by vacuum filters. The energy consumption of a vacuum pump is typically 2–15 kW/m^2 of the filter area, while other devices such as cloth drive and filtrate pumps consume only 0.2–0.4 kW/m^2 [17]. Therefore, optimization of the vacuum pump energy consumption can often lead to significant energy savings. When the filter cake is not washed, the separation process in a vacuum belt filter can be divided into two stages: filtration and dewatering. The aim of the filtration stage is to remove liquid from the slurry until a filter cake is formed. Problems in the filtration and dewatering stages may be caused for instance by the presence of fine particles, a wide particle size distribution, and an unfavorable particle shape [18, 19]. After the cake formation, air displaces liquid from the largest pores of the cake, provided that a cake-specific threshold pressure is exceeded [20, 21], and starts to flow through the cake at an increasing flow rate as a larger fraction of the total pore volume becomes empty of liquid [22]. As the air flow increases, the rate of dewatering decreases gradually until the saturation of the cake reaches an irreducible level [20, 23]. The energy consumption per mass unit of liquid removed increases sharply at this stage as a result of the slowdown of the liquid flow rate and acceleration of the air flow rate as

demonstrated previously by the authors [13]. The final moisture content of the cake depends on the cake properties and the applied pressure [24–26], the former being also influenced by the latter. According to Kemp [27, 28], a primary method of reducing the energy consumption of thermal drying of materials is efficient upstream dewatering prior to the drying stage.

The main objective of this paper is to investigate the energy consumption and enable energy conservation of cake dewatering using a pilot-scale vacuum belt filter equipped with the instrumentation required for process control and data acquisition. In addition to examining the influence of the process variables on the specific energy consumption, the paper provides information of energy consumption of two different types of vacuum pumps and shows a comparison between air dewatering and thermal drying of filter cakes. The effects of the mass of cake deposited per unit area on the moisture content of the filter cake, the energy consumption of filtration, and the air flow through the filter cake are studied. However, the influences of the particle size distribution and slurry solids content on the energy consumption fall outside the scope of this paper. A further objective of this paper is to compare the energy consumption of vacuum dewatering with the energy consumption of subsequent thermal drying.

2. Theory

2.1. Determination of filtration characteristics

The filtration equation used for calculation of the average specific cake resistance in constant pressure is based on Darcy's law, and after integration the equation becomes [29]

$$\frac{t}{V} = \frac{\alpha_{\mathrm{av}} \mu c}{2A^2 \Delta p} V + \frac{\mu R_m}{A \Delta p}, \tag{1}$$

where t is time elapsed since the start of the constant pressure period, V is the volume of filtrate, α_{av} is the average specific resistance of the cake, μ is the dynamic viscosity of filtrate, c is the mass of dry cake divided by the volume of filtrate, A is the effective filtration area, Δp is the pressure difference, and R_m is the resistance of the filter medium.

When only the resistance of the filter cake is considered, the equation can be simplified to the form

$$\alpha_{\mathrm{av}} = \frac{2aA^2 \Delta p}{\mu c}, \tag{2}$$

where a is the slope of the linear part of the experimentally obtained curve t/V vs. V.

For practical cases of compressible filtration, the variations of α can be presented by a power law type relationship [30]

$$\alpha = \alpha_0 \Delta p^n, \quad (3)$$

where α_0 is the specific resistance at unit applied pressure, which is obtained together with n by extrapolation and calculation from experimental data.

The average cake porosity can be calculated either by dividing the void volume of the cake by the total volume of the cake, or by subtracting the solids volume from the total volume using the formula [30]

$$\varepsilon_{\mathrm{av}} = 1 - \frac{m_{\mathrm{s}}}{\rho_{\mathrm{s}} A L}, \quad (4)$$

where m_{s} is the mass of solids, ρ_{s} is the density of solids, and L is the thickness of the filter cake. Equation (4) can be written for the case of a horizontal belt filter as

$$\varepsilon_{\mathrm{av}} = 1 - \frac{s q_{\mathrm{m,sl}}}{\rho_{\mathrm{s}} h_{\mathrm{B}} v_{\mathrm{B}} L}, \quad (5)$$

where s is the mass fraction of solids in the slurry, $q_{\mathrm{m,sl}}$ is the feed rate of the slurry in kg/s, ρ_{s} is the density of solids, h_{B} is the filter belt width, and v_{B} is the filter belt linear velocity.

2.2. Cake dewatering

Darcy's law is based on experiments on water flow through a bed of sand placed in a vertical iron pipe. The equation describing the observed relationship can be written as

$$u = \frac{-k}{\mu} \frac{dp}{dz}, \quad (6)$$

where dp is the dynamic pressure difference across the thickness dz of a porous medium of the permeability k, and u is the superficial velocity of liquid with a viscosity μ flowing through the bed [30].

In vacuum filtration, two immiscible fluids, gas and liquid, flowing through the filter medium form their unique pathways, which alter as the fluid saturation changes during filtration. As the liquid saturation is reduced to the minimum, the liquid pathways become discontinuous, the flow of the wetting fluid ceases, and the cake is at its irreducible wetting fluid saturation [30].

When Darcy's law is applied to each flowing phase, filtrate (l), and gas (g):

$$u_{\mathrm{l}} = \frac{-k_{\mathrm{l}}}{\mu_{\mathrm{l}}} \frac{dp_{\mathrm{l}}}{dz}, \quad (7)$$

and

$$u_{\mathrm{g}} = \frac{-k_{\mathrm{g}}}{\mu_{\mathrm{g}}} \frac{dp_{\mathrm{g}}}{dz}, \tag{8}$$

where dp_{l} and dp_{g} are the dynamic pressure differences across the thickness dz of a porous medium of permeabilities k_{l} and k_{g}, and u_{l} and u_{g} are the superficial velocities of the fluid with viscosities μ_{l} and μ_{g} flowing through the bed. Each phase has its own associated pressure, viscosity, and permeability. The difference between the two pressures is the capillary pressure, which is relative to the radius of the curvature of the interface between the phases, and it is dependent on the saturation of each phase. The terms k_{l} and k_{g} are effective permeabilities of the liquid and gas phases, respectively, and they are related to the permeability of the saturated medium through

$$k_{\mathrm{rl}} = k_{\mathrm{l}}/k \text{ and } k_{\mathrm{rg}} = k_{\mathrm{g}}/k, \tag{9}$$

where k_{rl} *and* k_{rg} are the cake relative permeabilities to the liquid and gas phases, respectively [30].

Darcy's equations for the flow of the two phases through the cake combined with the material balances for each phase give

$$\frac{\partial(\varepsilon S)}{\partial t} = -\frac{\partial u_{\mathrm{l}}}{\partial z} \tag{10}$$

and

$$\frac{\partial\left(\varepsilon\rho_{\mathrm{g}}(1-S)\right)}{\partial t} = -\frac{\partial\left(\rho_{\mathrm{g}}u_{\mathrm{g}}\right)}{\partial z}. \tag{11}$$

Using Eqs. (1) – (5) and solving the partial differential equations with boundary conditions for a particular operating point of the vacuum filter, one can calculate the final saturation of the filter cake and the gas and liquid flow through the cake. To facilitate these calculations, the equations have been solved, presented graphically, and curve fitted to a dimensionless form by [30]. Using these fittings, the reduced saturation S_{R} and the gas flow rate u_{g} through the cake can be estimated with the following simplified calculations.

Dimensionless terms used to calculate dewatering dynamics are written in terms of the average permeability k_{av} of the filter cake

$$k_{\mathrm{av}} = \frac{1}{\alpha_{\mathrm{av}}\rho_{\mathrm{s}}(1-\varepsilon_{\mathrm{av}})}, \tag{12}$$

where α_{av} is the average specific cake resistance, ρ_{s} is the density of solids, and $\varepsilon_{\mathrm{av}}$ is the average cake porosity.

Dimensionless deliquoring time θ is defined by

$$\theta = \frac{k_{\mathrm{av}} p_{\mathrm{b}}}{\mu_{\mathrm{l}} \varepsilon_{\mathrm{av}} (1 - S_{\infty}) L^2} t_{\mathrm{d}}, \tag{13}$$

where p_{b} is the threshold pressure at which the flow of the liquid begins, S_{∞} is the irreducible saturation at which the flow of the liquid ceases, L is the height of the cake, and t_{d} is the deliquoring time in seconds.

The threshold pressure p_{b} can be calculated by the equation

$$p_{\mathrm{b}} = \frac{4.6(1 - \varepsilon_{\mathrm{av}})\sigma}{\varepsilon_{\mathrm{av}} x}, \tag{14}$$

where σ is the cake liquid surface tension and x is the particle mean diameter.

The dimensionless gas flux u_{g}^* is calculated by

$$u_{\mathrm{g}}^* = \frac{u_{\mathrm{g}} \mu_{\mathrm{g}} L}{k_{\mathrm{av}} p_{\mathrm{b}}}. \tag{15}$$

the dimensionless pressure p^* is calculated by dividing the pressure p by the threshold pressure:

$$p^* = \frac{p}{p_{\mathrm{b}}}. \tag{16}$$

A value for the filter cake saturation is obtained by first determining a value for the reduced saturation S_{R} from Fig. 1 and applying it to the equation

$$S = S_{\infty} + S_{\mathrm{R}}(1 - S_{\infty}). \tag{17}$$

To evaluate a design gas flow rate u_{g} for vacuum pump or blower specification, the following calculations can be carried out. The dimensionless pressure difference across the cake is

$$p_{\mathrm{g}}^* = p_{\mathrm{gei}}^* - p_{\mathrm{geo}}^* = \frac{p_{\mathrm{B}}}{p_{\mathrm{b}}} - \frac{p_{\mathrm{B}} - \Delta p_{\mathrm{d}}}{p_{\mathrm{b}}} = \frac{\Delta p_{\mathrm{d}}}{p_{\mathrm{b}}}, \tag{18}$$

where the subscript g denotes pressure in the gas phase, i indicates the entry surface of the cake and o the exit surface of the cake in terms of gas flow direction, and e stands for the actual filter installation. The averaged dimensionless gas flow rate $\bar{u}_{\mathrm{g}}^*$ is obtained from Fig. 2, and the superficial gas velocity u_{g} is calculated by using Eqs. (19) and (20)

$$\bar{u}_{\mathrm{ge}}^* = \bar{u}_{\mathrm{g}}^* \frac{p_{\mathrm{go}}^*}{p_{\mathrm{geo}}^*} \left[\frac{\left(p_{\mathrm{geo}}^*\right)^2 - \left(p_{\mathrm{gei}}^*\right)^2}{\left(p_{\mathrm{go}}^*\right)^2 - \left(p_{\mathrm{gi}}^*\right)^2} \right], \tag{19}$$

$$u_{\mathrm{g}} = \bar{u}_{\mathrm{ge}}^* \frac{k_{\mathrm{av}} p_{\mathrm{b}}}{\mu_{\mathrm{g}} L}, \tag{20}$$

where $p_{\mathrm{gi}}^* = 100$, $p_{\mathrm{go}}^* = 100 - p_{\mathrm{g}}^*$ and μ_{g} is the gas viscosity.

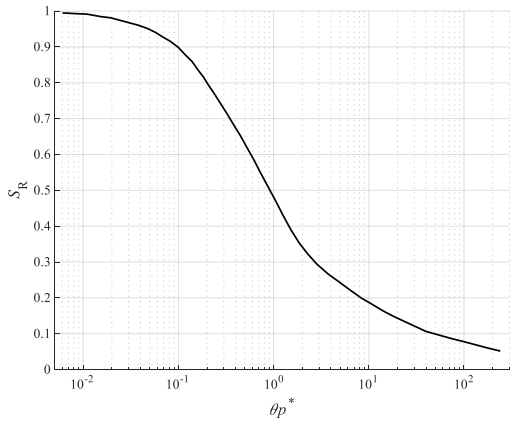

Fig. 1. Reduced saturation S_R of a filter cake as a function of the product of the dimensionless deliquoring time θ and the dimensionless pressure p^* according to [30].

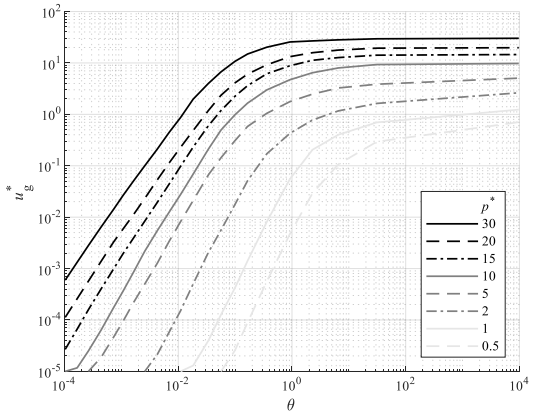

Fig. 2. Averaged dimensionless gas flow rate through the filter cake $\bar{u}_g^*$ as a function of the dimensionless deliquoring time θ and the pressure p^* according to [30].

2.3. Power demand in vacuum filtration

In vacuum filtration, the desired pressure difference across the filter cake is generated by a vacuum pump. The ideal isentropic power demand P_S for a given inlet volumetric flow rate $q_{V,in}$ generated by the vacuum pump can be calculated by the equation

$$P_{\mathrm{S}} = \frac{k}{k-1} q_{\mathrm{V,in}} p_{\mathrm{in}} \left[\left(\frac{p_{\mathrm{out}}}{p_{\mathrm{in}}} \right)^{\frac{k-1}{k}} - 1 \right], \tag{21}$$

where p_{in} is the pressure at the inlet of the vacuum pump, p_{out} is the outlet pressure of the vacuum pump, and k is the isentropic exponent. If the vacuum pump is cooled, the isothermal power demand P_{T} can be used to describe the ideal process, and it can be calculated using equation

$$P_{\mathrm{T}} = q_{\mathrm{V,in}} p_{\mathrm{in}} \ln \left(\frac{p_{\mathrm{out}}}{p_{\mathrm{in}}} \right). \tag{22}$$

Depending on whether the isothermal or isentropic compression is assumed, the required vacuum pump shaft power can be determined by the equation

$$P_{\mathrm{shaft}} = \frac{P_{\mathrm{T}}}{\eta_{\mathrm{T}}} \quad \text{or} \quad P_{\mathrm{shaft}} = \frac{P_{\mathrm{S}}}{\eta_{\mathrm{S}}}. \tag{23}$$

2.4. Power demand in thermal drying

If the moisture content of the filter cake after vacuum filtration is not low enough, additional drying of the product is required. In thermal drying, the moisture is removed from the cake by evaporation. The ideal power required for evaporation can be described by the equation [28]

$$P_{\mathrm{v}} = q_{\mathrm{m,v}} \Delta H_{\mathrm{v}} = q_{\mathrm{m,s}} \left(\frac{1}{s_{\mathrm{in}}} - \frac{1}{s_{\mathrm{out}}} \right) \Delta H_{\mathrm{v}}, \tag{24}$$

where q_{m} is the mass flow, ΔH_{v} is the latent heat of evaporation, and s is the weight-based solids content of the cake. The subscript v denotes vapor and s solids. For ideal energy consumption, it is assumed that all the supplied energy goes to the evaporation of water removed from the cake. This includes the energy required for heating up the water from 20 to 100 °C and for evaporation (ΔH_{v} = 2400 kJ/kg). The energy consumed in heating of solids is neglected.

The most commonly encountered dryer in the mineral processing industry is the rotary dryer, the thermal efficiencies of which typically range from 35 to 70 % [31]. In addition to rotary dryers, other convection type dryers suitable for filter cake drying are for instance flash, fluid bed, and tray dryers [31]. According to [28], convective dryers tend to have a low thermal efficiency (often below 50 %).

3. Materials and methods

3.1. Slurry

The slurry with a total solids content of 25 wt.% was prepared from Nordkalk Parfill H80 dry solids and tap water. The solids consisted mainly of ground calcium carbonate (89 %)

and small amounts of other components containing for instance Si, Al, Mg, and Na. The volumetric particle size distribution of the solids, measured by using a Malvern Mastersizer 3000 laser diffraction analyzer and shown as the average of several trials, is presented in Fig. 3. Mixing tanks equipped with propeller type impellers and baffles were used to keep the slurry mixed during the experiments.

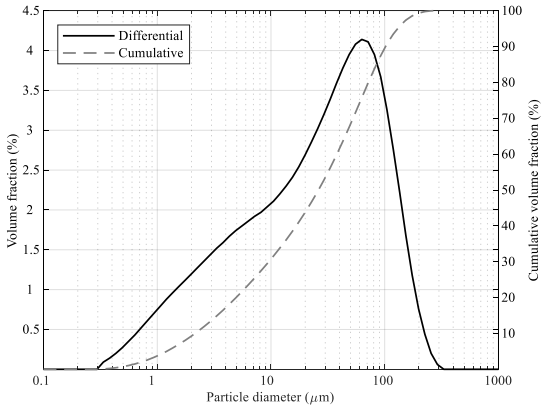

Fig. 3. Particle size distribution of Nordkalk Parfill H80.

3.2. Horizontal belt vacuum filter and related instrumentation

The horizontal belt vacuum filter used in this study and its device setup and instrumentation are illustrated in Fig. 4. The main operational parts of the machine are the slurry infeed, filter belt, vacuum generation, and filtrate handling. The physical layout of the devices is divided into three levels to enable sufficient vertical moving space for the filtrate level inside the barometric leg. The filtrate level moves inside the barometric leg according to the pressure difference applied to the filter. Manipulation of the operating point of the filter is implemented with the help of frequency-converter-operated pumps and a belt motor. The slurry infeed is controlled by two hose pumps. The first one circulates the slurry to avoid the settling of solids in the pumping line. The second pump controls the infeed flow to the filter belt, the feed flow rate being linearly proportional to the rotation speed of the pump. A vacuum is generated either with a liquid ring vacuum pump or with a claw vacuum pump. The filter has a reciprocating tray. The applied pressure difference joins the tray with the filter cloth, and thus, the tray moves with the filter belt for its operating distance of 10 cm. After this distance, the vacuum is cut off from the tray, the tray is returned to the starting point of the movement, and the vacuum is reapplied. The filter effective length is 2.1 m and the width is 0.1 m. With the liquid

ring vacuum pump, the filter is able to reach vacuum levels up to 0.4 bar and up to 0.6 bar with the claw vacuum pump.

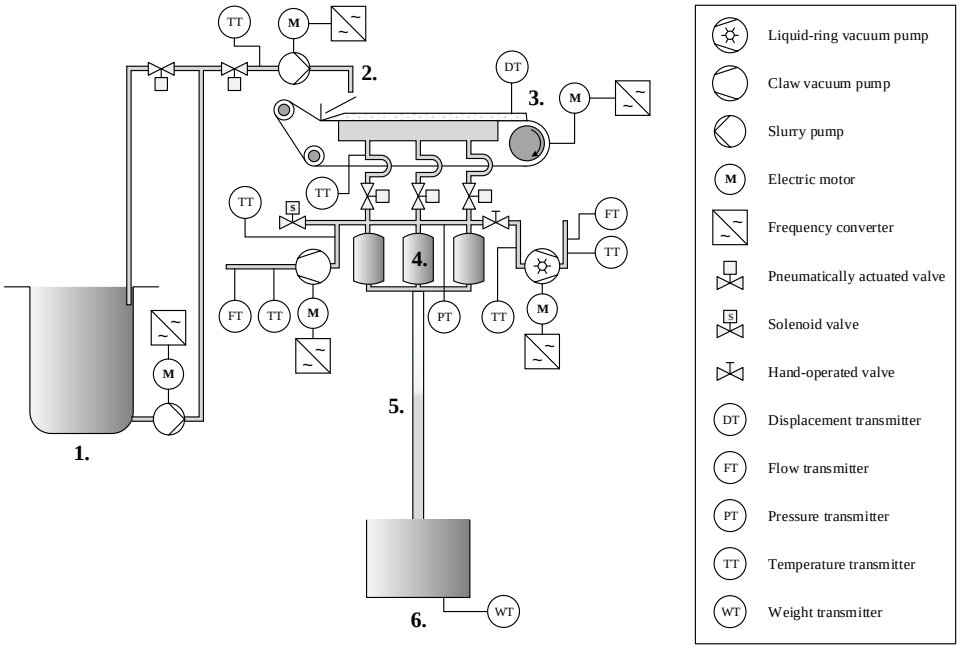

Fig. 4. Horizontal belt vacuum filter device setup and instrumentation: 1) slurry tank, 2) slurry infeed, 3) cake discharge, 4) filtrate intermediate tanks, 5) barometric leg, and 6) filtrate collection tank.

Frequency converter operation of the filter motors enables monitoring of energy consumption and calculation of the belt speed and the slurry infeed rate. Ideal energy consumption required to generate a pressure drop can be calculated on the basis of the vacuum pump flow rate and vacuum chamber pressure measurements. Vacuum pump flow rates were measured using flow velocity sensors based on the measuring principle of a thermal anemometer. The temperature measurements of the slurry infeed, the filtrate, and the vacuum pump inlet and outlet flow were collected. Filtrate production was measured using a digital scale for the filtrate collection tank. The cake thickness at the end of the dewatering phase was measured using a laser displacement sensor.

The separation process in the filter is continuous, including the slurry distribution on the belt, filtration until the cake is formed, and dewatering (i.e. drying) until the cake is discharged at the end of the belt. The discharged cake is collected in vessels located below the filter. After the cake discharge, the filter belt is spray washed with a large amount of

water until no remaining solid particles can be detected on the belt. Thus, the effect of the filter belt wash on the product quality and energy consumption is outside the scope of this study. There is also an option for cake washing and operation in an inert gas atmosphere, but those options are omitted in this study. The devices used for pilot-scale filter instrumentation are presented in Table 1.

3.3. Filtration experiments

The aim of the experimental work was to investigate the effect of the main process variables on the properties of the filter cake, as well as the air and energy consumption of dewatering, and to compare the laboratory results with those obtained by using the pilot-scale filter.

Experiments with a Büchner apparatus were conducted to determine the specific cake resistance and porosity. Pilot-scale experiments were carried out to study cake dewatering with a horizontal belt vacuum filter. A set of twelve experiments were carried out to study the effect of pressure difference and the mass of cake deposited per unit area w on the weight-based moisture content of the filtered cake and on the energy consumption of vacuum filtration. The mass of cake deposited per unit area was controlled by adjusting the slurry infeed rate and the belt speed. The experimental conditions are presented in Table 2.

4. Results

4.1. Filtration properties of the slurry

Results from the Büchner apparatus experiments are presented in Table 3. The solid content of the slurry, s, was constant 25 wt.% in all experiments. Shrinking of the filter cake was observed in experiments 4–9 at the beginning of the dewatering stage. The shrinking of the filter cake causes the average porosity of the cake to change during the dewatering stage. For this reason, a value of the average porosity and the cake thickness at the time of transition from the separation stage to the dewatering stage, $\varepsilon_{av,\,tr,\,calc}$, was also calculated using the volume of solids and liquid at this instance with the assumption that the cake was completely saturated. This value could be considered the initial value used for calculating the average porosity in the dewatering stage. The average specific cake resistance α_{av} was the higher, the larger was the filtration pressure difference, and thus, it can be concluded that the filter cakes were slightly compressible. The values of α_{av} were typical for vacuum filtration of calcium carbonate [32]. The capillary tests gave an average value for the irreducible saturation S_∞ of 0.61.

Results from the experiments using a pilot-scale horizontal belt filter with a liquid ring vacuum pump are presented in Table 4. The manipulated filtration variables are the

pressure difference Δp and the mass of cake deposited per unit area w, which was adjusted with the filter belt speed v_{belt} and the slurry infeed rate. The presented properties of the filter cakes are the filtration time t_f and the distance z_f, the dewatering time t_d and the distance z_d, the cake thickness L, the average porosity ε_{av}, the throughput of the cake solids M_s, and the moisture content M. The average porosity is calculated by using the cake thickness measurement at the end of the dewatering period.

The results show that a lower moisture content and average porosity of the filter cake are achieved by increasing the pressure difference. Furthermore, the moisture content and the average porosity vary depending on the mass of cake deposited per unit area w, the dewatering time, and the distance. The lowest moisture content and average porosity of the filter cake for a given pressure difference level are achieved when the dewatering time is longest. When comparing Tests 6 and 8, and 9 and 12 within the same pressure difference level for which the dewatering time is close to each other or exactly the same, it is observed that a lower moisture content is achieved with a thicker cake. Comparing the experiments within the same pressure difference levels of 0.3 and 0.4 bar with the w of 4.2 to 5.4 and 12.2 kg/m^2, a lower moisture content is achieved with the thicker filter cake while the shorter dewatering time and distance would indicate the contrary. This would suggest that there is an optimum value for the mass of cake deposited per unit area when seeking for the best dewatering performance. A similar observation was made with a different material in the previous study of the authors [13]. It can be speculated that the reason for a poor dewatering performance of the thinnest cakes may result from the uneven air flow, which, in turn, could be caused by the lack of a sufficient capillary structure in such cakes. Additionally, one factor omitted in this study is the effect of the filter medium: it might be possible that thin cakes are not effectively dewatered because the whole height profile of the cake is simply too close to the cake/medium interface, where the cake properties do not facilitate effective dewatering. In this study, the series w of 9.5 kg/m^2, which also has the longest dewatering times, gives the best results in terms of moisture content.

Results from the experiments using a pilot-scale horizontal belt filter with a claw vacuum pump are presented in Table 5. Similar results as with the liquid ring vacuum pump were achieved with the claw vacuum pump; a lower moisture content is achieved with a thicker cake. For this experiment series with Δp between 0.2 and 0.4 bar, the w of 10.3 kg/m^2 having the longest dewatering times gives the best results in terms of moisture content after dewatering. The lowest average porosity values for the claw vacuum pump experiments remained higher compared with the liquid ring pump experiments. The main reason for this is probably the slightly higher solids content of the slurry in the experiments with the claw pump. Increasing the solids content of the slurry typically results in a more rapid cake formation and a higher porosity.

4.2. Air flow rates

This is an original manuscript of an article published by Taylor & Francis in Drying Technology on March 7, 2019, available online: http://www.tandfonline.com/doi/full/10.1080/07373937.2019.1581214.

Volumetric air flow rates calculated from the flow velocity measurements of the pilot-scale experiments are presented in Table 6. To determine the leak flow of the horizontal belt filter vacuum system for the pressure difference region used in the experiments, a series of test runs were conducted. The infeed of the slurry and the speed of the filter belt were adjusted so that the filter cake was 100 % saturated over the whole area affected by the pressure difference. In this operating point, the fluid flow through the cake was assumed to be so low that it can be ignored and the air flow through the vacuum pump can be considered to originate from the vacuum system leaks. Linear correlation for the vacuum system leak flow with respect to the pressure difference across the filter cake is presented in Fig. 5. The behavior of vacuum system leaks in a standard volumetric air flow through the vacuum pump is linear as a function of pressure difference across the filter cake with a root-mean-squared error of 0.414, R-squared 0.998, and a p-value of $3.1 \cdot 10^{-5}$. Test 4 in both experiment series has a fully saturated filter cake along the whole distance of the filter belt. The air flow rate through the cake is zero in these tests, and the total air flow value serves as a reference point in determining the leak flow with the linear regression model for the other tests in the series.

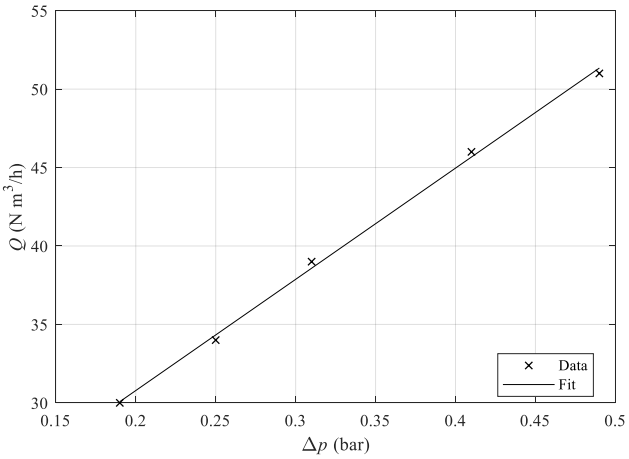

Fig. 5 Linear correlation for the leak air flow of the vacuum system of the pilot-scale belt filter with respect to the pressure difference across the filter cake.

The corresponding dimensionless dewatering time, pressure, and air flow rate for the experiments calculated using Eqs. (2)–(5), (12)–(16), and (18)–(20) and the results from Table 3–Table 6 are presented in Fig. 6. This representation of the results is analogous to Fig. 2. The average porosity value used for the calculations is an average value of $\varepsilon_{\mathrm{av,\,tr,\,calc}}$ of the Büchner experiments 1–9 (excluding the outlier Test 7) and the final average

This is an original manuscript of an article published by Taylor & Francis in Drying Technology on March 7, 2019, available online: http://www.tandfonline.com/doi/full/10.1080/07373937.2019.1581214.

porosity, ε_{av}, of each pilot filter test. By comparing the results presented in Fig. 2 with the same mass of cake deposited per unit area w in Fig. 6, it can be seen that the material used in the pilot-scale experiments shows a similar trend of the averaged dimensionless air flow rate as the theoretical curve. However, when the mass of cake deposited per unit area is increased from 4.6 to 10.3 kg/m^2, the averaged dimensionless air flow rate increases even if the dimensionless pressure decreases at the same time. Fig. 6 together with Table 6 also shows that increasing the mass of cake deposited per unit area within the same pressure difference level Δp increases the average air flux through the cake $u_{a,\,cake}$.

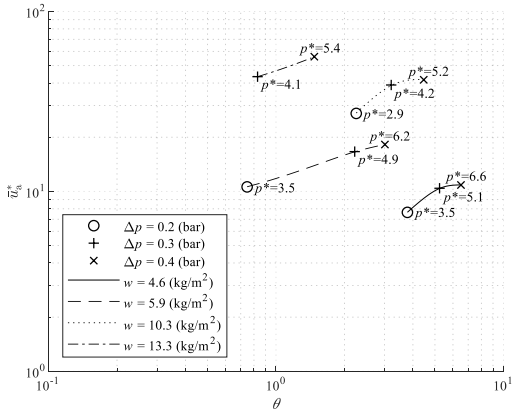

Fig. 6 Dimensionless air flow rates $\bar{u}_a^*$ with respect to the dimensionless deliquoring time θ for the horizontal belt filter and claw vacuum pump experiments calculated using Eqs. (2)–(5), (12)–(16), and (18)–(20).

4.3. Variations in the pressure difference

The cut-off and cut-in of suction to the vacuum box for the duration of the tray return movement induces transients to the pressure difference between the vacuum box and the ambient atmospheric pressure affecting through the filter cake as well as to the standard volumetric air flow rates. These transients, again, cause oscillation to the water level inside the barometric leg. The effect of these phenomena on the pressure difference can be seen in Fig. 7 (a) and on the standard volumetric air flow rates in Fig. 7 (b). To limit the water level oscillations inside the barometric leg, a diameter of 7 cm is selected for the barometric leg and an adjustable and controllable bypass valve is used to let air flow to the vacuum pump during the vacuum box suction cut-off. As can be seen in Fig. 7 (b),

the slowdown in the air flow rate induced by the resistance of the bypass valve is more significant at higher pressure differences and flow rates. Fig. 7 (a) illustrates the corresponding increase in the pressure difference.

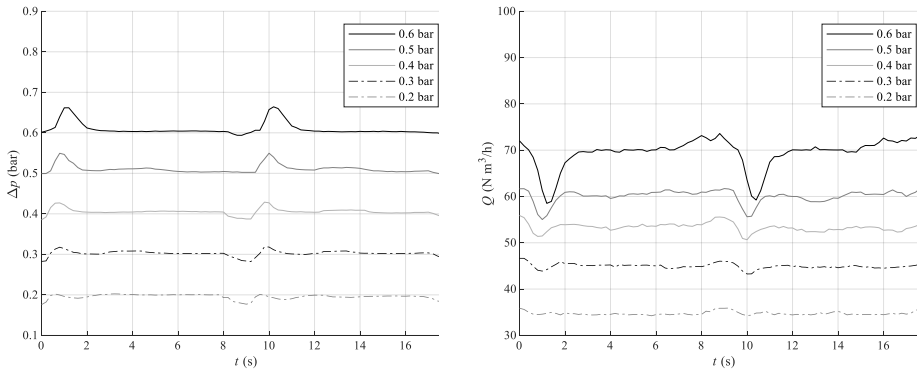

a) b)

Fig. 7 Example of transients in the pressure difference affecting the filter cake a) and in the standard volumetric air flow rate through the vacuum pump b). A sequence from claw pump experiments 1, 5, 9, 13, and 15.

4.4. Product quality and energy consumption

Fig. 8–10 present the specific energy consumption, $E_s = E/m_s$, for the pilot-scale horizontal belt filter experiments. Fig. 8 depicts the total ideal specific energy consumption for the claw pump experiments calculated using the air flow measurements and the isentropic power demand (Eq. (21)) and thermal drying to the zero moisture content with a thermal efficiency $\eta_{th} = 100$ % (Eq. (24)). The minimum total ideal energy consumption is achieved with Test 3 and values close to this one with Tests 6, 7, and 8 (see Table 6). Keeping the pressure difference and the belt speed fixed and increasing the mass of cake deposited per unit area decreases the ideal specific energy consumption of vacuum filtration. Moreover, with the exception of Test 4, where the filter cake does not have the chance to be dewatered with the vacuum filter, the total ideal energy consumption is decreased.

This is an original manuscript of an article published by Taylor & Francis in Drying Technology on March 7, 2019, available online: http://www.tandfonline.com/doi/full/10.1080/07373937.2019.1581214.

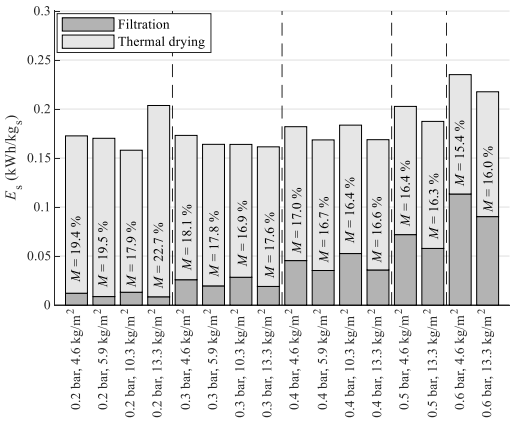

Fig. 8 Ideal specific energy consumption for achieving zero moisture content (M = 0 %) distinguishing between vacuum filtration and thermal drying (thermal efficiency η_{th}=100 %). The moisture content after vacuum filtration is shown for each experiment.

Fig. 9 presents the specific energy consumption of solid-liquid separation using a horizontal belt vacuum filter with a liquid ring vacuum pump in the first stage and thermal drying in the second stage to obtain the desired final zero moisture content. The corresponding results for the dry claw vacuum pump experiments are shown in Fig. 10. The energy consumption for filtration was calculated on the basis of power consumption data provided by the variable speed drive. The assumed thermal efficiency η_{th} = 50 % used for the thermal drying calculations is based on the heat efficiency of a spin-flash dryer reported by Kudra et al. [33]. The illustrations in Fig. 9 indicate that the minimum specific energy consumption to attain a zero moisture content with the liquid ring pump is reached in Test 3 with a 0.2 bar pressure difference and 9.5 kg of cake deposited per unit area. The specific energy consumption close to the minimum is also achieved with Tests 2, 6, and 8. As with the ideal case presented in Fig. 8, keeping the pressure difference and the belt speed fixed and increasing the mass of cake deposited per unit area decreases the specific energy consumption of vacuum filtration, and with the exception of Test 4, also the total energy consumption is decreased.

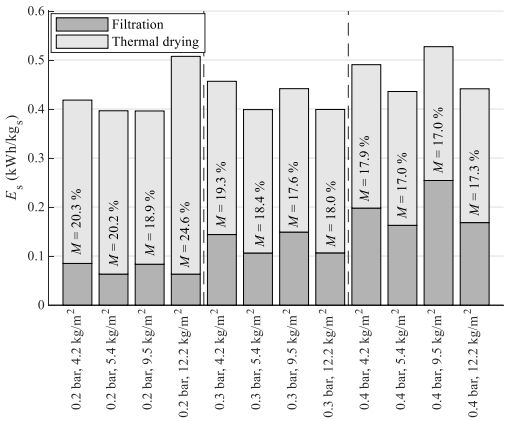

Fig. 9 Specific energy consumption for achieving zero moisture content (M = 0 %) for liquid ring vacuum pump experiments. Distinguishing between vacuum filtration and thermal drying (thermal efficiency η_{th}=50 %). The moisture content after vacuum filtration is shown for each experiment.

Fig. 10 indicates that the minimum specific energy consumption to attain a zero moisture content with the claw pump is achieved in Test 3 using a 0.2 bar pressure difference and 10.3 kg of cake deposited per unit area. The specific energy consumption close to the minimum is also reached in Tests 6 and 8. As can be observed in Fig. 10, it is not energy efficient to dewater the filter cake to the lowest achievable moisture content by using a high pressure difference. The highest specific energy consumption of the overall dewatering and drying process is caused by the unsuitable combination of a low solids loading and a high pressure difference. On the other hand, thermal drying of excessively wet filter cakes cannot be recommended when targeting at a low total energy consumption. The specific energy consumption of the claw vacuum pump is analogous to that of the liquid ring pump in the sense that keeping the pressure difference and the belt speed fixed and increasing the mass of cake deposited per unit area decreases the specific energy consumption of vacuum filtration. Additionally, with the exception of Test 4, the total energy consumption is decreased. Mainly because of the higher efficiency of the claw vacuum pump, the specific energy consumption of vacuum filtration is roughly half of that of the liquid ring pump operated at the same pressure difference.

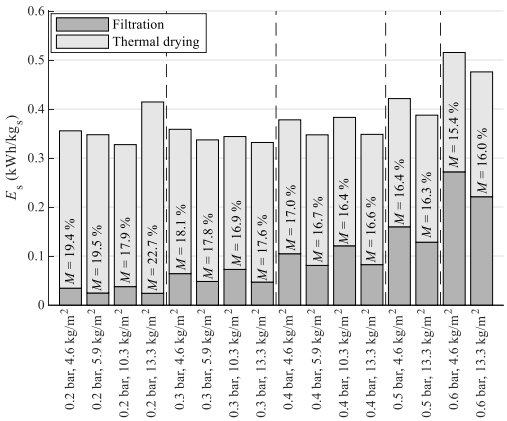

Fig. 10 Specific energy consumption for achieving zero moisture content (M = 0 %) for claw vacuum pump experiments. Distinguishing between vacuum filtration and thermal drying (thermal efficiency η_{th}=50 %). The moisture content after vacuum filtration is shown for each experiment.

A comparison of the measured specific energy consumptions obtained with the two types of pumps and the ideal isentropic specific energy consumption of cake dewatering (excl. thermal drying) is presented in Fig. 11. As mentioned above, cake dewatering with the liquid ring vacuum pump (LRVP) requires considerably more energy than dewatering with the claw pump. In addition to the comparison between the two different pump types, two alternative vacuum level control strategies using the liquid ring pump are compared. The bypass control strategy is implemented by running the pump at a full speed and inducing leak air flow into the vacuum system through a bypass valve, whereas the use of a variable speed drive (VSD) enables vacuum level control by manipulating the rotation speed of the vacuum pump directly. It is clearly illustrated in Fig. 9 that the use of a VSD reduces the specific energy consumption in cases where the pressure difference is small, and thus, below the maximum pressure difference obtainable by the pump. In this study, the maximum pressure difference obtainable by the LRVP was approximately 0.4 bar, which explains the negligible energy savings achieved by the use of a VSD when operating at Δp = 0.4 bar.

The ideal specific energy consumption in Fig. 11 was calculated using the isentropic power demand (Eq. (21)) and the air flow measurements from the claw vacuum pump experiments. Because of the efficiencies of the vacuum pumps, the ideal specific energy consumption is less than half of the actual energy consumption of the claw vacuum pump and less than one-quarter of the actual energy consumption of the liquid ring vacuum pump.

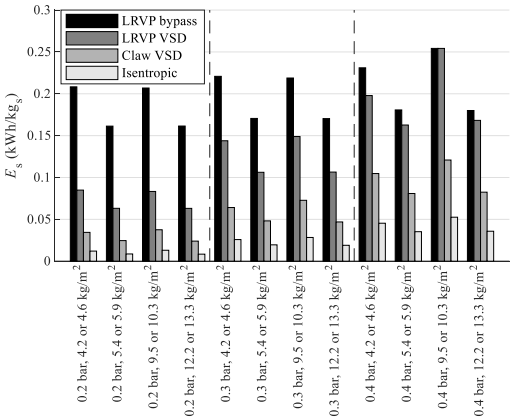

Fig. 11 Comparison of the specific energy consumption of filter cake dewatering with a horizontal belt vacuum filter. Dewatering by a liquid ring vacuum pump (LRVP) with a bypass valve and a variable speed drive (VSD) for pressure difference control. Dewatering by a claw vacuum pump with a variable speed drive (VSD) for pressure difference control. Ideal specific energy consumption of filter cake dewatering calculated using the isentropic power demand and the air flow measurements from the claw vacuum pump experiments.

5. Discussion

To reach a moisture level of zero percent with the combination of vacuum filtration and thermal drying, the specific energy consumption of vacuum filtration varies between 7 and 53 percent of the total specific energy consumption depending on the applied pressure difference. The lowest total specific energy consumptions are achieved with the pressure difference levels of 0.2 and 0.3 bar. The standard volumetric leak flow of the vacuum system of the pilot-scale vacuum filter used for the experiments increases linearly as a function of applied pressure difference. The increased air leak flow and the increased air flow through the filter cake have a nonlinear effect on the power demand and energy consumption of vacuum filtration as can be seen in Eqs. (21) and (22). The efficiency of vacuum pumps also behaves nonlinearly as a function of compression ratio [34, 35]. According to the experiments carried out with the pilot-scale horizontal belt vacuum filter, the specific energy consumption of vacuum filtration has a tendency to increase exponentially as the pressure difference is increased. A lower moisture content after vacuum filtration is achieved with a higher pressure difference, but the increased specific energy consumption of vacuum filtration adds to the total specific energy consumption with thermal drying to the extent that it is above optimal when the applied pressure difference is 0.4 bar or higher.

The claw vacuum pump used for the experiments has a significantly higher efficiency compared with the liquid ring vacuum pump. Typically, liquid ring vacuum pumps have

been used in filtration because of their ability to handle condensable vapors and availability for large capacities. Liquid ring pumps are available to capacities of over 37 000 m^3/h, while dry pumps are available only up to 2400 m^3/h [35]. The required capacities in vacuum filtration are often very high as a result of air flow from the leaks and through the cake; for instance in [36], for a 94 m^2 filter area, a vacuum pump with a suction capacity of 7000 m^3/h was used with a 0.45 bar pressure difference.

Controlling the vacuum level with a bypass valve should be avoided at all cost because of the high amount of energy wasted compared with controlling the vacuum level with a variable-speed-drive-operated vacuum pump. By adjusting the slurry infeed, the filter belt speed, and the vacuum level with variable speed drives, the moisture content of the filter cake could be controlled and the energy consumption of vacuum filtration could be optimized.

In process configurations where it is feasible to convey the filtrate flow several meters downwards inside a barometric leg, it might be possible to eliminate the energy consumption of filtrate pumping. Other devices in a horizontal belt vacuum filter besides the vacuum pump, such as cloth drive and filtrate pumps, typically consume 0.2–0.4 kW/m^2 of power [17]. This would make the energy saving potential of the barometric leg less than 0.2–0.4 kW/m^2. The use of the barometric leg could save energy by eliminating the need for a filtrate pump, but it also induces minor oscillation to the vacuum pressure, the air flow through the vacuum pump, and the filtrate level inside the barometric leg.

Using the method for identification of the leak flow of the vacuum system described in this article enables condition monitoring of the filter vacuum system and estimation of the flow through the filter cake. By this estimation, one could also calculate the efficiency of a vacuum filter for example in terms of the ratio of the leak flow and the flow through the filter cake.

6. Conclusions

According to the experiments carried out in this study, the main factors in minimizing the specific energy consumption of vacuum filtration are the usage of a variable-speed-controlled vacuum pump for controlling the pressure difference, the application of a moderate pressure difference of 0.2 to 0.3 bar, and the usage of an efficient vacuum pump. Claw-type vacuum pumps are more favorable than liquid ring pumps from the efficiency and energy consumption points of view.

The isentropic specific energy consumption calculated from the air flow data was significantly lower than the actual energy consumption obtained from the frequency converter. The vacuum system leak flow plays a considerable role in the total specific energy consumption of vacuum belt filters. However, the leak flow from the edges of the

filter cloth is not as great in large plant-scale filters, where the ratio between the edge length and the filtration area is smaller than in the pilot-scale filter used in this study.

The results of this study support the general assumption that thermal drying consumes the majority of the total energy consumption when dry solids are produced by a combination of mechanical solid-liquid separation and thermal drying. Furthermore, the results suggest that there is a combination of the pressure difference level and the mass of cake deposited per unit area that minimize the total energy consumption per solids mass of the filtration and thermal drying phases. For the experiments carried out in the study, taking into consideration also the throughput of cake solids, the most advantageous combination was to generate a 0.3 bar pressure difference with the claw vacuum pump and feed the slurry at the rate of 13.3 kg of cake deposited per unit area, which corresponded to a cake height of approximately 7.7 mm.

Acknowledgments

The authors would like to thank Hanna Niemelä for providing language help and The Finnish Funding Agency for Technology and Innovation (Tekes) for providing funding for the study.

References

[1] Zhu, Y.-F.; Qian, J.-Y.; Zhang, Q.-K.; Kuang, J.-Y.; Gao, X.-F.; Jin, Z.-J. Experimental Analysis on Filter Press and Energy Consumption Performance of Diaphragm Press Drying Device in Chemical Post-Processing Integrated Equipment. *Case Stud. Therm. Eng.* **2016**, *7*, 92–102. DOI: 10.1016/J.CSITE.2016.03.004.

[2] Eliseus, A.; Putra, Z. A.; Bilad, M. R.; Nordin, N. A. H. M.; Wirzal, M. D. H.; Jaafar, J.; Khan, A. L.; Aqsha. Energy Minimization of a Tilted Panel Filtration System for Microalgae Filtration: Performance Modeling and Optimization. *Algal Res.* **2018**, *34*, 104–115. DOI: 10.1016/J.ALGAL.2018.07.008.

[3] Danquah, M. K.; Ang, L.; Uduman, N.; Moheimani, N.; Forde, G. M. Dewatering of Microalgal Culture for Biodiesel Production: Exploring Polymer Flocculation and Tangential Flow Filtration. *J. Chem. Technol. Biotechnol.* **2009**, *84* (7), 1078–1083. DOI: 10.1002/JCTB.2137.

[4] Bilad, M. R.; Discart, V.; Vandamme, D.; Foubert, I.; Muylaert, K.; Vankelecom, I. F. J. Harvesting Microalgal Biomass Using a Magnetically Induced Membrane Vibration (MMV) System: Filtration Performance and Energy Consumption. *Bioresour. Technol.* **2013**, *138*, 329–338. DOI: 10.1016/J.BIORTECH.2013.03.175.

[5] Karabelas, A. J.; Koutsou, C. P.; Kostoglou, M.; Sioutopoulos, D. C. Analysis of Specific Energy Consumption in Reverse Osmosis Desalination Processes.

Desalination **2018**, *431*, 15–21. DOI: 10.1016/J.DESAL.2017.04.006.

[6] Zarzo, D.; Prats, D. Desalination and Energy Consumption. What Can We Expect in the near Future? *Desalination* **2018**, *427*, 1–9. DOI: 10.1016/J.DESAL.2017.10.046.

[7] Mazlan, N. M.; Peshev, D.; Livingston, A. G. Energy Consumption for Desalination — A Comparison of Forward Osmosis with Reverse Osmosis, and the Potential for Perfect Membranes. *Desalination* **2016**, *377*, 138–151. DOI: 10.1016/J.DESAL.2015.08.011.

[8] Sarai Atab, M.; Smallbone, A. J.; Roskilly, A. P. An Operational and Economic Study of a Reverse Osmosis Desalination System for Potable Water and Land Irrigation. *Desalination* **2016**, *397*, 174–184. DOI: 10.1016/J.DESAL.2016.06.020.

[9] Ghaffour, N.; Missimer, T. M.; Amy, G. L. Technical Review and Evaluation of the Economics of Water Desalination: Current and Future Challenges for Better Water Supply Sustainability. *Desalination* **2013**, *309*, 197–207. DOI: 10.1016/J.DESAL.2012.10.015.

[10] Al-Karaghouli, A.; Kazmerski, L. L. Energy Consumption and Water Production Cost of Conventional and Renewable-Energy-Powered Desalination Processes. *Renew. Sustain. Energy Rev.* **2013**, *24*, 343–356. DOI: 10.1016/J.RSER.2012.12.064.

[11] Avlonitis, S. A.; Kouroumbas, K.; Vlachakis, N. Energy Consumption and Membrane Replacement Cost for Seawater RO Desalination Plants. *Desalination* **2003**, *157* (1–3), 151–158. DOI: 10.1016/S0011-9164(03)00395-3.

[12] Zhao, R.; Porada, S.; Biesheuvel, P. M.; van der Wal, A. Energy Consumption in Membrane Capacitive Deionization for Different Water Recoveries and Flow Rates, and Comparison with Reverse Osmosis. *Desalination* **2013**, *330*, 35–41. DOI: 10.1016/J.DESAL.2013.08.017.

[13] Huttunen, M.; Nygren, L.; Kinnarinen, T.; Häkkinen, A.; Lindh, T.; Ahola, J.; Karvonen, V. Specific Energy Consumption of Cake Dewatering with Vacuum Filters. *Miner. Eng.* **2017**, *100*, 144–154. DOI: 10.1016/J.MINENG.2016.10.025.

[14] Karvonen, V.; Huttunen, M.; Kinnarinen, T.; Häkkinen, A. Research Focus and Research Trends in Vacuum Filtration – Bibliographical Analysis. *Filtration* **2018**, *18*, 40–44.

[15] Sparks, T. Solid-Liquid Filtration: Understanding Filter Presses and Belt Filters. *Filtr. + Sep.* **2012**, *49* (4), 20–24. DOI: 10.1016/S0015-1882(12)70193-3.

[16] Sparks, T. (Trevor). *Solid-Liquid Filtration: A User's Guide to Minimizing Cost and Environmental Impact, Maximizing Quality and Productivity*; Butterworth-Heinemann: Oxford, 2012.

[17] Henriksson, B. Focus on Separation in the Mining Industry. *Filtr. Sep.* **2000**, *37* (7), 26–29. DOI: 10.1016/S0015-1882(00)80139-1.

[18] Besra, L.; Sengupta, D. K.; Roy, S. K. Particle Characteristics and Their Influence on Dewatering of Kaolin, Calcite and Quartz Suspensions. *Int. J. Miner. Process.* **2000**, *59* (2), 89–112. DOI: 10.1016/S0301-7516(99)00065-4.

[19] Kinnarinen, T.; Tuunila, R.; Häkkinen, A. Reduction of the Width of Particle Size

Distribution to Improve Pressure Filtration Properties of Slurries. *Miner. Eng.* **2017**, *102*, 68–74. DOI: 10.1016/J.MINENG.2016.12.009.
[20] Tien, C. *Principles of Filtration*; Elsevier: Oxford, 2012.
[21] Wakeman, R. J.; Tarleton, E. S. Modelling, Simulation and Process Design of the Filter Cycle. *Filtr. Sep.* **1990**, *27* (6), 412–419. DOI: 10.1016/0015-1882(90)80534-R.
[22] Wakeman, R. J. An Improved Analysis for the Forced Gas Deliquoring of Filter Cakes and Porous Media. *J. Sep. Process Technol.* **1982**, *3* (1), 32–38.
[23] Hoşten, Ç.; Şan, O. Reassessment of Correlations for the Dewatering Characteristics of Filter Cakes. *Miner. Eng.* **2002**, *15* (5), 347–353. DOI: 10.1016/S0892-6875(02)00038-9.
[24] Wakeman, R. The Influence of Particle Properties on Filtration. *Sep. Purif. Technol.* **2007**, *58* (2), 234–241. DOI: 10.1016/J.SEPPUR.2007.03.018.
[25] Condie, D. J.; Hinkel, M.; Veal, C. J.; Boissy, K.; Leclerc, D. Modeling the Vacuum Filtration of Fine Coal. III. Comparison of Models for Predicting Desaturation Kinetics. *Sep. Sci. Technol.* **2000**, *35* (10), 1467–1484. DOI: 10.1081/SS-100100236.
[26] Fan, Y.; Dong, X.; Li, H. Dewatering Effect of Fine Coal Slurry and Filter Cake Structure Based on Particle Characteristics. *Vacuum* **2015**, *114*, 54–57. DOI: 10.1016/J.VACUUM.2015.01.003.
[27] Kemp, I. C. Reducing Dryer Energy Use by Process Integration and Pinch Analysis. *Dry. Technol.* **2005**, *23* (9–11), 2089–2104. DOI: 10.1080/07373930500210572.
[28] Kemp, I. C. Fundamentals of Energy Analysis of Dryers. In *Modern Drying Technology Volume 4: Energy Savings*; Wiley-VCH Verlag GmbH & Co. KGaA: Weinheim, Germany, 2012; pp 1–45. DOI: 10.1002/9783527631681.ch1.
[29] Svarovsky, L. *Solid-Liquid Separation*, 4th ed.; Butterworth-Heinemann, 2000.
[30] Tarleton, S.; Wakeman, R. *Solid/Liquid Separation : Principles of Industrial Filtration.*; Elsevier Science, 2005.
[31] Mujumdar, A. S. *Handbook of Industrial Drying*, 4rd ed.; CRC Press, 2014.
[32] Holdich, R. G. Solid–liquid Separation Equipment Selection and Modelling. *Miner. Eng.* **2003**, *16* (2), 75–83. DOI: 10.1016/S0892-6875(02)00178-4.
[33] Kudra, T.; Pallai, E.; Bartczaki, Z.; Peter, M. Drying of Paste-like Materials in Screw-Type Spouted-Bed and Spin-Flash Dryers. *Dry. Technol.* **1989**, *7* (3), 583–597. DOI: 10.1080/07373938908916612.
[34] Ryans, J. L.; Croll, S. Selecting Vacuum-Systems. *Chem. Eng.* **1981**, *88* (25), 72.
[35] Ryans, J.; Bays, J. Run Clean with Dry Vacuum Pumps. *CEP Magazine*. 2001.
[36] Taylor, J. L. An Operational Review of the Belt-Filtration Plant at Chemwes Limited. *J. South African Inst. Min. Metall.* **1983**, No. 10, 237–245.

Tables

Table 1. Actuator and sensor devices installed in the pilot-scale horizontal belt filter.

Device	**Manufacturer and model**	**Electrical motor**	**Variable speed drive**
Liquid ring vacuum pump	Robuschi RMV 14	Three-phase motor, 4.0 kW, 1430 rpm	ABB ACS580
Claw vacuum pump	Busch Mink MM1202AVA3	Three-phase motor, 5.1 kW, 3000 rpm	ABB ACS850
Slurry circulation pump	Larox LPP-D 20	Three-phase motor, 0.55 kW, 1400 rpm	Nordac SK300E
Slurry feed pump	Cole-Parmer Masterflex	Three-phase motor, 0.55 kW, 1360 rpm	ABB ACS580
Filter cloth drive	Heynau mini drive	Three-phase motor, 0.18 kW, 1400 rpm	ABB ACS580
Vacuum valves	Gemü		
Slurry control valves	Flowrox PVE25		
Bypass solenoid valve	Schmalz DRV 25 NC		
Cake thickness sensor	Keyence LB-1201 W		
Vacuum pump flow sensors	Schmidt SS 20.260		
Vacuum pressure difference transmitter	Aplisens APR-2000ALW		
Temperature sensors	Aplisens CT-I6		
Filtrate weight scale and transmitter	Dini Argeo PBE300 & DGT20AN		

This is an original manuscript of an article published by Taylor & Francis in Drying Technology on March 7, 2019, available online: http://www.tandfonline.com/doi/full/10.1080/07373937.2019.1581214.

Table 2. Laboratory experiments carried out to study the material properties and energy consumption of cake dewatering using vacuum filtration. The equipment consisted of a Büchner apparatus and a pilot-scale horizontal belt vacuum filter.

Büchner experiments			**Pilot experiments, liquid ring pump**			**Pilot experiments, claw pump**		
Test	**Δp (bar)**	**w (kg/m^2)**	**Test**	**Δp (bar)**	**w (kg/m^2)**	**Test**	**Δp (bar)**	**w (kg/m^2)**
1	0.2	7.2	1	0.2	4.2	1	0.2	4.6
2	0.2	12.5	2	0.2	5.4	2	0.2	5.9
3	0.2	17.7	3	0.2	9.5	3	0.2	10.3
4	0.4	7.2	4	0.2	12.2	4	0.2	13.3
5	0.4	12.5	5	0.3	4.2	5	0.3	4.6
6	0.4	17.9	6	0.3	5.4	6	0.3	5.9
7	0.6	7.3	7	0.3	9.5	7	0.3	10.3
8	0.6	12.7	8	0.3	12.2	8	0.3	13.3
9	0.6	17.8	9	0.4	4.2	9	0.4	4.6
			10	0.4	5.4	10	0.4	5.9
			11	0.4	9.5	11	0.4	10.3
			12	0.4	12.2	12	0.4	13.3
						13	0.5	4.6
						14	0.5	13.3
						15	0.6	4.6
						16	0.6	13.3

Table 3. Büchner experiment variables, properties of the filter cakes, and separation time. Slurry temperature T = 22 °C and s = 25 wt.% in all experiments.

Test	**Δp (bar)**	**m_{sl} (g)**	**w (kg/m^2)**	**t_{sep} (s)**	**L_{meas} (mm)**	**$L_{tr,\,calc}$ (mm)**	**$\varepsilon_{av,\,meas}$ (-)**	**$\varepsilon_{av,\,tr,\,calc}$ (-)**	**$\alpha_{av} \cdot 10^{10}$ (m/kg)**
1	0.2	300	7.2	186	4.5	5.2	0.41	0.48	4.53
2	0.2	500	12.5	470	6.7	8.5	0.31	0.46	4.51
3	0.2	700	17.7	929	10.6	12.1	0.38	0.46	4.51
4	0.4	300	7.2	108	4.3	5.3	0.38	0.49	4.90
5	0.4	500	12.5	281	7.5	8.7	0.39	0.47	4.93
6	0.4	700	17.9	534	10.8	13.2	0.38	0.50	5.04
7	0.6	300	7.3	78	4.6	7.2	0.41	0.63	4.04
8	0.6	500	12.7	205	7.8	9.3	0.40	0.49	4.99
9	0.6	700	17.8	387	10.8	13.1	0.39	0.50	5.14

Table 4. Pilot experiments with a horizontal belt filter and a liquid ring vacuum pump. Slurry temperature T = 24 °C and s = 26 wt.% in all experiments.

Test	Δp (bar)	w (kg/m^2)	v_{belt} (cm/s)	t_f (s)	z_f (cm)	t_d (s)	z_d (cm)	L (mm)	ε_{av} (-)	M_s (g/s)	M (wt.%)
1	0.2	4.2	1.1	105	115	77	85	2.5	0.38	4.6	20.3
2	0.2	5.4	1.1	157	173	25	27	3.6	0.44	6.0	20.2
3	0.2	9.5	0.5	293	143	117	57	5.0	0.30	4.6	18.9
4	0.2	12.2	0.5	409	200	0	0	7.2	0.37	6.0	24.6
5	0.3	4.2	1.1	75	83	106	117	2.3	0.32	4.6	19.3
6	0.3	5.4	1.1	114	125	68	75	3.5	0.43	6.0	18.4
7	0.3	9.5	0.5	215	105	194	95	5.0	0.30	4.6	17.6
8	0.3	12.2	0.5	348	170	61	30	6.9	0.35	6.0	18.0
9	0.4	4.2	1.1	59	65	123	135	2.3	0.32	4.6	17.9
10	0.4	5.4	1.1	86	95	95	105	3.4	0.41	6.0	17.0
11	0.4	9.5	0.5	164	80	246	120	4.9	0.28	4.6	17.0
12	0.4	12.2	0.5	286	140	123	60	6.9	0.35	6.0	17.3

Table 5. Pilot experiments with a horizontal belt filter and a claw vacuum pump. Slurry temperature T = 22 °C and s = 28 wt.% in all experiments.

Test	Δp (bar)	w (kg/m^2)	v_{belt} (cm/s)	t_f (s)	z_f (cm)	t_d (s)	z_d (cm)	L (mm)	ε_{av} (-)	M_s (g/s)	M (wt.%)
1	0.2	4.6	1.1	105	115	77	85	3.3	0.48	5.0	19.4
2	0.2	5.9	1.1	164	180	18	20	4.2	0.48	6.5	19.5
3	0.2	10.3	0.5	276	135	133	65	6.3	0.39	5.0	17.9
4	0.2	13.3	0.5	409	200	0	0	8.1	0.39	6.5	22.7
5	0.3	4.6	1.1	77	85	105	115	3.2	0.47	5.0	18.1
6	0.3	5.9	1.1	118	130	64	70	4.0	0.45	6.5	17.8
7	0.3	10.3	0.5	225	110	184	90	6.1	0.37	5.0	16.9
8	0.3	13.3	0.5	358	175	61	25	7.7	0.36	6.5	17.6
9	0.4	4.6	1.1	59	65	123	135	3.1	0.45	5.0	17.0
10	0.4	5.9	1.1	100	110	77	90	3.9	0.44	6.5	16.7
11	0.4	10.3	0.5	184	90	225	110	5.8	0.34	5.0	16.4
12	0.4	13.3	0.5	286	140	123	60	7.6	0.35	6.5	16.6
13	0.5	4.6	1.1	55	60	127	140	2.9	0.41	5.0	16.4
14	0.5	13.3	0.5	235	115	174	85	7.3	0.33	6.5	16.3
15	0.6	4.6	1.1	50	55	132	145	2.8	0.39	5.0	15.4
16	0.6	13.3	0.5	215	105	194	95	7.2	0.32	6.5	16.0

Table 6. Measured standard volumetric air flow rates for the total flow through the vacuum pump, the estimated volumetric air flow rate, and the air flux through the filter cake dewatering area calculated on the basis of leak flow measurements.

This is an original manuscript of an article published by Taylor & Francis in Drying Technology on March 7, 2019, available online: http://www.tandfonline.com/doi/full/10.1080/07373937.2019.1581214.

Liquid ring vacuum pump experiments						**Claw vacuum pump experiments**					
Test	**Δp (bar)**	**w (kg/m^2)**	**$Q_{a,\,total}$ (m^3/h)**	**$Q_{a,\,cake}$ (m^3/h)**	**$u_{a,\,cake}$ (m^3/h·m^2)**	**Test**	**Δp (bar)**	**w (kg/m^2)**	**$Q_{a,\,total}$ (m^3/h)**	**$Q_{a,\,cake}$ (m^3/h)**	**$u_{a,\,cake}$ (m^3/h·m^2)**
1	0.2	4.2	35.0	2.0	23.7	1	0.2	4.6	31.5	3.5	41.3
2	0.2	5.4	33.5	0.5	19.0	2	0.2	5.9	29.2	1.2	60.6
3	0.2	9.5	36.0	3.0	52.8	3	0.2	10.3	33.7	5.7	87.9
4	0.2	12.2	33.0	0.0	-	4	0.2	13.3	28.0	0.0	-
5	0.3	4.2	45.0	4.9	42.1	5	0.3	4.6	41.0	5.9	51.5
6	0.3	5.4	43.0	2.9	39.0	6	0.3	5.9	40.0	4.9	70.3
7	0.3	9.5	49.0	8.9	93.9	7	0.3	10.3	45.5	10.4	115.8
8	0.3	12.2	43.5	3.4	114.1	8	0.3	13.3	38.8	3.7	124.1
9	0.4	4.2	53.0	5.8	43.2	9	0.4	4.6	49.0	6.8	50.6
10	0.4	5.4	55.0	7.8	74.6	10	0.4	5.9	48.5	6.3	74.5
11	0.4	9.5	63.0	15.8	132.0	11	0.4	10.3	55.5	13.3	121.2
12	0.4	12.2	57.0	9.8	163.9	12	0.4	13.3	50.0	7.8	130.6
						13	0.5	4.6	56.0	6.7	48.2
						14	0.5	13.3	58.0	8.7	102.9
						15	0.6	4.6	66.0	9.7	66.6
						16	0.6	13.3	65.0	8.7	91.1

Publication IV

Huttunen, M., Nygren, L., Kinnarinen, T., Ekberg, B., Lindh, T., Karvonen, V., Ahola, J., and Häkkinen, A..
Real-time monitoring of the moisture content of filter cakes in vacuum filters by a novel soft sensor

Reprinted with permission from
Separation and Purification Technology
Vol. 223, pp. 282–291, 2019

Separation and Purification Technology 223 (2019) 282–291

Contents lists available at ScienceDirect

Separation and Purification Technology

journal homepage: www.elsevier.com/locate/seppur

Real-time monitoring of the moisture content of filter cakes in vacuum filters by a novel soft sensor

Manu Huttunen[a,*], Lauri Nygren[a], Teemu Kinnarinen[b], Bjarne Ekberg[b], Tuomo Lindh[a], Vesa Karvonen[b], Jero Ahola[a], Antti Häkkinen[b]

[a] LUT School of Energy Systems, LUT University, P.O. Box 20, FI-53851 Lappeenranta, Finland
[b] LUT School of Engineering Science, LUT University, P.O. Box 20, FI-53851 Lappeenranta, Finland

ARTICLE INFO

Keywords:
Thermodynamics
Vacuum filtration
Dewatering
Moisture content prediction
Soft sensor

ABSTRACT

The moisture content of filter cakes is probably the most important characteristic that should be kept at a desired level in industrial cake filtration applications to maintain consistent product quality and minimize energy consumption. Most of the currently applied methods for contactless real-time monitoring of the moisture content are based for example on x-ray or microwave techniques, and therefore, the equipment for the purpose is highly specialized. This paper introduces a novel soft sensor for filter cake moisture estimation that uses machine learning algorithms and data collected with basic process instrumentation. The method is primarily based on the cooling effect observed in the cake and air, caused by evaporation of liquid from the cake during the dewatering period, and it can be supported by other process data. The specific energy consumption of vacuum filtration and the subsequent thermal drying to zero moisture is also analyzed. The results of pilot-scale experiments with calcite slurry and a horizontal belt vacuum filter show that in order to minimize the specific energy consumption of vacuum filtration, it is crucial to find the right combination of slurry concentration, vacuum level, and mass of filter cake per unit area. The proposed method for estimating the filter cake moisture content is especially suitable for real-time monitoring and control, enabling also considerable reduction in the energy consumption of the overall process. When applying the proposed soft sensor method in a pilot-scale process, the mean absolute error of the estimated moisture content of the filter cake is ~0.4 percentage points when the temperature of air at the vacuum pump inlet and the vacuum pump air flow rate are included in the input variables.

1. Introduction

Filtration and dewatering operations of easily filtering slurries are commonly performed with vacuum filters, which provide a robust and reliable technology for industrial dewatering. There are several vacuum cake filter designs available, including for instance rotary discs, drum and horizontal belt filters, and table and tilting pan filters [1]. Depending on the filter design, vacuum filters are operated by using different filter media, such as polymeric filter cloths or ceramic filter elements. Most industrial vacuum filters are continuously operating devices with high production capacities and energy requirements. The importance of vacuum filtration has increased considerably over the past decades [2].

In the cake dewatering stage in vacuum filters, the air flow rate through the cake and the filter medium is high, provided that the applied pressure difference is higher than the capillary threshold pressure of the cake and the filter medium [1,3]. In belt filters equipped with filter cloths there is also a significant ineffective bypass flow at the imperfectly sealed edges of the filter medium. For these reasons, large vacuum pumps consuming considerable amounts of energy are required to maintain the target level of pressure difference. In many vacuum filtration plants, however, the operators typically have no online information about the cake moisture content, nor have the possibility of controlling the rotational speeds of the vacuum pumps to reduce the energy consumption of the process.

The moisture content of the cake at the point of its discharge is one of the most important factors reflecting the filtration and dewatering performance. Determination of the cake moisture content after a dewatering process can be carried out by measuring the weight of a cake sample before and after drying it to complete dryness, according to an appropriate standard (e.g. ASTM D2216). To make it possible to monitor the dewatering process online, without delays caused by the laboratory determination, some indirect methods for the moisture determination have been developed. As an example, the MoistScan®

* Corresponding author.
E-mail address: manu.huttunen@lut.fi (M. Huttunen).

https://doi.org/10.1016/j.seppur.2019.03.091
Received 19 November 2018; Received in revised form 19 February 2019; Accepted 28 March 2019
Available online 29 March 2019
1383-5866/

Nomenclature

A	filtration area (m^2)
a	experimentally determined slope t/V^2
c	filtration concentration ($kg/m^3_{filtrate}$)
E	energy consumption (J)
E_S	specific energy consumption (kJ/kg)
L	thickness of the filter cake (mm)
M	moisture content (% kg/kg)
M_s	solids mass flow rate (g/s)
$\dot{m}$	mass flow (kg/s)
m_s	mass of solids (kg)
P	power (W)
p	pressure (bar)
Δp	applied pressure difference (bar)
Q	standard volumetric flow rate (Nm^3/h), heat transfer
q_m	mass flow rate (kg/s)
q_{sl}	slurry mass flow rate (kg/min)
q_V	volumetric flow rate (m^3/s)
R_m	resistance of the filter medium (1/m)
s	solids content (kg/kg)
T	temperature (°C)
ΔT	temperature difference (°C)
t	time (s)
V_f	volume of the filtrate (m^3)
v	velocity (mm/s)
w_a	specific humidity of air (kg_v/kg_a)
w	mass of cake deposited per unit area (kg/m^2)
z	length on filter belt (cm)

Dimensionless number

k	isentropic exponent
R^2	coefficient of determination

Greek symbols

α	specific cake resistance (m/kg)
ε	cake porosity (volume of voids per unit cake volume)
η	efficiency (%)
μ	dynamic viscosity of the filtrate (N s/m^2)
ρ	density (kg/m^3), Pearson correlation coefficient (–)

Subscripts and superscripts

a	air
av	average
belt	filter belt
c	filter cake
dw	dewatering
e	evaporation
f	filtrate, filtration
in	input value
m	medium
out	output value
S	isentropic, specific
s	solids
sl	slurry
T	isothermal
t	thermal
V	volumetric
v	vapor
vp	vacuum pump
w	water

technology by Callidan Instruments, based on a microwave transmission technique, represents an indirect method for online moisture determination in vacuum filters [4]. Other potential methods for the purpose include for instance NMR spectroscopy [5], NIR spectroscopy [6], neutron scattering, and gamma-ray attenuation [7]. Most of these methods have been considered for soil moisture determination, not for continuous filters, where the studied material is in constant movement. On the other hand, theoretical approximation of the cake moisture content is even more challenging because of inevitable variation in the slurry properties and filtration conditions in time, as well as inaccuracy or unavailability of process data. The major factors affecting the filterability have been discussed for example in [8].

The objective of this paper is to introduce a novel soft sensor technique that is suitable for online determination of cake moisture content in industrial vacuum filters. Additionally, the energy consumption of the dewatering stage and the overall material drying process is evaluated.

2. Theory

2.1. Filtration and dewatering of filter cakes

In cake filtration, the solid particles in the slurry are retained on the filter medium during the filtration phase, forming a matrix of solid particles with a void space, i.e., a filter cake. When applying a pressure difference greater than the threshold pressure over the filter cake, air may enter the filter cake and start displacing the liquid. The capillary retention forces holding the liquid in the pores of the filter cake depend on the size range and surface properties of the particles in the cake.

Darcy's basic filtration equation describing the flow rate u of a filtrate with a viscosity μ through a porous medium can be written as

$$u = \frac{-k}{\mu}\frac{dp}{dz}, \tag{1}$$

where dp is the dynamic pressure difference across the thickness dz of a porous medium of the permeability k [9].

For cake filtration, there is also a minimum moisture content, called irreducible saturation, at which the flow of the liquid ceases at any pressure. As can be seen in Eq. (1), increasing the pressure difference over the filter cake increases the flow rate of the filtrate, thereby decreasing the time required to achieve a certain moisture content or, on the other hand, a lower moisture content is achieved in the same amount of time [9,10].

In the conventional filtration theory, the average specific cake resistance α_{av} is determined from experimental constant pressure filtration data and by using the equation:

$$\frac{t}{V_f} = \frac{\alpha_{av}\mu c}{2A^2\Delta p}V_f + \frac{\mu R_m}{A\Delta p}, \tag{2}$$

where t is time, V_f is the volume of the filtrate, μ is the dynamic viscosity of the filtrate, c is the filtration concentration, i.e., mass of solids collected per volume of the filtrate, A is the filtration area, Δp is the applied pressure difference, and R_m is the resistance of the filter medium [10].

When omitting the resistance of the filter medium and solving Eq. (2) with respect to α_{av}, where a denotes the experimentally determined slope t/V^2, the average specific resistance of the cake is expressed by:

$$\alpha_{av} = \frac{2aA^2\Delta p}{\mu c}. \tag{3}$$

The average cake porosity is the ratio of the void volume of the cake to the total volume of the cake, which can also be calculated by subtracting the solids volume from the total cake volume applying the formula

$$\varepsilon_{av} = 1 - \frac{m_s}{\rho_s A L}, \tag{4}$$

where m_s is the mass of solids, ρ_s is the density of solids, and L is the thickness of the filter cake [9].

In addition to the properties in Eqs. (2)–(4), the mathematical dewatering models derived from the classical filtration theory require the irreducible saturation and threshold pressure of the filter cake as inputs [11]. Furthermore, the assumption underlying the conventional theory is that the specific cake resistance and the porosity are functions of applied pressure only. In reality, the cake porosity and specific resistance depend on time (creep effect) and solids concentration (rate of cake formation) [10,12].

2.2. Thermodynamic background of vacuum dewatering

When considering the thermodynamics of the flow of air through a filter cake with a partially water-saturated void space, the evaporation of water has to be included in the analysis (Fig. 1). The driving force for evaporation of water in the filter cake is the difference of vapor pressures at the saturation and interface temperatures. If the air being forced through the filter cake ($\dot{m}_a$) is unsaturated, there will be a difference in vapor pressures. Because of the difference, some of the water will evaporate ($\dot{m}_w$). The latent heat required for this change of state (Q_e) will be drawn from the sensible heat of the water in the cake. As a result, the water will be slightly cooled ($T_w^1 > T_w^2$). The flow of sensible heat from the air and the solids in the filter cake to the water provides the latent heat to evaporate a part of it and a thermal balance is pursued [13].

As a section of the filter cake moves from the start of the dewatering period to the end of the belt, water is both mechanically removed from the filter cake with suction and evaporated. The mechanically removed water is extracted from the process as filtrate, and the evaporated water is extracted in the air evacuated by the vacuum pump. The saturation of the filter cake section decreases as it travels on the filter belt and the flow of air through the filter cake increases. The rates of heat transfer between the liquid and gas phases depend on the properties of the volatile fluid, the dimensions of the interface, and the velocities of flow [13]. Throughout the thickness of the filter cake, heat (Q) is transferred between the liquid water, the cake solids, and the air flowing through. As a result, the filter cake and the air in the vacuum box are at a lower temperature than the room temperature air entering the filter cake ($T_a^1 > T_a^2$). The decreasing saturation and the increasing air flow through the filter cake in the horizontal direction towards the end of the dewatering zone, and the changing temperature through the filter cake in the vertical direction render the phenomena into a multiphase flow and transient heat flow process. Moreover, as the filter cake height decreases in the axial direction owing to the sloping edges of the filtration area and there is a leak flow of air around the edges of the filter cake, an axial temperature profile is produced on the surface of the cake, where the edges are colder than the longitudinal centerline of the cake. For a more detailed account of the governing equations for flow and transport in porous media, the reader is directed to [14].

The mass transfer from water to air by evaporation is proportional to the air mass flow through a filter cake and to the difference between the specific humidity of the outlet and inlet air

$$\dot{m}_w = \dot{m}_a (w_a^{out} - w_a^{in}), \tag{5}$$

where $\dot{m}$ is the mass flow, the subscripts w and a denote water and air, and w_a is the specific humidity of air [15]. On the other hand, in an air-water vapor mixture, the rate of mass transfer is roughly proportional to the rate of heat transfer at the interface [13].

2.3. Power demand

In vacuum filtration processes, the pressure difference across the filter cake is generated by a vacuum pump. The ideal isentropic power demand P_S of a dry claw vacuum pump for a given inlet volumetric flow rate $q_{V,in}$ generated by the pump can be calculated by the equation

$$P_S = \frac{k}{k-1} q_{V,in} p_{in} \left[\left(\frac{p_{out}}{p_{in}} \right)^{\frac{k-1}{k}} - 1 \right], \tag{6}$$

where p_{in} is the pressure at the inlet of the vacuum pump, p_{out} is the outlet pressure of the vacuum pump, and k is the isentropic exponent. For a cooled vacuum pump, such as a liquid-ring vacuum pump, the isothermal power demand P_T can be used to describe the ideal process,

$$P_T = q_{V,in} p_{in} \ln\left(\frac{p_{out}}{p_{in}} \right). \tag{7}$$

If the moisture content of the product after vacuum filtration is too high, additional drying is required. In thermal drying, the moisture is removed from the cake by evaporation. Ideally, the power P_v required to provide the heat for evaporation can be calculated by using the equation

$$P_v = q_{m,v} \Delta H_v = q_{m,s} \left(\frac{1}{s_{in}} - \frac{1}{s_{out}} \right) \Delta H_v, \tag{8}$$

where q_m is the mass flow, ΔH_v is the latent heat of evaporation, and s_{in} is the weight per weight solids content of the filter cake after vacuum filtration [16]. The subscript v denotes vapor and s solids. For ideal evaporation, it is assumed that all the supplied energy goes to heating of the matter and evaporation of water. The specific heat used in the calculations for water and calcite solids is $c_w = 4.186\,kJ/(kg\,K)$ and $c_s = 0.8\,kJ/(kg\,K)$ respectively, and the latent heat for evaporation of

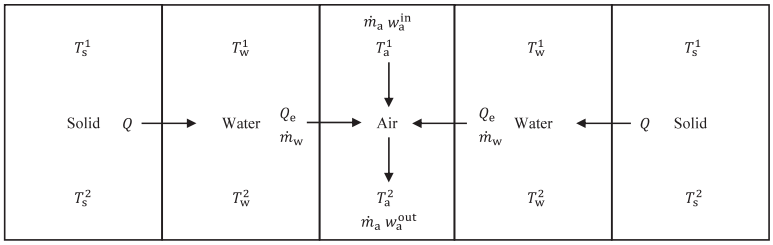

Fig. 1. Diagram illustration of the heat transfer inside the filter cake caused by evaporation. The latent heat Q_e required for evaporation of water will be drawn from the sensible heat of the water. The sensible heat is transferred from the cake solids to the cooled water. In this case $T_x^1 > T_x^2$ and $w_a^{in} < w_a^{out}$.

water ΔH_v = 2256 kJ/kg [17].

3. Materials and methods

3.1. Preparation of slurries

The slurries used for the experiments were prepared from Nordkalk Parfill H80 calcite and tap water to form a variety of slurries with dimensionless weight based solids contents in the range of 0.26–0.44. The particle size distribution of solids was measured with a Malvern Mastersizer 3000 laser diffraction particle size analyzer. Five parallel measurements were performed, and the characteristic diameters of the volumetric undersize distribution were Dx (10) = 1.85 µm, Dx (50) = 22.4 µm, and Dx (90) = 95.7 µm.

3.2. Equipment and instrumentation

Filtration experiments were conducted using a pilot-scale horizontal belt vacuum filter with a reciprocating tray. The main operational parts of the machine comprise slurry infeed, filter belt, vacuum generation by a claw or a liquid-ring vacuum pump, and filtrate handling. The filter belt effective length is 2.1 m and the width is 10 cm. The instrumentation of the device is illustrated in Fig. 2. The majority of the experiments were run with the claw vacuum pump and 16 experiments with the liquid-ring vacuum pump.

3.3. Experimental work

Experiments were conducted with various weight based slurry solids contents s_{sl} and masses of cake solids deposited per unit area w varying also the pressure difference Δp over the filter cake. The mass of cake deposited per unit area was varied by varying the feed flow rate q_{sl} and the belt speed v_{belt}. The varied experiment settings determined the slurry density ρ_{sl} and the solids mass flow rate M_s. Summary statistics of the experiment settings with mean μ, standard deviation σ, minimum, 25th percentile, median, 75th percentile, and maximum values are presented in Table 1. The subscripts sl, s, and belt denote the slurry, solids, and the filter belt. The complete settings and measurement results for a total of 80 experiments are presented in an [dataset] additional file.

Table 1
Summary statistics of the settings for all the experiments. The symbols μ and σ denote mean and standard deviation.

	Δp (bar)	s_{sl} (-)	ρ_{sl} (kg/m^3)	q_{sl} (kg/min)	M_s (g/s)	v_{belt} (mm/s)	w (kg/m^2)
μ	0.34	0.33	1259	1.1	5.8	6.6	9.7
σ	0.11	0.07	69	0.2	0.9	2.3	3.2
min	0.20	0.26	1192	0.6	4.4	5.0	4.4
25%	0.30	0.28	1214	1.0	5.0	5.0	6.5
50%	0.31	0.29	1221	1.1	5.8	5.0	10.1
75%	0.40	0.39	1323	1.2	6.5	10.0	12.1
max	0.61	0.44	1384	1.5	7.4	10.0	14.7

When running the experiments, the filtration process was allowed to stabilize to a steady state, in other words, to a steady filtration length before data collection was started. The pressure difference was held at a constant level using a programmable logic controller (PLC) and a variable speed drive (VSD) for the vacuum pump. The slurry infeed rate and the belt speed were also kept constant during the data collection with the help of variable speed drives. Data were collected from the filter instrumentation using the PLC and a 100 ms sampling rate. For a number of experiments, the surface temperature of the filter cake in the dewatering zone was measured with a PeakTech 4695 infrared thermometer. The device has a measuring range from −50 °C to +380 °C and a distance/spot ratio of 12:1. The measurement distance perpendicular to the filter cake was 10 cm, and the measurements were made along the centerline of the filter cake.

Cake samples were collected from the scraper located at the end of

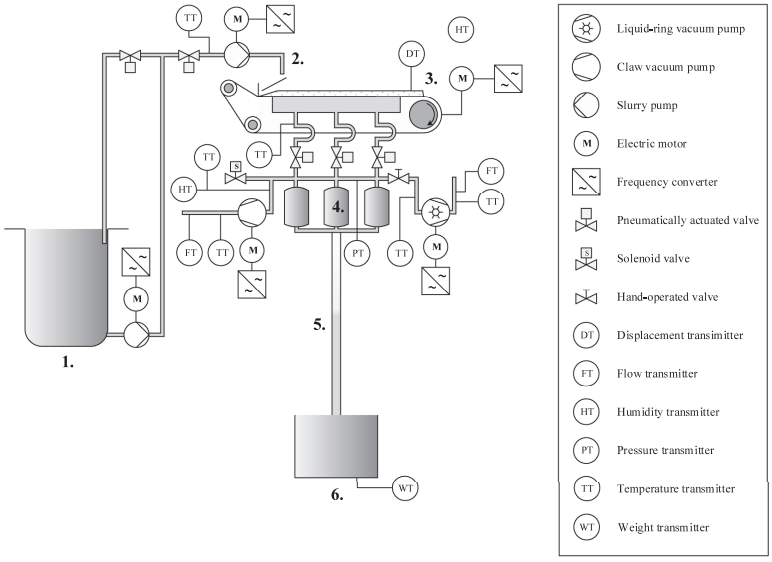

Fig. 2. Horizontal belt vacuum filter device setup and instrumentation: (1) slurry tank, (2) slurry infeed, (3) cake discharge, (4) filtrate intermediate tanks, (5) barometric leg, and (6) filtrate collection tank.

the filter belt to determine their dimensionless weight based solids contents s and the weight based moisture contents percentage M. The cake samples were weighed wet immediately after sampling, dried to zero moisture, and reweighed. The total solids content of each slurry was determined by collecting two parallel samples from the slurry recirculation loop and processed in the same way as the cake samples.

3.4. Regression models

Mathematical models of processes that are designed based on experimental data to estimate relevant process variables are known as inferential models, virtual sensors, or soft sensors [18]. Data-driven methods for building soft sensor models to estimate difficult to measure quality variables of a process have gained much attention in recent years [19–26]. Machine learning algorithms serve as basic tools for constructing models from relationships between difficult to measure quality or key variables and easy to measure variables [27]. Contactless online measurement of the filter cake moisture content requires special equipment that uses for instance x-rays or microwave radiation. A reliable soft sensor model for moisture content could possibly render the use of special equipment and radiation obsolete.

The development of a special soft sensor regression algorithm for the solids content of the filter cake is beyond the scope of this study. The aim of experimenting with machine learning algorithms was to find the simplest model with reliable estimation results. To this end, soft sensor regression was experimented with five standard machine-learning algorithms, namely regularized linear regression algorithms Lasso, Ridge, and Elastic-Net as well as ensemble decision tree algorithms Random Forest and Gradient Boosting capable of modeling non-linear relationships between variables.

The data set was randomly divided into training and testing sets with 80% and 20% of data respectively. The models were trained with fivefold cross-validation using algorithms provided in the Scikit-Learn software package. For hyperparameter tuning, the strengths of penalty for Lasso, Ridge, and Elastic-Nets were 0.001, 0.005, 0.01, 0.05, 0.1, 0.5, 1, 5, and 10, and for Elastic-Net the L_1-ratios were 0.1, 0.3, 0.5, 0.7, and 0.9. The number of estimators for the decision tree algorithms were 10, 20, 40, 60, 80, 100, and 200. The tuned maximum features settings for the Random Forest Algorithm were auto, sqrt, and 0.33. The Gradient Boosting tuned learning rates were 0.05, 0.1, and 0.2, and the maximum depths 1, 3, and 5.

4. Results and discussion

4.1. Summary statistics of filtration results

The pressure difference range for the experiments was from 0.2 to 0.6 bar, and the mass of solids per unit area on the filter belt varied between 4.4 and 14.7 kg/m^2. This resulted in a filter cake height L_c varying between 2.1 and 8.0 mm. Experiments with extremely short and long filtration lengths z_f were also ran for values between 30 and 190 cm. The mean moisture content of the filter cakes M was 16.6% with a standard deviation of 1.3 percentage points (pp). Summary statistics of filter cake properties are presented in Table 2. The subscripts f, dw, c, and av denote filtration, dewatering, filter cake, and average. Filtration results for all the experiments are presented in an [dataset] additional file.

4.2. Solids contents of filter cakes

The filter cake solids content after dewatering s_c with respect to the dewatering time is depicted on the left in Fig. 3. In general, a higher solids content is achieved with a higher pressure difference and a longer dewatering time. A higher pressure difference also leads to a higher air flow rate, which, in turn, leads to a greater temperature difference between the vacuum pump suction air and the slurry infeed, see Supplementary Fig. 1. The correlation of the filter cake solids content with the pressure difference and the dewatering time arouses interest to study how the interaction feature of the pressure difference and the dewatering time correlates with the solids content. As can be seen on the right in Fig. 3, the product of these two features yields a stronger correlation with the filter cake solids content.

As expected, a higher pressure difference and a higher vacuum pump air flow rate, maintaining that pressure difference, yields a drier cake as can be seen as a general trend on the left in Fig. 4. In most cases, a greater temperature difference between the vacuum pump suction air and the slurry feed seems to indicate a drier cake as illustrated on the right in Fig. 4. Variations in the interdependence of these two features could be caused for example by the increased leak flow around the edges of the filter cake, which would increase the gas temperature in the vacuum box. As the air entering the filter cake was at a room temperature, the deviation in that temperature is small and thus neglected in this study. The correlation between the solids content of the cake and the temperature difference between the vacuum pump suction air and the slurry feed is in line with the thermodynamic background of vacuum dewatering described in the theory section.

For a limited number of experiments, the surface temperature of the filter cake on the longitudinal centerline of the filter belt in the dewatering region was measured, and the minimum, mean, and maximum values for each vacuum level are depicted in Fig. 5. The slurry solids content for these experiments was held constant, but the slurry infeed and filter belt speed were adjusted to vary the slurry loading on the belt. As more and more water was evaporated from the pore space of the filter cake towards the end of the belt, more and more sensible heat was removed from the cake and the temperature of the filter cake decreased. The slope of the temperature profile suggests that the cooling effect would continue for some time if the filter belt were longer. As can be clearly seen in Fig. 5, the greater the pressure difference over the filter cake is, the greater is the temperature change on the surface of the filter cake.

From the limited number of experiments with cake surface temperature measurements, it can be concluded that the change in the cake temperature seems to give an indication of the solids content of the filter cake as depicted in Fig. 6. In general, the greater the pressure difference is, the greater is the temperature change of the filter cake in the dewatering zone and the drier is the filter cake. It was also found that the cake surface temperature varies greatly also in the direction perpendicular to the filter belt movement. Hence, in the future research, it would be a good idea to measure the filter cake temperature along the whole width of the cake.

4.3. Specific energy consumption

To investigate the specific energy consumption of vacuum filtration and to minimize the variation in results arising from the two different types of vacuum pumps used in the study, theoretical power demand calculations for the two pumps were made using Eqs. (6) and (7). The power demand of thermal drying of the filtration product to zero

Table 2
Summary statistics of filter cake properties for all the experiments. The symbols μ and σ denote mean and standard deviation. For other symbol definitions, see Nomenclature.

	z_f (cm)	t_f (s)	t_{dw} (s)	L_c (mm)	ε_{av} (–)	s (–)	M (%)
μ	110	189	162	5.2	0.34	0.834	16.6
σ	35	85	63	1.7	0.08	0.013	1.3
min	30	30	30	2.1	0.04	0.797	14.7
25%	94	115	118	3.9	0.28	0.829	15.7
50%	110	199	160	5.6	0.35	0.836	16.4
75%	130	249	209	6.6	0.40	0.843	17.1
max	190	379	349	8.0	0.46	0.853	20.3

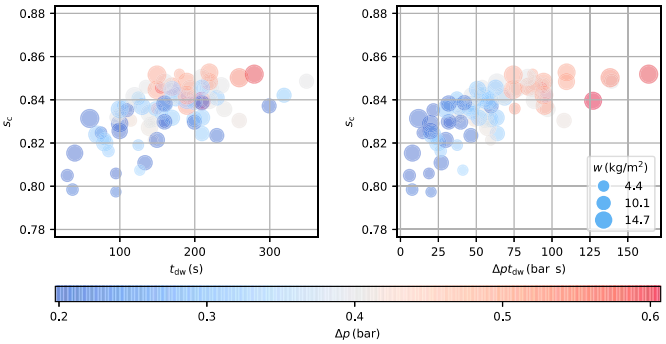

Fig. 3. Filter cake solids content s_c plotted against the dewatering time t_{dw} (left) and the pressure difference multiplied by the dewatering time Δpt_{dw} (right). The size of the marker is varied according to the mass of cake deposited per unit area w and the color according to the pressure difference Δp.

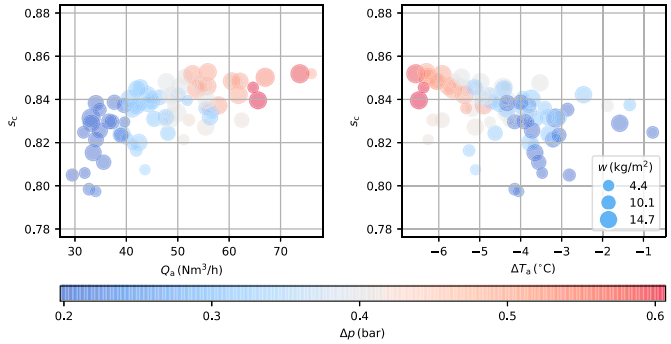

Fig. 4. Filter cake solids content s_c plotted against air flow rates through the vacuum pump Q_a (left) and the temperature difference ΔT_a between the vacuum pump suction air and the slurry feed (right). The size of the marker is varied according to the mass of cake deposited per unit area w and the color according to the pressure difference Δp.

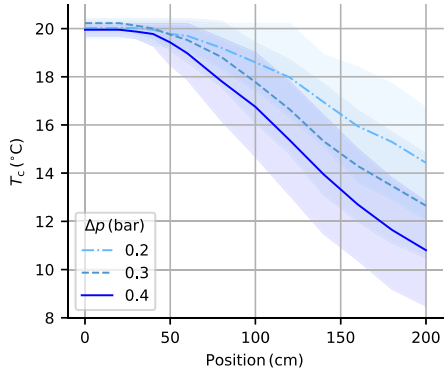

Fig. 5. Mean filter cake surface temperature T_c profiles along the filter belt (lines) and variation between the minimum and maximum temperatures due to varying slurry loadings (filled area) at the corresponding pressure difference levels.

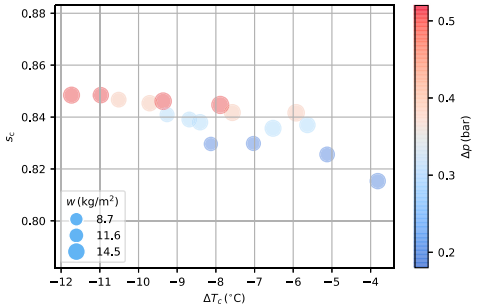

Fig. 6. Filter cake solids content s_c plotted against temperature difference ΔT_c between the filter cake surface at the end of the dewatering region and slurry feed. The size of the marker is varied according to the mass of cake deposited per unit area w and the color according to the pressure difference Δp.

moisture was calculated by Eq. (8). The specific energy consumption of vacuum filtration, $E_S^f = E^f/m_s$, versus the filter cake solids content is illustrated on the left in Fig. 7. The specific energy requirement of

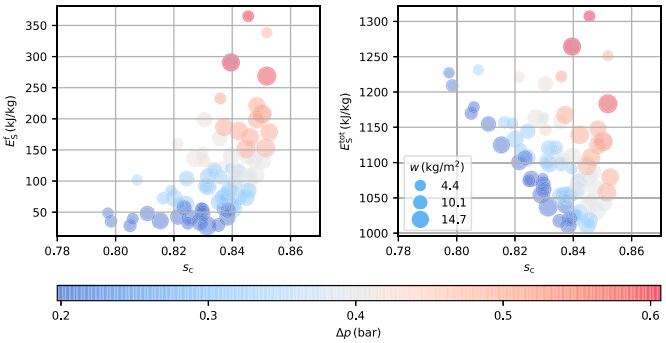

Fig. 7. Specific energy consumption of vacuum filtration E_S^f (left) and the total specific energy consumption to zero moisture E_S^{tot} (right) plotted against filter cake solids content s_c. The size of the marker is varied according to the mass of cake deposited per unit area w and the color according to the pressure difference Δp.

Table 3
Filtration experiments with the total specific energy consumption in the lowest 10%. For symbol definitions, see Nomenclature.

s_{sl} (–)	ρ_{sl} (kg/m^3)	w (kg/m^2)	M_s (g/s)	Δp (bar)	L_c (mm)	z (cm)	t_f (s)	t_{dw} (s)	s (–)	ε_{av}	M (%)	E_S^{tot}(kJ/kg)
0.39	1323	10.4	5.2	0.20	5.1	130	259	160	0.838	0.27	16.2	1010
0.39	1323	11.7	5.9	0.30	5.7	125	249	170	0.845	0.27	15.5	1011
0.44	1384	7.4	7.4	0.20	4.2	100	100	110	0.835	0.36	16.5	1017
0.39	1323	10.4	5.2	0.30	5.0	105	209	209	0.846	0.24	15.4	1018
0.39	1323	9.1	4.6	0.20	4.4	105	209	209	0.839	0.25	16.1	1020
0.44	1384	14.7	7.4	0.30	7.6	115	229	190	0.840	0.31	16.0	1022
0.44	1384	7.4	7.4	0.30	3.9	85	85	125	0.841	0.31	15.9	1025
0.34	1270	12.1	6.1	0.30	5.8	120	239	180	0.842	0.25	15.8	1029

Table 4
Features selected for different feature sets for experimentation as model inputs to predict the cake solids content s_c.

	Feature Set								
Features	1	2	3	4	5	6	7	8	9
s_{sl}						x	x	x	x
w	x	x	x	x	x	x	x	x	x
Δp	x	x	x			x	x	x	x
t_{dw}		x							x
T_{sl}									x
T_{vp}			x		x	x	x	x	x
Q_a					x	x	x	x	x
ΔT_a				x			x	x	x
Δpt_{dw}				x	x			x	x

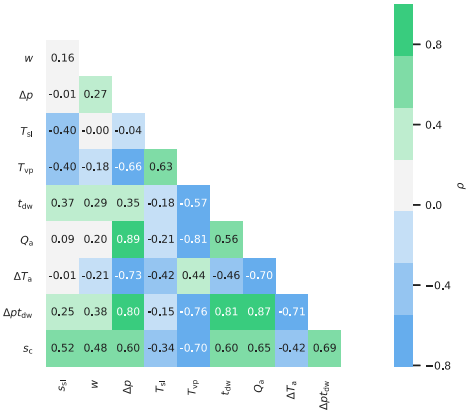

Fig. 8. Correlation map presenting the Pearson correlation coefficients ρ between the experiment settings, process variables, the two interaction features ΔT_a and Δpt_{dw}, and the filter cake solids content s_c.

vacuum filtration increases exponentially as the pressure difference is increased. Similar findings were also observed by the authors of [28] in experiments conducted using a Büchner filter. For experiments with the filter cake solids content between 0.835 and 0.845, the results show nearly a tenfold increase in the specific energy consumption of vacuum filtration from 29.5 to 291 kJ/kg as a result of the increasing pumping demand for maintaining a higher pressure difference. When increasing the solids content of the filter cake from 0.84 to 0.85, the specific energy consumption nearly tripled from 56.1 to 153 kJ/kg. For experiments with the pressure difference of 0.2 bar, the solids content varied by 4.1 pp between 0.797 and 0.838 while the specific energy consumption remained below 50 kJ/kg.

The theoretical specific energy consumption of thermal drying, $E_S^t = E^t/m_s$, i.e., evaporation of the residual moisture content in the filter cake was calculated with the help of Eq. (8) and assuming a thermal efficiency $\eta = 50\%$ of the drying process based on the heat efficiency of a spin-flash dryer reported by Kudra et al. [29]. The moist solids are heated to 100 °C from the initial temperature, which is assumed to be the same as the vacuum pump inlet air temperature. A higher solids content decreases the energy required in the thermal drying stage. The majority of the energy in drying is consumed by the evaporation of water and the small deviations from the decreasing

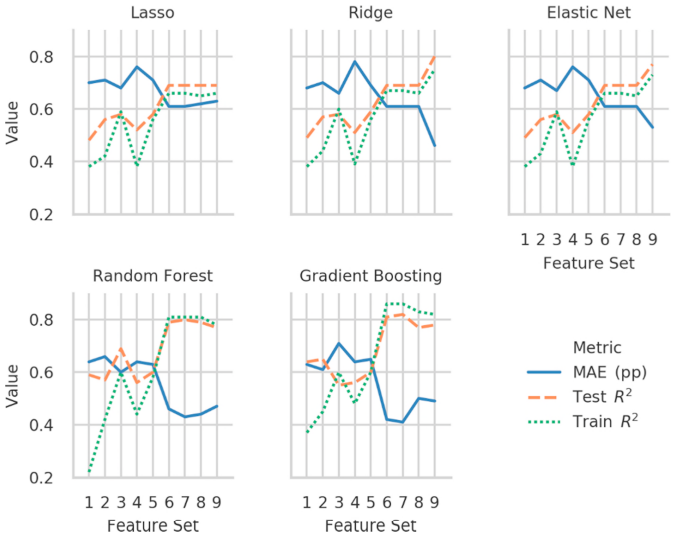

Fig. 9. Performance of the trained models for the filter cake solids content. The mean absolute error MAE is presented as percentage points of the target value. The coefficients of determination R^2 are presented both for the regression model training and testing.

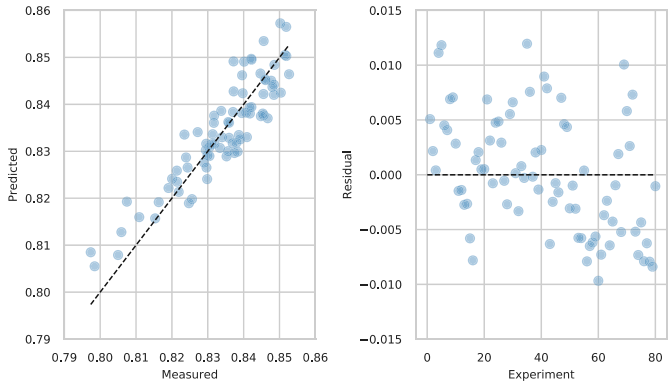

Fig. 10. Soft sensor predictions versus measured values (left) and residuals per experiment (right) for the Ridge regression model with feature set 9 as the model input.

linear energy demand trend are due to the differences in the initial temperature (after dewatering) of the filter cake. The total specific energy consumption to zero moisture, i.e., the sum of the specific energy consumption of vacuum filtration and the specific energy consumption of thermal drying (evaporation), $E_S^{tot} = E_S^f + E_S^t$, versus the filter cake solids content after dewatering, is presented on the right in Fig. 7. The optimum operating conditions in terms of specific energy consumption for the pilot-scale filter and the slurry in question seem to concentrate around the solids content of 0.84, emphasizing the importance of online tracking of the filter cake solids content. Given that the total specific energy consumption mostly varies from 1000 to 1150 kJ/kg, the potential for energy conservation by optimizing slurry concentration, pressure difference, and cake deposited per unit area could be as high as 13% in this case. In order to identify the optimum operating point within the range of variability of the manipulated process variables in this study, the experiments with the total specific energy consumption in the lowest 10% are presented in Table 3 in an ascending order according to the total specific energy consumption.

Within the range of variability of the manipulated process variables, the total specific energy consumption to zero moisture within the lowest 10% is achieved with pressure differences ranging from 0.2 to 0.3 bar. All these experiments with the exception of one are from the test series with two of the highest levels of the slurry solids content. The majority of the experiments with a low total specific energy consumption are from experiments with a slow filter belt speed and a high mass of cake deposited per unit area w. The solids contents after vacuum

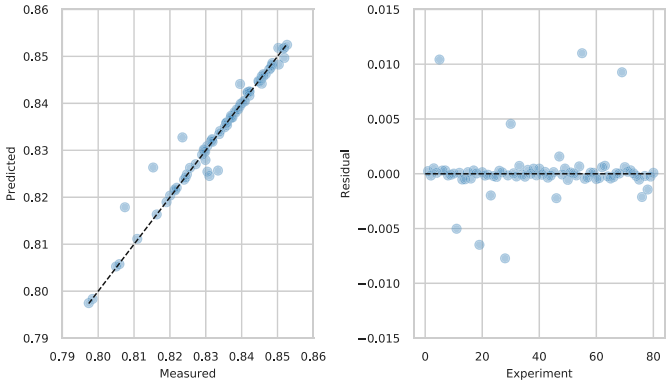

Fig. 11. Soft sensor predictions versus measured values (left) and residuals per experiment (right) for the Gradient Boosting regression model with feature set 7 as model input.

filtration for the experiments in Table 3 is between 0.835 and 0.846. With one exception, the porosities of the experiments are within the 50th percentile, and six of them deviate from the 25th percentile by 3 pp or less. The two minimum energy consumption values are achieved with the slurry solids content of 0.39 and long filtration times, the second-row experiment having an increase in the mass of cake deposited per unit area w and in the pressure difference compared with the first-row experiment. Compared with the two minimum specific energy consumption experiments, increasing the slurry solids content to 0.44 and shortening the filtration time by increasing the filter belt speed, produces a thinner, higher porosity cake with only a 6–7 kJ/kg (0.6–0.7%) increase in the total specific energy consumption but a 25–42% increase in the solids throughput M_s.

4.4. Prediction of the moisture contents of filter cakes

Nine combinations of experiment settings, measured process values, and interaction features were used as inputs to the regression models (Table 4) to predict the filter cake solids content s_c after dewatering. The correlation map of the correlation coefficients ρ between these inputs is presented in Fig. 8. The values of $|\rho| \geq 0.60$ with the cake solids content are found for the pressure difference Δp, air temperature at the vacuum pump inlet T_{vp}, the dewatering time t_{dw}, the air flow rate at the vacuum pump outlet Q_a, the temperature difference ΔT_a between the vacuum pump suction air and the slurry feed, and the interaction feature $\Delta p t_{dw}$. Other features presented in the correlation map were also considered to have an impact on the filter cake solids content and were thus included in the analysis.

The selection of features for the nine feature sets used as inputs to model the cake solids content s_c was started from the bare minimum of Δp and w and increased and varied from set to set to see which features would be advantageous to the modeling and to keep the number of input features at a reasonable level. As these two features were the main controlled process variables in the experiments, they were included in each of the feature sets, in two of which Δp was included only in the interaction feature $\Delta p t_{dw}$. 80% of the experiments were randomly selected for training the regression models, and 20% of the experiments were reserved for testing the trained models.

For all other algorithms except Gradient Boosting, the selection between the dewatering time and the vacuum pump inlet air temperature favors the latter as can be seen in Fig. 9. This suggests that the temperature of air after passing through the filter cake would be a better indicator of the cake moisture content than the dewatering time. When relying on the two interaction features and the mass of solids deposited per unit area, regression results for all the other algorithms except for Gradient Boosting, again, take a turn to the worse. Selecting both the temperature and flow rate of air as inputs in addition to w and $\Delta p t_{dw}$ helps all the algorithms to perform better.

For feature sets 6, 7, 8, and 9, which all also include the solids content of slurry and the pressure difference as inputs, the coefficients of determination R^2 for the ensemble decision tree algorithms Random Forest and Gradient Boosting rise to the 0.8 region. This indicates that these models are able to explain ~80% of the variability in the cake solids content. The fact that the training and test scores for Random Forest are close to each other indicates a good fit of the algorithm for the non-linear regression problem. When including all the features as inputs, the linear regression algorithms Ridge and Elastic Net also achieve R^2 values above 0.7 and the Ridge mean absolute error (MAE) falls close to that of the Random Forest. The smallest MAE of 0.41 pp is achieved using the Gradient Boosting regression algorithm and the feature set 7 with the R^2 values for training and testing of 0.86 and 0.82 respectively.

Regarding the linear regression models, the best fit was achieved with the Ridge algorithm and feature set 9 as the model input. The predictions and residuals for this model are presented in Fig. 10. The residuals seem to be randomly dispersed around zero, which would indicate the applicability of this model to predict the filter cake solids content with residuals generally between ± 0.01 (± 1 pp).

The Gradient Boosting regression algorithm with feature set 7 as the input produced the best results considering all the experimented models. As can be seen in Fig. 11, the predictions align with the measured values with only a few deviations by ± 0.011 (± 1.1 pp) or less. One experiment with these high prediction errors had a filter cake height of 2.3 mm and the other had either a considerably longer or shorter dewatering time compared with all the other experiments. It seems that the algorithm would have needed more data around these extreme values to properly train and predict them.

An important aspect to be considered about the modeling capability of these data-driven models is the constraint that the process variables used as inputs to the model should be within the same range as when training the models in order for the model to output a proper prediction. The application of the method in industry would require a proper instrumentation of the filter to measure the variables used as inputs for the model. Sufficient number of recordings of the input variables and an analysis of the corresponding cake samples at a sufficiently wide range of operating points of the filter would be required to train a useful

model. The solids content of the slurry as input variable could be replaced by a density measurement of the slurry.

5. Conclusions

The previously unexplored application of thermodynamics to cake vacuum filtration has proven highly beneficial for predicting the filter cake moisture content. The heat transfer between air forced through the filter cake, the water inside the filter cake, and the solids of the filter cake resulting from evaporation of water can be seen clearly from the results of this study. Predicting the cake solids content by using regression modeling with the vacuum pump inlet air temperature and the air flow rate as inputs in addition to the traditional vacuum filtration process variables makes it possible to explain 80% of the variance in the target variable by the model, while keeping the mean absolute error below 0.5 pp.

An interesting approach for predicting the filter cake moisture content would be the use of cake surface temperature as an input variable for modeling. The room temperature leak flow air mixes with the cooled air that has passed through the filter cake, warming the air/vapor mixture in the vacuum box especially at higher pressure differences with the increased leak flow. This moderates the cool down effect of evaporation in the vacuum box, which could be prevented by using the surface temperature of the filter cake as a key variable in the prediction. In addition to horizontal belt vacuum filters, the proposed method for real-time monitoring of the moisture content of the filter cake is applicable to other types of filters where similar temperature measurements can be made. However, the applicability of the method to air drying in pressure filters would require further investigation. Given the promising results of this pilot-scale research, next steps for future investigation of the technology could include a trial setup on an industrial scale. Another topic for future research could be the development of a rigorous mathematical model for evaporation using the governing equations for mass, momentum, and energy.

Regarding the energy consumption of vacuum filtration and the subsequent thermal drying of the calcite material investigated in this study, the following conclusions can be made:

(1) The lowest total energy demand is achieved in the pressure difference range from 0.2 to 0.3 bar, when the cake is dewatered to approximately 84 wt% solids content prior to thermal drying.
(2) Finding the right combination of slurry solids content, mass of cake per unit area, and pressure difference is crucial in minimizing the specific energy consumption of vacuum filtration.

LUT University has patented the methods for the filter cake moisture estimation described in this publication.

Acknowledgements

The authors would like to thank Hanna Niemelä for providing language help during the writing process.

Funding: This work was supported by The Finnish Funding Agency for Technology and Innovation (Tekes).

Appendix A. Supplementary material

Supplementary data to this article can be found online at https://doi.org/10.1016/j.seppur.2019.03.091.

References

[1] E.S. Tarleton, R.J. Wakeman, Institution of Chemical Engineers (Great Britain), Solid/liquid Separation: Equipment Selection and Process Design, Butterworth-Heinemann, 2007.
[2] V. Karvonen, M. Huttunen, T. Kinnarinen, A. Häkkinen, Research focus and research trends in vacuum filtration – bibliographical analysis, Filtration 18 (2018) 40–44.
[3] L. Besra, D.K. Sengupta, S.K. Roy, Particle characteristics and their influence on dewatering of kaolin, calcite and quartz suspensions, Int. J. Miner. Process. 59 (2000) 89–112, https://doi.org/10.1016/S0301-7516(99)00065-4.
[4] G. France, A. von Muralt, Horizontal vacuum belt filter control using on-line moisture analysis at Gregory coal mine, in: 11th Aust. Coal Prep. Conf. Exhib. Proc., 2007: pp. 82–93.
[5] H. Mao, F. Wang, F. Mao, Y. Chi, S. Lu, K. Cen, Measurement of water content and moisture distribution in sludge by 1 H nuclear magnetic resonance spectroscopy, Dry. Technol. 34 (2016) 267–274, https://doi.org/10.1080/07373937.2015.1047952.
[6] K. Phetpan, P. Sirisomboon, Evaluation of the moisture content of tapioca starch using near-infrared spectroscopy, J. Innov. Opt. Health Sci. 08 (2015) 1550014, https://doi.org/10.1142/S1793545815500145.
[7] T.J. Schmugge, T.J. Jackson, H.L. McKim, Survey of methods for soil moisture determination, Greenbelt, Maryland, 1979.
[8] R. Wakeman, The influence of particle properties on filtration, Sep. Purif. Technol. 58 (2007) 234–241, https://doi.org/10.1016/J.SEPPUR.2007.03.018.
[9] S. Tarleton, R. Wakeman, Solid/Liquid Separation : Principles of Industrial Filtration, Elsevier Science, 2005.
[10] L. Svarovsky, Solid-liquid Separation, 4th ed., Butterworth-Heinemann, 2000.
[11] D.J. Condie, M. Hinkel, C.J. Veal, K. Boissy, D. Leclerc, Modeling the vacuum filtration of fine coal. III. Comparison of models for predicting desaturation kinetics, Sep. Sci. Technol. 35 (2000) 1467–1484, https://doi.org/10.1081/SS-100100236.
[12] A. Rushton, M. Hosseini, I. Hassan, The effects of velocity and concentration on filter cake resistance, in: Proc. Symp. Solid-Liquid Sep. Pract., Leeds, 1978, pp. 78–91.
[13] G.H. Hundy, A.R. Trott, T. Welch, Refrigeration, Air Conditioning and Heat Pumps, Fifth, Butterworth-Heinemann, Oxford, 2016.
[14] M.K. Das, P.P. Mukherjee, K. Muralidhar, Equations Governing Flow and Transport in Porous Media, in: Model. Transp. Phenom. Porous Media with Appl., Springer International Publishing, 2018, pp. 15–63. http://doi.org/10.1007/978-3-319-69866-3_2.
[15] I. Kovačević, M. Sourbron, The numerical model for direct evaporative cooler, Appl. Therm. Eng. 113 (2017) 8–19, https://doi.org/10.1016/J.APPLTHERMALENG.2016.11.025.
[16] I.C. Kemp, Fundamentals of Energy Analysis of Dryers, in: Mod. Dry. Technol. Vol. 4 Energy Savings, Wiley-VCH Verlag GmbH & Co. KGaA, Weinheim, Germany, 2012, pp. 1–45. http://doi.org/10.1002/9783527631681.ch1.
[17] J.R. Rumble, D.R. Lide, T.J. Bruno, CRC handbook of chemistry and physics, 99 th, CRC Press, 2018. https://www.crcpress.com/CRC-Handbook-of-Chemistry-and-Physics-99th-Edition/Rumble/p/book/9781138561632 (accessed November 15, 2018).
[18] L. Fortuna, S. Graziani, A. Rizzo, M.G. Xibilia, Soft Sensors for Monitoring and Control of Industrial Processes, Springer, London, London, 2007. http://doi.org/10.1007/978-1-84628-480-9.
[19] B. Lin, B. Recke, J.K.H. Knudsen, S.B. Jørgensen, A systematic approach for soft sensor development, Comput. Chem. Eng. 31 (2007) 419–425, https://doi.org/10.1016/J.COMPCHEMENG.2006.05.030.
[20] P. Kadlec, B. Gabrys, S. Strandt, Data-driven Soft Sensors in the process industry, Comput. Chem. Eng. 33 (2009) 795–814, https://doi.org/10.1016/J.COMPCHEMENG.2008.12.012.
[21] P. Kadlec, R. Grbić, B. Gabrys, Review of adaptation mechanisms for data-driven soft sensors, Comput. Chem. Eng. 35 (2011) 1–24, https://doi.org/10.1016/J.COMPCHEMENG.2010.07.034.
[22] F.A.A. Souza, R. Araújo, J. Mendes, Review of soft sensor methods for regression applications, Chemom. Intell. Lab. Syst. 152 (2016) 69–79, https://doi.org/10.1016/J.CHEMOLAB.2015.12.011.
[23] Z. Ge, Review on data-driven modeling and monitoring for plant-wide industrial processes, Chemom. Intell. Lab. Syst. 171 (2017) 16–25, https://doi.org/10.1016/J.CHEMOLAB.2017.09.021.
[24] B. Bidar, J. Sadeghi, F. Shahraki, M.M. Khalilipour, Data-driven soft sensor approach for online quality prediction using state dependent parameter models, Chemom. Intell. Lab. Syst. 162 (2017) 130–141, https://doi.org/10.1016/J.CHEMOLAB.2017.01.004.
[25] L. Yao, Z. Ge, Variable selection for nonlinear soft sensor development with enhanced Binary Differential Evolution algorithm, Control Eng. Pract. 72 (2018) 68–82, https://doi.org/10.1016/J.CONENGPRAC.2017.11.007.
[26] E. Szymańska, Modern data science for analytical chemical data – a comprehensive review, Anal. Chim. Acta. 1028 (2018) 1–10, https://doi.org/10.1016/J.ACA.2018.05.038.
[27] Z. Ge, Z. Song, S.X. Ding, B. Huang, Data mining and analytics in the process industry: the role of machine learning, IEEE Access 5 (2017) 20590–20616, https://doi.org/10.1109/ACCESS.2017.2756872.
[28] M. Huttunen, L. Nygren, T. Kinnarinen, A. Häkkinen, T. Lindh, J. Ahola, V. Karvonen, Specific energy consumption of cake dewatering with vacuum filters, Miner. Eng. 100 (2017) 144–154, https://doi.org/10.1016/J.MINENG.2016.10.025.
[29] T. Kudra, E. Pallai, Z. Bartczaki, M. Peter, Drying of paste-like materials in screw-type spouted-bed and spin-flash dryers, Dry. Technol. 7 (1989) 583–597, https://doi.org/10.1080/07373938908916612.

ACTA UNIVERSITATIS LAPPEENRANTAENSIS

848. ALMPANOPOULOU, ARGYRO. Knowledge ecosystem formation: an institutional and organisational perspective. 2019. Diss.

849. AMELI, ALIREZA. Supercritical CO2 numerical modelling and turbomachinery design. 2019. Diss.

850. RENEV, IVAN. Automation of the conceptual design process in construction industry using ideas generation techniques. 2019. Diss.

851. AVRAMENKO, ANNA. CFD-based optimization for wind turbine locations in a wind park. 2019. Diss.

852. RISSANEN, TOMMI. Perspectives on business model experimentation in internationalizing high-tech companies. 2019. Diss.

853. HASSANZADEH, AIDIN. Advanced techniques for unsupervised classification of remote sensing hyperspectral images. 2019. Diss.

854. POPOVIC, TAMARA. Quantitative indicators of social sustainability applicable in process systems engineering. 2019. Diss.

855. RAMASAMY, DEEPIKA. Selective recovery of rare earth elements from diluted aqueous streams using N- and O –coordination ligand grafted organic-inorganic hybrid composites. 2019. Diss.

856. IFTEKHAR, SIDRA. Synthesis of hybrid bio-nanocomposites and their application for the removal of rare earth elements from synthetic wastewater. 2019. Diss.

857. HUIKURI, MARKO. Modelling and disturbance compensation of a permanent magnet linear motor with a discontinuous track 2019. Diss.

858. AALTO, MIKA. Agent-based modeling as part of biomass supply system research. 2019. Diss.

859. IVANOVA, TATYANA. Atomic layer deposition of catalytic materials for environmental protection. 2019. Diss.

860. SOKOLOV, ALEXANDER. Pulsed corona discharge for wastewater treatment and modification of organic materials. 2019. Diss.

861. DOSHI, BHAIRAVI. Towards a sustainable valorisation of spilled oil by establishing a green chemistry between a surface active moiety of chitosan and oils. 2019. Diss.

862. KHADIJEH, NEKOUEIAN. Modification of carbon-based electrodes using metal nanostructures: Application to voltammetric determination of some pharmaceutical and biological compounds. 2019. Diss.

863. HANSKI, JYRI. Supporting strategic asset management in complex and uncertain decision contexts. 2019. Diss.

864. OTRA-AHO, VILLE. A project management office as a project organization’s strategizing tool. 2019. Diss.

865. HILTUNEN, SALLA. Hydrothermal stability of microfibrillated cellulose. 2019. Diss.

866. GURUNG, KHUM. Membrane bioreactor for the removal of emerging contaminants from municipal wastewater and its viability of integrating advanced oxidation processes. 2019. Diss.

867. AWAN, USAMA. Inter-firm relationship leading towards social sustainability in export manufacturing firms. 2019. Diss.

868. SAVCHENKO, DMITRII. Testing microservice applications. 2019. Diss.

869. KARHU, MIIKKA. On weldability of thick section austenitic stainless steel using laser processes. 2019. Diss.

870. KUPARINEN, KATJA. Transforming the chemical pulp industry – From an emitter to a source of negative CO2 emissions. 2019. Diss.

871. HUJALA, ELINA. Quantification of large steam bubble oscillations and chugging using image analysis. 2019. Diss.

872. ZHIDCHENKO, VICTOR. Methods for lifecycle support of hydraulically actuated mobile working machines using IoT and digital twin concepts. 2019. Diss.

873. EGOROV, DMITRY. Ferrite permanent magnet hysteresis loss in rotating electrical machinery. 2019. Diss.

874. PALMER, CAROLIN. Psychological aspects of entrepreneurship – How personality and cognitive abilities influence leadership. 2019. Diss.

875. TALÁSEK, TOMÁS. The linguistic approximation of fuzzy models outputs. 2019. Diss.

876. LAHDENPERÄ, ESKO. Mass transfer modeling in slow-release dissolution and in reactive extraction using experimental verification. 2019. Diss.

877. GRÜNENWALD, STEFAN. High power fiber laser welding of thick section materials - Process performance and weld properties. 2019. Diss.

878. NARAYANAN, ARUN. Renewable-energy-based single and community microgrids integrated with electricity markets. 2019. Diss.

879. JAATINEN, PEKKO. Design and control of a permanent magnet bearingless machine. 2019. Diss.

880. HILTUNEN, JANI. Improving the DC-DC power conversion efficiency in a solid oxide fuel cell system. 2019. Diss.

881. RAHIKAINEN, JARKKO. On the dynamic simulation of coupled multibody and hydraulic systems for real-time applications. 2019. Diss.

882. ALAPERÄ, ILARI. Grid support by battery energy storage system secondary applications. 2019. Diss.

883. TYKKYLÄINEN, SAILA. Growth for the common good? Social enterprises' growth process. 2019. Diss.

884. TUOMISALO, TEEMU. Learning and entrepreneurial opportunity development within a Finnish telecommunication International Venture. 2019. Diss.

885. OYEDEJI, SHOLA. Software sustainability by design. 2019. Diss.

ISBN 978-952-335-458-6
ISBN 978-952-335-459-3 (PDF)
ISSN-L 1456-4491
ISSN 1456-4491
Lappeenranta 2019